



VCU

Virginia Commonwealth University
VCU Scholars Compass

Theses and Dissertations


Graduate School

2023

Patterns, Mechanisms, and Characterization of Carbon Cycling Stability Following Partial Forest Disturbance

Kayla C. Mathes
Virginia Commonwealth University

Follow this and additional works at: <https://scholarscompass.vcu.edu/etd>

 Part of the [Forest Biology Commons](#), [Forest Management Commons](#), [Other Forestry and Forest Sciences Commons](#), [Plant Sciences Commons](#), and the [Terrestrial and Aquatic Ecology Commons](#)

© The Author

Downloaded from

<https://scholarscompass.vcu.edu/etd/7290>

This Dissertation is brought to you for free and open access by the Graduate School at VCU Scholars Compass. It has been accepted for inclusion in Theses and Dissertations by an authorized administrator of VCU Scholars Compass. For more information, please contact libcompass@vcu.edu.

**PATTERNS, MECHANISMS, AND CHARACTERIZATION OF CARBON CYCLING
STABILITY FOLLOWING PARTIAL FOREST DISTURBANCE**

A dissertation submitted in partial fulfillment of the requirements for the degree of Doctor of
Philosophy at Virginia Commonwealth University

By

Kayla C. Mathes
B.S. Environmental Sciences,
University of Michigan-Ann Arbor 2018

Advisor:
Dr. Christopher M. Gough
Associate Professor, Department of Biology, VCU

Virginia Commonwealth University
Richmond, VA
May, 2023

This dissertation is dedicated to my parents, Glenda and John Mathes, for every single reason I could possibly image.

Acknowledgements

First and foremost, I want to express my deep gratitude for my advisor, Chris Gough. He showed me what it means to be an incredible mentor and I cannot express enough how much his enthusiasm and integrity as a scientist and kindness and dedication as an advisor has meant to my academic growth over the last five years. Thank you to the University of Michigan Biological Station for not only hosting all my PhD research, but for being my summer home and community for the last 8 years. I found my love for forests and a passion for ecology in those North Woods along Douglas Lake and I have never looked back. I would like to acknowledge the ILS program and director, Dr. Fong, for giving me the opportunity and resources to advance my scientific education amongst such talented peers. A big shoutout to all lab mates, past and present. Getting to share the *humbling* experience of graduate school with such incredible scientists and caring people was an honor. Cheers to (mostly) hitting the sweet spot between work and play. To my partner, Max, thank you for being my rock throughout this journey and always helping me live and cherish the present. And finally, to my parents, for whom this dissertation is dedicated, thank you for always trusting me to continue finding the best version of myself and for, somehow, always knowing what I am capable of long before I do.

Table of Contents

Executive Summary.....	5-10
Table Captions.....	11-12
Figure Captions.....	12-18
Chapter 1: <i>A multidimensional stability framework enhances interpretation and comparison of carbon cycling response to disturbance</i>	19
Abstract.....	20
Section 1.....	21-23
Section 2.....	23-25
Section 3.....	25-30
Conclusions and Recommendations.....	30-31
Literature Cited.....	32-42
Tables and Figures.....	43-50
Appendix.....	51
Chapter 2: <i>Sustained three-year declines in forest soil respiration are proportional to disturbance severity</i>	52
Abstract.....	53
Introduction.....	54-57
Methods.....	57-65
Results.....	65-68
Discussion.....	69-75
Literature Cited.....	76-86
Tables and Figures.....	87-96
Appendix.....	97-107
Chapter 3: <i>Sustained net ecosystem production across a disturbance severity gradient</i>	108
Abstract.....	109
Introduction.....	110-112
Methods.....	113-123
Results.....	124-126
Discussion.....	126-131
Literature Cited.....	131-141
Tables and Figures.....	142-151
Appendix.....	152-158
Chapter 4: <i>Dynamic rhizosphere processes drive immediate soil respiration response to phloem disruption</i>	159
Abstract.....	160
Introduction.....	161-162
Methods.....	163-170
Results.....	170-172
Discussion.....	172-177
Literature Cited.....	177-184
Tables and Figures.....	185-192
Appendix.....	193-195
Conclusions & Recommendations.....	196-197
Vita.....	198

Executive Summary (Abstract)

PATTERNS, MECHANISMS, AND CHARACTERIZATION OF CARBON CYCLING STABILITY FOLLOWING PARTIAL FOREST DISTURBANCE

By

Kayla C. Mathes

Virginia Commonwealth University, 2023

Advisor:

Dr. Christopher M. Gough

Associate Professor, Department of Biology, VCU

Among the most essential questions in the era of global climate change is how the forest carbon (C) cycle will respond to an increase in the extent of biotic disturbances from insects and pathogens. While considerable research has focused on stand-replacing disturbance regimes, less is known about C cycling stability following partial disturbances that produce gradients of disturbance severity (Cohen et al. 2016, Sommerfeld et al. 2018, Edgar and Westfall 2022). Belowground C cycling responses to disturbance are especially poorly understood, even though temperate forest soils and roots contain up to 50% of total ecosystem C (Pan et al. 2011). In particular, soil respiration (R_s) accounts for more than half of temperate forest C loss (Bond-Lamberty et al. 2018, Lei et al. 2021) and even small shifts in this globally important flux from rising disturbance could tip the C balance from net sink to source (Schlesinger and Andrews 2000; Janssens et al. 2001; Curtis et al. 2005). Interpreting trends and mechanisms of C cycling

disturbance response requires the integration of cross-scaled experiments and refined ecological theory. The overarching goal of my dissertation is to lay a foundation for the use of a multi-dimensional stability framework for the C cycling community, and through manipulative ecosystem experiments, assess patterns and advance mechanistic understanding of how partial disturbances impact forest C cycling.

To begin, **chapter one** demonstrates the utility of a multi-dimensional stability framework for interpreting and comparing forest C flux responses to disturbance (Mathes et al. 2021, published in *Ecosphere*). I adapted a framework that includes four interrelated but distinct dimensions of stability (resistance, resilience, temporal stability and recovery), first described in Hillebrand et al. 2018. Leveraging flux data following disturbance, I found this framework provides a powerful complement to analyses of absolute fluxes, allowing for direct comparisons of functional disturbance response across sites and among C fluxes with variable units and magnitudes. To continue assessing its value, I integrated elements of this framework into subsequent chapters, focusing on the *resistance* stage (i.e. initial direction and magnitude of disturbance response), and provided further context for the strengths as well as the current limitations of this framework for interpreting C flux disturbance response.

Diving into my empirical assessments of C cycling following disturbance, in **chapter two**, I quantify how soil respiration (R_s) responds to a large-scale experimental manipulation of disturbance severity via phloem-disruption (Forest Resilience Threshold Experiment, FoRTE) (minor revision, *Ecosystems*). Phloem-disruption was used to mimic disturbances from wood-boring insects that are increasing in North American forests (Edgar and Westfall 2022). I found

immediate and sustained declines in R_s for the first three years following disturbance that were proportional to severity. By comparing R_s and heterotrophic respiration (i.e. microbial decomposition) *resistance*, and assessing the temperature sensitivity and basal respiration rates, I concluded that this immediate and sustained decline in R_s was primarily driven by suppression of autotrophic (i.e. root) respiration.

Observations from FoRTE showing sustained wood net primary production and declining R_s following phloem-disruption (Chapter two; Niedermaier et al. 2022; Gough et al. 2021) prompted the hypothesis that C balance, or net ecosystem production (NEP), may be sustained during the resistance phase of disturbance response. In **chapter three**, I test this hypothesis by performing a biometric accounting of C fluxes and estimate NEP across the disturbance severity gradient. In support for my hypothesis, NEP was stable across the severity gradient for the first three years even at the highest level of severity (85% gross defoliation) as a result of stable total net primary production (NPP) and heterotrophic respiration (R_h).

Finally, I was motivated to understand the mechanisms that drive immediate, short-term R_s response to partial disturbance. In **chapter four**, I present results from a separate, small-scale phloem-disrupting experiment (Short-term Response to Experimental Disturbance, ShRRED) that I designed and implemented to assess fine-scale rhizosphere responses that could regulate stand-level R_s following phloem-disruption. In contrast to results from chapter 2, I found R_s was completely *resistant* (i.e. no change relative to control) in the first year following disturbance, highlighting the variability in R_s response to phloem-disruption that exists at our site and in the literature (Levy-Varon et al. 2014, Aubrey and Teskey 2018, Nottingham et al. 2022). I suggest

mechanisms that regulate rates of C allocated belowground, such as site productivity and temporal climatic variation, may support variable R_s response. Additionally, I found surviving trees responded to enriched soil nitrogen *before* complete functional decline of disturbed trees, which may have helped sustain stand-level R_s .

Synthesizing across chapters, I highlight three overarching conclusions from my dissertation. First, temperate forests can sustain C balance following disturbances across a gradient of severities in the initial resistance phase as a result of stable heterotrophic respiration and net primary production. Second, soil respiration can exhibit variable responses to the same partial disturbance, which could partly be determined by dynamic fine-scale rhizosphere responses from both surviving and disturbed trees on a landscape. Third, leveraging components of a multi-dimensional stability framework into assessments of C flux disturbance response revealed the utility of applying such a framework—more commonly used by community ecologists—to analyses of ecosystem function.

Literature Cited

- Aubrey, D. P., & Teskey, R. O. (2018). Stored root carbohydrates can maintain root respiration for extended periods. *New Phytologist*, *218*(1), 142–152.
- Bond-Lamberty, B., Bailey, V. L., Chen, M., Gough, C. M., & Vargas, R. (2018). Globally rising soil heterotrophic respiration over recent decades. *Nature*, *560*(7716), 80–83.
- Cohen, W. B., Yang, Z., Stehman, S. V., Schroeder, T. A., Bell, D. M., Masek, J. G., Huang, C., & Meigs, G. W. (2016). Forest disturbance across the conterminous United States from 1985-2012: The emerging dominance of forest decline. *Forest Ecology and*

- Management*, 360, 242–252.
- Curtis, P. S., Vogel, C. S., Gough, C. M., Schmid, H. P., Su, H. B., & Bovard, B. D. (2005). Respiratory carbon losses and the carbon-use efficiency of a northern hardwood forest, 1999-2003. *New Phytologist*, 167(2), 437–456.
- Edgar, C. B., & Westfall, J. A. (2022). Timing and extent of forest disturbance in the Laurentian Mixed Forest. *Frontiers in Forests and Global Change*, 5(August), 1–15.
- Gough, C. M., Atkins, J. W., Bond-Lamberty, B., Agee, E. A., Dorheim, K. R., Fahey, R. T., Grigri, M. S., Haber, L. T., Mathes, K. C., Pennington, S. C., Shiklomanov, A. N., & Tallant, J. M. (2021). Forest Structural Complexity and Biomass Predict First-Year Carbon Cycling Responses to Disturbance. *Ecosystems*, 24(3), 699–712.
- Hillebrand, H., S. Langenheder, K. Lebet, E. Lindström, Ö. Östman, and M. Striebel. (2018). Decomposing multiple dimensions of stability in global change experiments. *Ecology Letters* 21:21–30.
- Janssens, I. A., Lankreijer, H., Matteucci, G., Kowalski, A. S., Buchmann, N., Epron, D., Pilegaard, K., Kutsch, W., Longdoz, B., Grunwald, T., Montagnani, L., Dore, S., Rebmann, C., Moors, E. J., Grelle, A., Rannik, U., Morgenstern, K., Oltchev, S., Clement, R., Valentini, R. (2001). Productivity overshadows temperature in determining soil and ecosystem respiration across European forests. *Global Change Biology*, 7(3), 269–278.
- Lei, J., Guo, X., Zeng, Y., Zhou, J., Gao, Q., & Yang, Y. (2021). Temporal changes in global soil respiration since 1987. *Nature Communications*, 12(1), 1–9.
- Levy-Varon, J. H., Schuster, W. S. F., & Griffin, K. L. (2014). Rapid rebound of soil respiration following partial stand disturbance by tree girdling in a temperate deciduous forest.

- Oecologia*, 174(4), 1415–1424.
- Mathes, K. C., Ju, Y., Kleinke, C., Oldfield, C., Bohrer, G., Bond-Lamberty, B., Vogel, C. S., Dorheim, K., & Gough, C. M. (2021). A multidimensional stability framework enhances interpretation and comparison of carbon cycling response to disturbance. *Ecosphere*, 12(11).
- Niedermaier, K. M., Atkins, J. W., Grigri, M. S., Bond-lamberty, B., & Gough, C. M. (2022). Structural complexity and primary production resistance are coupled in a temperate forest. *Frontiers in Forests and Global Change*.
- Nottingham, A. T., Cheesman, A. W., Riutta, T., Doughty, C. E., Telford, E., Huaraca Huasco, W., Svátek, M., Kvasnica, J., Majalap, N., Malhi, Y., Meir, P., & Arn Teh, Y. (2022). Large contribution of recent photosynthate to soil respiration in tropical dipterocarp forest revealed by girdling. *Journal of Ecology*, 110(2), 387–403.
- Pan, Y., Birdsey, R. A., Fang J., Houghton R., Kauppi P. E., Kurz W. A., Phillips O. L., & Shvidenko A. (2011). A Large and Persistent Carbon Sink in the World's Forests. *Science*, 333(6045), 988–933.
- Schlesinger, W. H., & Andrews, J. A. (2000). Soil respiration and the global carbon cycle. In *Biogeochemistry*, 48.
- Sommerfeld, A., Senf, C., Buma, B., D'Amato, A. W., Després, T., Díaz-Hormazábal, I., Fraver, S., Frelich, L. E., Gutiérrez, Á. G., Hart, S. J., & and others. (2018). Patterns and drivers of recent disturbances across the temperate forest biome. *Nature Communications*, 9(1), 4355.

Table Captions

Table 1.1: Multidimensional stability metrics for UMBS gross primary production (GPP), ecosystem respiration (R_e), soil respiration (R_s) and net ecosystem production (NEP) from the log response ratios of treatment and control estimates (Figure 1.1). R_s resistance could not be calculated because data were not available the year following disturbance. To account for pre-treatment site differences, the response ratios of control and treatment C fluxes were normalized to pre-disturbance values.

Table 1.2: Critical knowledge gaps in ecology that could benefit from a multidimensional stability analytical framework.

Table 2.1: The vegetation characteristics, landforms and soil textures of treatment replicates in the Forest Resilience Threshold Experiment (FoRTE) before disturbance severity and type treatments were implemented (2018). Species abbreviations are as follows: POGR (*Populus grandidentata*), ACSA (*Acer saccharum*), ACRU (*Acer rubrum*), FAGR (*Fagus grandifolia*), QURU (*Quercus rubra*), PIST (*Pinus strobus*).

Table 3.1: The vegetation characteristics, landforms and soil textures of treatment replicates in the Forest Resilience Threshold Experiment (FoRTE) before disturbance severity treatments were implemented. Species abbreviations are as follows: POGR (*Populus grandidentata*), ACSA (*Acer rubrum*), FAGR (*Fagus grandifolia*), QURU (*Quercus rubra*), PIST (*Pinus strbous*).

Table 3.2: Mean (\pm SE) NPP fluxes ($\text{Mg C ha}^{-1} \text{ yr}^{-1}$) across disturbances severities and years. SE represents variation across experimental replicates. Canopy and subcanopy ANPP_w = Aboveground woody net primary production, BNPP_w = Belowground woody net primary

production, NPP_{ll} = leaf litter primary production, NPP_{fwd} = fine woody debris primary production, NPP_{fr} = fine-root primary production.

Table 3.3: Mean (\pm SE) R_h fluxes ($Mg\ C\ ha^{-1}\ yr^{-1}$) across disturbances severities and years from 3 and 4 independent estimates of R_{cwd} and R_h , respectively. SE represents quadratic sum of compounding error from spatial variation (replicates) and uncertainty around modeled soil temperature estimates. R_{cwd} = coarse woody debris respiration and R_{sh} = soil heterotrophic respiration.

Table 3.4: Mean (\pm SE) net ecosystem production (NEP, $Mg\ C\ ha^{-1}\ yr^{-1}$) across disturbances severities and years. 12 independent estimates are the result of all combinations of R_{cwd} and R_h methods. SE represents quadratic sum of compounding error across component fluxes.

Table 4.1: Physical and ecological site characteristics between the disturbance and control plots. Landform, soil type and soil drainage information was taken from Pearsall et al. 1995 and vegetation and soil micrometeorology measurements were taken one week prior to disturbance initiation.

Figure Captions

Figure 1.1: A multidimensional stability framework (MDSF) with four distinct dimensions of stability adopted from Hillebrand et al. 2018 and revised to capture dynamic C cycling responses to disturbance. Conceptual figure shows two example C flux stability profiles following disturbance, one increasing (presented with positive stability dimension labels, e.g. r_{s+}) and one decreasing (presented with negative stability dimension labels, e.g. r_{s-}) immediately following disturbance. Illustration panels provide snapshots of the various stages of disturbance response corresponding with different stability dimensions. Table details mathematical and written

definitions of each dimension. “ F ” represents the C flux rate from the y-axis, “ t ” represents time from the x-axis and “ i ” represents the intercept of the resilience regression line.

Figure 1.2: Time-series (2008-2019) of disturbance treatment via stem girdling (US-UMd) and control (US-UMB) forests analyzed with simple linear regression. A) Annual gross primary production (GPP) \pm uncertainty: Girdled (p-value: n.s.), Control (p-value: n.s.) B) Annual net ecosystem production (NEP) \pm uncertainty: Girdled (p-value < 0.01 , Adjusted $R^2 = 0.53$), Control (p = 0.02, Adjusted $R^2 = 0.36$) C) Annual ecosystem respiration (R_e) \pm uncertainty: Girdled (p-value = 0.01, Adjusted $R^2 = 0.45$), control (p-value: n.s.) and D) Average growing season soil respiration (R_s) \pm plot-level standard error, Girdled (p-value: n.s.), Control (p-value: n.s). The derivation of C fluxes and their uncertainty is detailed in Gough et al. 2021.

Figure 1.3: Linear regression showing calculated gross primary production (GPP), net ecosystem production (NEP), ecosystem respiration (R_e) and soil respiration (R_s) recovery as a function of C flux resilience from US-UMB and US-UMd flux tower sites.

Figure 1.4: Time-series of net ecosystem production (NEP) in years since disturbance (yr 0 = yr of disturbance, indicated with vertical dashed line) for seven forested sites that experienced either a fire (prescribed or natural) or defoliating insect disturbance. See Appendix Table S1.1 for site information.

Figure 1.5: Comparison of average net ecosystem production (NEP) stability (resistance, resilience, temporal stability) between fire (n = 4) and insect (n = 3) disturbances presented in figure 1.4.

Figure 2.1: Forest Resilience Threshold Experiment (FoRTE) A) plot distribution map, B) experimental design and layout of *in situ* bulk soil respiration (R_s) collars and C) layout of soil sampling locations for *in-vitro* heterotrophic respiration (R_h) estimates.

Figure 2.2: A) Mean aboveground wood biomass \pm SE by disturbance severity and disturbance type prior to girdling in 2018 (whole bar) and remaining ungirdled biomass following disturbance treatment applications in 2019 (solid shade only). B) Median, interquartile range (middle 50% of range) and minimum and maximum vegetative area index (VAI) values by disturbance severity for pre-disturbance (2018, gray shading) and post-disturbance (2019-2021) years. Different letters indicate significant within-year differences among disturbance severities ($\alpha = 0.05$, $F = 2.045$, $p = 0.047$).

Figure 2.3: Mean (± 1 SE) discrete measurements of soil respiration (R_s ; **A, B**), soil temperature (T_s ; **C, D**), and volumetric water content (VWC; **E, F**) by disturbance severity (left panels) and disturbance type (right panels), 2018-2021. Red vertical dashed line delineates pre- and post-disturbance measurement periods.

Figure 2.4: Boxplots displaying median, interquartile range (middle 50% of range) and minimum and maximum soil respiration (R_s) values by disturbance severity for pre-disturbance (2018, gray shading) and post-disturbance (2019-2021) years. Different letters indicate significant within-year differences among disturbance severities ($\alpha = 0.05$, $F = 4.42$, $p < 0.001$).

Figure 2.5: Boxplots displaying median, interquartile range (middle 50% of range) and minimum and maximum soil respiration (R_s) values by “top-down” and “bottom-up” disturbance types for pre-disturbance (2018, gray shading) and post-disturbance (2019-2021) years. Within-year comparisons yielded no significant differences ($\alpha = 0.05$, $F = 0.942$, $p = 0.42$).

Figure 2.6: Post-disturbance (2019-2021) relationship between soil temperature and R_s using a two-parameter exponential model by **A**) disturbance severity (0,45,65,85% gross defoliation) and **B**) by disturbance type (“top-down” and “bottom-up”). Average Q10 values (increase in R_s for

every 10 °C in T_s) by **C**) Disturbance severity ($F = 1.847$, $p = 0.21$) and **D**) disturbance type ($F = 1.343$, $p = 0.27$). Average basal R_s rates (BR) at 10 °C by **E**) Disturbance severity ($F = 4.418$, $p=0.04$, and **F**) Disturbance type ($F = 0.17$, $p = 0.690$).

Figure 2.7: Boxplots displaying median, interquartile range (middle 50% of range) and minimum and maximum soil heterotrophic respiration estimates (R_h) of incubated root-free soils (10 cm depth) averaged across all post-disturbance years (2019-2021) by: **A**) disturbance severity ($\alpha = 0.05$, $F = 4.369$, $p = 0.042$) and **B**) “top-down” and “bottom-up” disturbance type ($\alpha = 0.05$, $F = 6.837$, $p = 0.024$). Different letters indicate significant differences among disturbance severities or disturbance type.

Figure 2.8 Average R_s as a function of fine-root production, 2019-2021 (p -value <0.001 , Adjusted $R^2 = 0.50$). Solid gray line represents linear relationship between R_s and fine-root production in the control and dotted gray line represents linear relationship between R_s and fine-root production in across disturbance severities. Slopes of the two lines are significantly different from each other (T -value = 2.24, p -value = 0.03).

Figure 2.9: **A**) Average R_s resistance and **B**) Average R_h resistance as a function of disturbance severity (% gross defoliation), 2018-2021. Gray line indicates significant linear decline in R_s resistance with increasing disturbance severity between 2019-2021 (p -value: <0.001 , Adjusted $R^2 = 0.93$). No significant relationship between R_h resistance and disturbance severity.

Figure 3.1: Forest Resilience Threshold Experiment (FoRTE) **A**) plot distribution map, **B**) experimental design and layout of all component NPP flux measurements **C**) layout of soil sampling locations for *in-vitro* heterotrophic soil respiration (R_{sh}) estimates.

Figure 3.2: Boxplots displaying median, interquartile range (middle 50% of range) and minimum and maximum **A**) Total NPP (sum of all NPP component fluxes) ($F = 1.147$; p -value =

0.36), and **B**) total R_h (sum of R_{sh} and R_{cwd} averaged across methods) ($F = 0.332$, p -value = 0.91) across disturbance severities (2019-2021). Fluxes are presented as $Mg\ C\ ha^{-1}\ yr^{-1}$.

Figure 3.3: Boxplots displaying median, interquartile range (middle 50% of range) and minimum and maximum **A**) Canopy $ANPP_w$ ($F = 0.622$, $p = 0.71$), **B**) Subcanopy $ANPP_w$ ($F = 7.04$, $p = <0.001$), **C**) $BNPP_w$ ($F = 0.62$, $p = 0.71$), **D**) NPP_{ll} ($s\ F = 2.39$, $p = 0.05$), **E**) NPP_{fwd} ($F = 0.77$, $p = 0.60$), and **F**) NPP_{fr} (p -value = 0.05) across disturbance severities (2019-2021).

Asterisks (*) indicates pair-wise significant differences from the control. All fluxes are presented as $Mg\ C\ ha^{-1}\ yr^{-1}$.

Figure 3.4: Boxplots displaying median, interquartile range (middle 50% of range) and minimum and maximum **A**) R_{cwd} , averaged across 3 methods ($F = 1.4$, p -value = 0.26), and **B**) R_{sh} ($F = 0.35$, p -value = 0.9) averaged across 4 methods and across disturbance severities (2019-2021). Fluxes are presented as $Mg\ C\ ha^{-1}\ yr^{-1}$.

Figure 3.5: Boxplots displaying median, interquartile range (middle 50% of range) and minimum and maximum NEP across disturbance severities (2019-2021) and averaged across methods.

Figure 3.6: NEP averaged across methods as a function of pre-disturbance biomass, 2019-2021. Colored lines represent significant interaction between pre-disturbance biomass and disturbances severity (Adjusted $R^2 = 0.35$, $F = 4.8$, p -value = 0.002).

Figure 4.1: Illustration of hypothesized changes in stand and root-level rhizosphere processes following phloem-disruption and the consequences for stand-scale R_s .

Figure 4.2: ShRRED experiment design. **A**) Four $100m^2$ squared treatment (disturbance) and control plots randomly assigned with at least a 10 m buffer in between plots. **B**) Layout of disturbance plots centered around a > 20 cm DBH canopy oak tree (“focal surviving tree”) with

surrounding subcanopy (> 1.4 m height) and canopy (>8 cm DBH) girdled trees. Colored dots represent various rhizosphere measurements. Control plots contained the same layout as illustrated above, but all trees were left ungirdled.

Figure 4.3: **A)** Time series of mean instantaneous R_s values (\pm S.E.) between the disturbance and control plots (F-value = 0.032, p-value = 0.86), and **B)** log response ratios of R_s in disturbance as compared to control, or “resistance”. Values overlapping with zero indicate complete resistance. Time series shows 4 days before girdling disturbance to 99 days after disturbance. Dashed horizontal red line indicates day of disturbance (May 31, 2022).

Figure 4.4: Boxplots showing median, interquartile range (middle 50% of range) and minimum and maximum root NSC concentration (%) between control trees and girdled trees in the disturbance plots. (F-value = 0.01, p-value = 0.9). Values were averaged across measurement times (44-58 days after girdling).

Figure 4.5: Boxplots showing median, interquartile range (middle 50% of range), minimum and maximum **A)** soil available ammonium (NH_4^+) between control (ungirdled) and disturbance (girdled) plots. (F = 3.76, p = 0.08) and **B)** soil available nitrate (NO_3^-) between control (ungirdled) and disturbance (girdled) plots (F = 0.06, p = 0.8). Values were averaged across measurement times (28-56 days after girdling).

Figure 4.6: Boxplots shows median, interquartile range (middle 50% of range), minimum and maximum fine-root structural and functional traits in control focal trees and surviving focal trees within the disturbance. **A)** Average fine-root surface area (cm^2):volume (cm^3) ratio (F-value = 0.137, p-value = 0.7), **B)** Average fine-root diameter (mm) (F-value = 0.12, p-value = 0.73), **C)** Average fine-root exudation (F-value = 0.17, p-value = 0.68), **D)** coefficient of variance (C_v) for Fine-root SAV (D'AD = 4.65, p - value = 0.03) and **E)** C_v of average fine-root diameter (mm)

(D'AD = 3.66, p-value = 0.05) between the control and the surviving focal trees in the disturbance plots. Values were averaged across measurement times (28-56 days after girdling).

Figure 4.7: Root NSC concentrations in control focal trees and surviving focal trees within the disturbance plots as a function of soil available ammonium (NH_4^+). ($R^2 = 0.51$, $F = 3.79$, p-value = 0.017).

Chapter 1: A multidimensional stability framework enhances interpretation and comparison of carbon cycling response to disturbance

Kayla C. Mathes*¹, Yang Ju², Callie Kleinke³, Callie Oldfield⁴, Gil Bohrer², Ben Bond-Lamberty⁵, Christoph S. Vogel⁶, Kalyn Dorheim⁵, Christopher M. Gough¹

¹Department of Biology, Virginia Commonwealth University

²Department of Civil, Environmental and Geodetic Engineering, Ohio State University

³Department of Chemical and Biomedical Engineering, Ohio State University

⁴Department of Plant Biology, University of Georgia Franklin College of Arts and Sciences

⁵Joint Global Change Research Institute, Pacific Northwest National Laboratory

⁶University of Michigan Biological Station, Pellston

Corresponding author: matheskc@vcu.edu

Published in *Ecosphere* (2021)

DOI: <https://doi.org/10.1002/ecs2.3800>

Abstract

The concept of stability is central to the study and sustainability of vital ecosystem goods and services as disturbances increase globally. While ecosystem ecologists, including carbon (C) cycling scientists, have long-considered multiple dimensions of disturbance response, our discipline lacks an agreed-upon analytical framework for characterizing multidimensional stability. Here, we advocate for the broader adoption of a standardized and normalized multidimensional stability framework for analyzing disturbance response. This framework includes four dimensions of stability: the degree of initial change in C fluxes (i.e., *resistance*); rate (i.e., *resilience*) and variability (i.e., *temporal stability*) of return to pre-disturbance C fluxes; and the extent of return to pre-disturbance C fluxes (i.e., *recovery*). Using this framework, we highlight findings not readily seen from analysis of absolute fluxes, including: trade-offs between initial and long-term C flux responses to disturbance; different overall stability profiles among fluxes; and, using a pilot dataset, similar relative stability of net primary production following fire and insect disturbances. We conclude that ecosystem ecologists' embrace of a unifying multidimensional stability framework as a complement to approaches focused on absolute C fluxes could advance global change research by aiding in the novel interpretation, comprehensive synthesis, and improved forecasting of ecosystems' response to an increasing array of disturbances.

Keywords: carbon, disturbance, ecosystem ecology, forests, resilience, resistance, stability, synthesis.

Section 1: Introduction

Quantifying ecosystems' functional response to disturbance is a long-standing focus of ecologists that has become more crucial in this era of unprecedented global change (Hicke et al. 2012, Cohen et al. 2016, Sommerfeld et al. 2018). Ecologists have long considered how disturbance affects ecosystem functions such as primary production, nutrient and water cycling, and carbon fluxes, recognizing both the multidimensional behavior of disturbance response and varying degrees of stability among ecosystems (Holling 1973). For example, 20th century theorists hypothesized a pattern of primary production decline and recovery following succession-resetting disturbance (Odum 1969, Bormann and Likens 1979, Vitousek 1982); empiricists used chronosequences and long-term observations to test this theory, documenting and comparing the stability of primary production following disturbance (Amiro et al. 2010, Hicke et al. 2012, Gough et al. 2013); and modelers used theoretical and empirical information to build, parameterize, and challenge earth-system models' representation of disturbance responses (Cao and Woodward 1998, Dorheim et al. 2021). Following Holling's (1973) definition of resilience as the capacity of ecosystems to withstand and recover from perturbation (Holling 1973), ecosystem ecologists have also characterized the temporal dynamics and degrees of functional change that follow disturbances varying in scale, source, severity and frequency (Turner et al. 1993, Nave et al. 2011, Goulden et al. 2011, Gough et al. 2020).

Despite these advances, ecosystem ecologists, including carbon (C) cycling scientists, have not embraced the theories and analytical tools developed and applied by other disciplines for assessing the stability of ecological properties and processes following disturbance.

Multidimensional stability frameworks (MDSFs) offer a conceptual and analytical basis for

deriving and interpreting the many components of disturbance response, including the rate, magnitude, variability, and direction of compositional and functional change that proceeds disturbance (Box 1.1). These frameworks decompose absolute responses into discrete standardized and normalized components of stability, which can be compared against one another (i.e., to evaluate response trade-offs) and across ecosystems, fluxes and disturbance sources (Harrison 1979, Peterson et al. 1998, Donohue et al. 2016, Kéfi et al. 2019).

Applied broadly by population and community ecologists, MDSFs have been used to assess the multidimensional stability of populations or taxonomic composition following disturbance (Donohue et al. 2016, Kéfi et al. 2019). These studies have led to several new insights, including, ecological and evolutionary trade-offs among short-and long-term disturbance responses (Stuart-Haëntjens et al. 2018, Cabrerizo et al. 2019, Hillebrand and Kunze 2020); differences in stability among disturbance types and spatial scales (Radchuk et al. 2019); the coupling of compositional and biomass change throughout disturbance recovery cycles (Gao et al. 2017); and recognition that –because dimensions of stability may relate to one another – initial changes in populations and communities could foreshadow long-term stability and the degree of full recovery (Hillebrand and Kunze 2020). However, despite the utility and widespread adoption of MDSFs for assessing population and community-level responses to disturbance, a meta-analysis found that none of the 508 studies utilizing these frameworks examined ecosystem-scale functions, including C fluxes, which are routinely characterized by ecosystem ecologists (Hillebrand and Kunze 2020).

In this *Innovative Viewpoint*, we use ecosystem-scale C flux data to illustrate how a normalized, standardized and multidimensional stability framework offers a powerful complementary tool to approaches focused on absolute fluxes for interpreting, comparing, and synthesizing ecosystem functional responses to disturbance. We first show how a multidimensional stability framework developed for and largely applied to populations and communities can be modified to compare how different C fluxes respond to disturbance. Next, we apply this analytical framework to C flux time-series collected after insect or fire disturbance, illustrating how the approach may facilitate future syntheses of disturbance response. We demonstrate how the adoption of this type of framework by C cycling and other ecosystem ecologists could advance our ability to interpret, forecast, and manage for functional stability, particularly as advances in open data provide increasingly long-term, cross-scale C flux observations following disturbances.

Section 2: A multidimensional stability framework for analysis of carbon flux response to disturbance

While several MDSFs have been proposed (Egli et al. 2019, Downing et al. 2020), we highlight that of (Hillebrand et al. 2018) for three reasons. First, it is designed to enable analysis of compositional *and* functional responses to disturbance; this is appealing because compositional (e.g., taxonomic diversity) or structural (e.g., leaf area index, LAI) change may foreshadow or co-vary with C cycling responses to disturbance (Stuart-Haëntjens et al. 2015). Despite this knowledge, the study of compositional changes following disturbance is historically the domain of community ecologists and ecosystem-scale functional responses such as primary production the focus of ecosystem ecologists (Gough et al. 2020). Second, while population and community

properties such as species diversity and richness more commonly decline after disturbance (Armesto and Pickett 1985, Murphy and Romanuk 2014), the analytical approach used here acknowledges that C fluxes may decrease or increase. For example, disturbance may initially increase soil respiration and organic mineralization as legacy detritus stimulates decomposition (Harmon et al. 2011a), while intermediate levels of disturbance may prompt “overyielding” or increased primary production as suppressed vegetation is released from competition (Stuart-Haëntjens et al. 2015). Lastly, the MDSF is well-suited to burgeoning time-series data generated from remote sensing platforms, meteorological flux towers, and on-the-ground inventories. Such open datasets are growing in number, duration, and spatial coverage with the deployment of satellite remote sensing platforms including NASA’s Orbiting Carbon Observatory 2 (OCO-2) (Eldering et al. 2017), meteorological C flux tower networks including AmeriFlux and the National Ecological Observatory Network (NEON) (Keller et al. 2008, Pastorello et al. 2020), and national inventories including the USDA Forest Inventory and Analysis (McRoberts et al. 2005).

An additional strength of the (Hillebrand et al. 2018) framework is its standardization and normalization of stability dimensions, which allows for direct comparisons of disturbance response not readily made using absolute C fluxes. When control and treatment time-series data are paired or observations (without a control) span pre-disturbance through recovery, four stability dimensions can be calculated: *resistance*, *resilience*, *temporal stability* and *recovery* (Figure 1.1). Each dimension is calculated from the log response ratios of C fluxes (e.g., soil respiration) before and after disturbance or between a control and disturbance treatment; such log response ratios improve the normality of distributions and provide uniform contrasts between a

treatment and reference value (Hedges et al. 1999). *Resistance* (r_s), a static variable, captures the initial magnitude and direction of disturbance response, and is calculated from the log response ratio of pre-post or control-treatment C fluxes initially following disturbance. *Resilience* (r_i), a dynamic variable (i.e. changing over time), captures the rate and directionality of change over time following the initial disturbance response and is calculated as the slope of the log response C flux ratio. *Temporal stability* (s_t), also a dynamic variable, is calculated from the residuals of resilience (C flux vs time) slopes, and represents the interannual variability of C fluxes during this period. Finally, *recovery* (r_v) summarizes the degree to which the C fluxes return to or exceed pre-disturbance rates and is a static variable calculated from the log response ratio after the period of resilience. Because the timing of disturbance response may differ among disturbance sources and ecosystems, static variable such as resistance are ideally calculated when initial changes in log response ratios have peaked and recovery estimated once log response ratios no longer change over time (e.g., through change-point analysis, Gough et al. 2021). All dimensions, aside from temporal stability, which can only be positive, can be positive, negative or zero, representing an increase, decrease, or no change, respectively. A conceptual illustration of C flux time-series data and their relationship with multiple dimensions of stability, along with the mathematical derivation of each stability variable is found in Figure 1.1.

Section 3: Applying a multidimensional stability framework to carbon flux datasets

Application #1: Calculating carbon flux stability using experiments with controls

Motivated by the prevalence of ecosystem experiments with controls (Hanson and Walker 2020), our first example compares the multidimensional stability of C fluxes using a paired control-

treatment disturbance manipulation. This approach could be applied to experiments with controls evaluating C flux responses to precipitation change (Rustad and Campbell 2012), temperature stress (Chivers et al. 2009), biomass removal and harvesting (Fakhraei et al. 2020), nutrient additions (Cusack et al. 2011), and elevated CO₂ (Selsted et al. 2012). We use data from the Forest Accelerated Succession Experiment (FASET) (Gough et al. 2013), available through AmeriFlux (Pastorello et al. 2020) and COSORE (COntinuous SOil REspiration; (Bond-Lamberty et al. 2020) open data repositories. The FASET study was implemented in 2008 via the stem girdling of >6,700 trees within a 39 ha meteorological flux tower footprint to assess how a ~40% stem basal area reduction affects forest C cycling (Gough et al. 2013, Stuart-Haëntjens et al. 2015). We compare the multidimensional stability profiles of annual gross primary production (GPP), ecosystem respiration (R_e), net ecosystem production (NEP), and instantaneous soil respiration (R_s), which, prior to normalization, spanned a range of absolute numeric values and possessed different units. Extensive descriptions of the study site, experimental design and C flux methods are detailed in a series of research articles (Nave et al. 2011, Gough et al. 2013; Gough et al. 2021).

We used regression analyses to assess absolute changes in C fluxes following implementation of the FASET treatment (Figure 1.2). We found that 10-yr NEP in the treatment and control forests increased significantly by 1.4 and 0.36 Mg C ha⁻¹yr⁻¹, respectively, following disturbance ($p < 0.01$, $R^2 = 0.53$; $p = 0.02$, $R^2 = 0.36$). In contrast, GPP exhibited no significant decadal change in the treatment or control forest. R_e significantly declined in the treatment forest ($p = 0.01$, $R^2 = 0.45$) but did not change in the control forest. Treatment declines in R_e of 1.51 Mg C ha⁻¹ over 10 years suggests that lower C losses rather than higher C uptake drove increases in NEP. Similar

comparisons of absolute C fluxes feature prominently in the literature and are critical for understanding how disturbances affect C sink-source dynamics (Seidl et al. 2014, Williams et al. 2014), C allocation within ecosystems (Litton et al. 2007), and for the parametrization and benchmarking of earth and ecosystem models (Shiklomanov et al. 2020).

Interpreting the same datasets using an MDSF elucidates three findings less-obvious from our analysis of absolute fluxes. First, while GPP and R_e initially increased following disturbance, and therefore exhibited positive resistance values, NEP decreased, resulting in a negative resistance value (Table 1.1). This contrasting pattern indicates that the initial direction and magnitude of change by NEP and its component fluxes differed (Table 1.1). Second, correlations between some but not all stability dimensions suggest that early responses to disturbance may predict long-term responses or the degree of recovery. For example, resilience, the rate of C flux recovery following disturbance, was positively correlated with recovery, the extent to which fluxes returned to their pre-disturbance values (Figure 1.3, $R^2 = 0.95$, $p = 0.015$). Comparable analyses of absolute fluxes, in the absence of standardized and normalized expressions of stability, may obscure such relationships because of differences among fluxes in units, scales and timing of disturbance response. Lastly, our analysis indicates that the relative temporal stability of fluxes varies by an order of magnitude, a comparison that requires normalization (Table 1.1). This example illustrates how a MDSF powerfully complements absolute flux analyses; absolute flux analyses are essential to predicting the quantitative changes in ecosystem and earth system properties while MDSFs provide new, potentially generalizable, information on the similarities, differences and relationships among fluxes and features of stability.

Application #2: Deriving multidimensional stability values from carbon flux time-series

Our second example uses time-series data without controls to compare the resistance, resilience, and temporal stability of forests affected by two well-studied disturbance sources: fire and insect pests. This example highlights how an MDSF can be applied to long-term datasets that lack controls but include pre-disturbance observations as a reference. For example, multi-decadal open C flux datasets are available for forests disturbed by insects (Finzi et al. 2020) and fire (Kashian et al. 2013). To identify datasets for our example, we conducted a Web of Science search with the following keywords: “Net Ecosystem Product*” AND “insect” and “Net Ecosystem Product*” AND “fire”. The criteria for inclusion were that annual NEP observations span at least one year before and four years after fire or insect disturbance. Our search yielded seven datasets, three documenting NEP after defoliating insect outbreaks and four after either prescribed burns or natural fire disturbances (Table S1.1).

We focus first, again, on absolute NEP values. The time-series convey similar patterns of decline and rebound following fire and insect invasion, while illustrating a wide range in production among study sites (Figure 1.4). For example, pre-disturbance NEP ranged from 49 to 780 g C m⁻² yr⁻¹ among sites, which was generally greater than within site-level temporal variability following disturbance. Insect and fire disturbances were followed by initial declines in NEP during the year of disturbance of up to 386 g C m⁻² yr⁻¹ and 141 g C m⁻² yr⁻¹, respectively (Figure 1.4).

When an MDSF is applied, we find that, despite large site differences in absolute NEP values, forests responded similarly to insect and fire disturbance. Specifically, mean differences between insect and fire *resistance*, *resilience*, and *temporal stability* were not statistically significant (Figure 1.5). In relative terms, both disturbances were followed by a similar initial drop in NEP or displayed a similar level of negative *resistance*, had overlapping rates of rebounding NEP or positive *resilience*, and exhibited comparable levels of interannual NEP variation during the period of resilience or *temporal stability* (Figure 1.5). These similarities were not obvious from our unstandardized, non-normalized comparison of NEP. While the NEP stability profiles were similar for the two disturbances, forests affected by fire displayed high variation within each stability dimension, while forests responded more uniformly to insect disturbance. We did not calculate *recovery* because, like many ecological studies of disturbance, observations did not extend to the period of recovery, when the ecosystems have attained a newly stable post-disturbance level of functioning.

Here, analysis of absolute NEP and relative responses viewed through the lens of an MDSF supplies complementary information, highlighting shared stability among disturbance types and sites, despite large differences in net C balance. While our sample size is small relative to meta-analyses summarizing mature areas of scientific investigation (Ainsworth et al. 2002, Nave et al. 2010), our example highlights the potential for syntheses of stability once a critical mass of C flux time-series overlapping with disturbance events becomes available through ecological networks. Similar analyses of absolute C fluxes have yielded important insights, demonstrating how quantitatively variable the net C balance of ecosystems is among sites and disturbances over time (Amiro et al. 2010, Hicke et al. 2012). However, given the wide range in magnitude of NEP

values, duration of measurement, and temporal variation among sites, comparisons of stability between common disturbances, such as fire and insect pests, are challenging without a standardized and normalized analytical framework.

Conclusions and recommendations

We conclude that the broader adoption of an agreed upon multidimensional stability framework by C cycling scientists could greatly enhance understanding of disturbance responses by advancing standardized terminology, enabling new comparisons, supporting ecological forecasting, and providing a template for quantitative syntheses. Just as basins of attraction were conceived as a theoretical and analytical model with which to better conceptualize, assess, and compare state changes (Folke et al. 2004), the utilization of MDSFs by ecosystem ecologists will complement C flux and other ecosystem-scale functional analyses focused on absolute responses. Moreover, an MDSF that applies to multiple scales of biological organization—from organisms to ecosystems—will enable new discoveries only possible at the intersection of ecological disciplines (Table 1.2). Such interdisciplinary and integrative knowledge is essential for assessing coupled structural and functional mechanisms driving responses to disturbance at multiple scales, and could provide fundamental insights relevant to ecosystem management focused on sustaining resources under changing disturbance regimes (Albrich et al. 2018). In addition, greater understanding of how initial (i.e., resistance) and long-term (i.e., recovery) measures of stability relate to one another could constrain ecological forecasts of disturbance response and improve mechanistic representation of disturbance in ecosystem and Earth System

Models (ESMs) (Deser et al. 2020) (Fisher and Koven 2020), which often fail to simulate observed disturbance responses (Bond-Lamberty et al. 2015).

Rather than our *Innovative Viewpoint* serving as a static commentary and tutorial on MDSFs, significant advances in stability research will require further consideration and contributions by multiple ecological disciplines along with the expertise and cooperation of data providers, modelers, managers, and technologists. For example, synthesizing stability across scales of biological organization is increasingly possible with data from open science networks such as FLUXNET, NEON, and Europe's Integrated Carbon Observation System (ICOS), which are accumulating years to decades of data through complete disturbance response cycles. However, such cross-scale syntheses necessitate broad analytical and ecological expertise. In addition, important questions for MDSF users and developers remain, including: What other dimensions of stability could or should be routinely characterized? What novel ecological and environmental questions will benefit from the broader, integrated application of MDSFs? How can MDSFs be revised to better accommodate temporal variability and the range of functional response to disturbance? Continuing to advance MDSFs to transform understanding of stability in an era of rapid global change necessitates greater integration of ecological disciplines and, moving forward, will require ecologists studying different levels of organization to intentionally intersect, drawing from equally rich, but often separate, areas of knowledge and theory.

Acknowledgments: Funding for AmeriFlux core sites US-UMB and US-UMd was provided by the U.S. Department of Energy's Office of Science. We thank the University of Michigan Biological Station for hosting our work.

Data Availability Statement: Data and code are available via:

<https://doi.org/10.6084/m9.figshare.14238008.v4>. Data were analyzed using R version 4.0.1 (2020-06-06). Meteorological and carbon flux data for US-UMB (Gough et al. 1999) and US-Umd (Gough et al. 2016) are available through AmeriFlux: <https://ameriflux.lbl.gov>; soil respiration data are available through COntinuous SOil REspiration (COSORE) open data repository (Bond-Lamberty et al. 2020): <https://doi.org/10.1111/gcb.15353>.

Literature Cited

- Ainsworth, E. A., P. A. Davey, C. J. Bernacchi, O. C. Dermody, E. A. Heaton, D. J. Moore, P. B. Morgan, S. L. Naidu, H. S. Y. Ra, X. G. Zhu, P. S. Curtis, and S. P. Long. (2002). A meta-analysis of elevated [CO₂] effects on soybean (*Glycine max*) physiology, growth and yield. *Global Change Biology* 8:695–709.
- Albrich, K., W. Rammer, D. Thom, and R. Seidl. (2018). Trade-offs between temporal stability and level of forest ecosystem services provisioning under climate change. *Ecological Applications* 28:1884–1896.
- Amiro, B. D., A. G. Barr, J. G. Barr, T. A. Black, R. Bracho, M. Brown, J. Chen, K. L. Clark, K. J. Davis, A. R. Desai, S. Dore, V. Engel, J. D. Fuentes, A. H. Goldstein, M. L. Goulden, T. E. Kolb, M. B. Lavigne, B. E. Law, H. A. Margolis, T. Martin, J. H. McCaughey, L. Misson, M. Montes-Helu, A. Noormets, J. T. Randerson, G. Starr, and J. Xiao. (2010). Ecosystem carbon dioxide fluxes after disturbance in forests of North America. *Journal of Geophysical Research: Biogeosciences*, 115. doi : 10.1029/2010JG001390
- Armesto, J. J., and S. T. A. Pickett. (1985). Experiments on disturbance in old-field plant

communities: impact on species richness and abundance. *Ecology* 66:230–240.

Bond-Lamberty, B., D. S. Christianson, A. Malhotra, S. C. Pennington, D. Sihi, A.

AghaKouchak, H. Anjileli, M. Altaf Arain, J. J. Armesto, S. Ashraf, M. Ataka, D.

Baldocchi, T. Andrew Black, N. Buchmann, M. S. Carbone, S. C. Chang, P. Crill, P. S.

Curtis, E. A. Davidson, A. R. Desai, J. E. Drake, T. S. El-Madany, M. Gavazzi, C. M.

Görres, C. M. Gough, M. Goulden, J. Gregg, O. Gutiérrez del Arroyo, J. S. He, T. Hirano,

A. Hoppo, H. Hughes, J. Järveoja, R. Jassal, J. Jian, H. Kan, J. Kaye, Y. Kominami, N.

Liang, D. Lipson, C. A. Macdonald, K. Maseyk, K. Mathes, M. Mauritz, M. A. Mayes, S.

McNulty, G. Miao, M. Migliavacca, S. Miller, C. F. Miniati, J. G. Niets, M. B. Nilsson, A.

Noormets, H. Norouzi, C. S. O’Connell, B. Osborne, C. Oyonarte, Z. Pang, M. Peichl, E.

Pendall, J. F. Perez-Quezada, C. L. Phillips, R. P. Phillips, J. W. Raich, A. A. Renchon, N.

K. Ruehr, E. P. Sánchez-Cañete, M. Saunders, K. E. Savage, M. Schrumppf, R. L. Scott, U.

Seibt, W. L. Silver, W. Sun, D. Szutu, K. Takagi, M. Takagi, M. Teramoto, M. G. Tjoelker,

S. Trumbore, M. Ueyama, R. Vargas, R. K. Varner, J. Verfaillie, C. Vogel, J. Wang, G.

Winston, T. E. Wood, J. Wu, T. Wutzler, J. Zeng, T. Zha, Q. Zhang, and J. Zou. (2020).

COSORE: A community database for continuous soil respiration and other soil-atmosphere greenhouse gas flux data. *Global Change Biology*, 26:7268–7283.

Bond-Lamberty, B., J. P. Fisk, J. A. Holm, V. Bailey, G. Bohrer, and C. M. Gough. (2015).

Moderate forest disturbance as a stringent test for gap and big-leaf models. *Biogeosciences* 12:513–526.

Bormann, F. H., and G. E. Likens. (1979). Catastrophic Disturbance Steady State in Northern

Hardwood Forests A new look at the role of disturbance in the Northern Hardwood forests.

American Scientist, 67:660–669.

- Buma, B., C. D. Brown, D. C. Donato, J. B. Fontaine, and J. F. Johnstone. (2013). The impacts of changing disturbance regimes on serotinous plant populations and communities. *BioScience*, 63:866–876.
- Cabrerizo, M. J., J. M. Medina-Sánchez, M. Villar-Argaiz, and P. Carrillo. (2019). Interplay between resistance and resilience governs the stability of a freshwater microbial food web under multiple stressors. *Science of the Total Environment* 691:908–918.
- Cao, M., and F. I. Woodward. (1998). Dynamic responses of terrestrial ecosystem carbon cycling to global climate change. *Nature*, 393:249–252.
- Chivers, M. R., M. R. Turetsky, J. M. Waddington, J. W. Harden, and A. D. McGuire. (2009). Effects of experimental water table and temperature manipulations on ecosystem CO₂ fluxes in an Alaskan rich fen. *Ecosystems*, 12:1329–1342.
- Clark, K. L., H. J. Renninger, N. Skowronski, M. Gallagher, and K. V. R. Schäfer. (2018). Decadal-scale reduction in forest net ecosystem production following insect defoliation contrasts with short-term impacts of prescribed fires. *Forests*, 9:1–25.
- Clark, K. L., N. Skowronski, H. Renninger, and R. Scheller. (2014). Climate change and fire management in the mid-Atlantic region. *Forest Ecology and Management*, 327:306–315.
- Cohen, W. B., Z. Yang, S. V. Stehman, T. A. Schroeder, D. M. Bell, J. G. Masek, C. Huang, and G. W. Meigs. (2016). Forest disturbance across the conterminous United States from 1985-2012: The emerging dominance of forest decline. *Forest Ecology and Management* 360:242–252.
- Cusack, D. F., W. L. Silver, M. S. Torn, and W. H. McDowell. (2011). Effects of nitrogen additions on above- and belowground carbon dynamics in two tropical forests. *Biogeochemistry*, 104:203–225.

- Deser, C., F. Lehner, K. B. Rodgers, T. Ault, T. L. Delworth, P. N. DiNezio, A. Fiore, C. Frankignoul, J. C. Fyfe, D. E. Horton, J. E. Kay, R. Knutti, N. S. Lovenduski, J. Marotzke, K. A. McKinnon, S. Minobe, J. Randerson, J. A. Screen, I. R. Simpson, and M. Ting. (2020). Insights from Earth system model initial-condition large ensembles and future prospects. *Nature Climate Change*, 10:277–286.
- Domínguez-García, V., V. Dakos, and S. Kéfi. (2019). Unveiling dimensions of stability in complex ecological networks. *Proceedings of the National Academy of Sciences of the United States of America*, 116:25714–25720.
- Donohue, I., H. Hillebrand, J. M. Montoya, O. L. Petchey, S. L. Pimm, M. S. Fowler, K. Healy, A. L. Jackson, M. Lurgi, D. McClean, N. E. O’Connor, E. J. O’Gorman, and Q. Yang. (2016). Navigating the complexity of ecological stability. *Ecology letters*, 19:1172–1185.
- Donohue, I., O. L. Petchey, J. M. Montoya, A. L. Jackson, L. McNally, M. Viana, K. Healy, M. Lurgi, N. E. O’Connor, and M. C. Emmerson. (2013). On the dimensionality of ecological stability. *Ecology Letters*, 16:421–429.
- Dorheim, K., S. J. Smith, and B. Bond-Lamberty. (2021). HIRM v1.0: A hybrid impulse response model for climate modeling and uncertainty analyses. *Geoscientific Model Development*, 14:365–375.
- Downing, A. L., C. Jackson, C. Plunkett, J. Ackerman Lockhart, S. M. Schlater, and M. A. Leibold. (2020). Temporal stability vs. community matrix measures of stability and the role of weak interactions. *Ecology Letters*, 23:1468–1478.
- Egli, L., H. Weise, V. Radchuk, R. Seppelt, and V. Grimm. (2019). Exploring resilience with agent-based models: State of the art, knowledge gaps and recommendations for coping

with multidimensionality. *Ecological Complexity* 40. doi:

10.1016/j.ecocom.2018.06.008

Eldering, A., P. O. Wennberg, D. Crisp, D. S. Schimel, M. R. Gunson, A. Chatterjee, J. Liu, F.

M. Schwandner, Y. Sun, C. W. O'Dell, C. Frankenberg, T. Taylor, B. Fisher, G. B.

Osterman, D. Wunch, J. Hakkarainen, J. Tamminen, and B. Weir. (2017). The Orbiting

Carbon Observatory-2 early science investigations of regional carbon dioxide fluxes.

Science 358. doi: 10.1126/science.aam5745

Fakhraei, H., T. J. Fahey, and C. T. Driscoll. (2020). The Biogeochemical Response of Nitrate

and Potassium to Landscape Disturbance in Watersheds of the Hubbard Brook

Experimental Forest, New Hampshire, USA. Pages 537–563 in D. F. Levia, D. E. Carlyle-

Moses, S. Lida, B. Michalzik, K. Nanko, editors. Forest-Water Interactions. Ecological

Studies (Analysis and Synthesis). Springer Nature Switzerland, Cham, Switzerland.

Fellows, A. W., G. N. Flerchinger, K. A. Lohse, and M. S. Seyfried. (2018). Rapid Recovery of

Gross Production and Respiration in a Mesic Mountain Big Sagebrush Ecosystem

Following Prescribed Fire. *Ecosystems*, 21:1283–1294.

Finzi, A. C., M. A. Giasson, A. A. Barker Plotkin, J. D. Aber, E. R. Boose, E. A. Davidson, M.

C. Dietze, A. M. Ellison, S. D. Frey, E. Goldman, T. F. Keenan, J. M. Melillo, J. W.

Munger, K. J. Nadelhoffer, S. V. Ollinger, D. A. Orwig, N. Pederson, A. D. Richardson,

K. Savage, J. Tang, J. R. Thompson, C. A. Williams, S. C. Wofsy, Z. Zhou, and D. R.

Foster. (2020). Carbon budget of the Harvard Forest Long-Term Ecological Research

site: pattern, process, and response to global change. *Ecological Monographs*, 90.

doi: 10.1002/ecm.1423

Fisher, R. A., and C. D. Koven. (2020). Perspectives on the Future of Land Surface Models and

- the Challenges of Representing Complex Terrestrial Systems. *Journal of Advances in Modeling Earth Systems* 12. doi: 10.1029/2018MS001453
- Folke, C., S. Carpenter, B. Walker, M. Scheffer, T. Elmqvist, L. Gunderson, and C. S. Holling. (2004). Regime shifts, resilience, and biodiversity in ecosystem management. *Annual Review of Ecology, Evolution, and Systematics*, 35:557–581.
- Fraterrigo, J. M., and J. A. Rusak. (2008). Disturbance-driven changes in the variability of ecological patterns and processes. *Ecology Letters*, 11:756–770.
- Führer, E. (2000). Forest functions, ecosystem stability and management. *Forest Ecology and Management*, 132:29–38.
- Gao, D., X. Wang, S. Fu, and J. Zhao. (2017). Legume plants enhance the resistance of soil to ecosystem disturbance. *Frontiers in Plant Science*, 8. doi: 10.3389/fpls.2017.01295
- Gough, C.M., G. Bohrer, B. S. Hardiman, L. E. Nave, C.S. Vogel, J. Atkins, B. Bond-Lamberty, R. T. Fahey, A. T. Fotis, M. S. Grigri, L. T. Haber, Y. Ju, C. L. Kleinke, K. C. Mathes, K. J. Nadelhoffer, E. Stuart-Haëntjens, P. S. Curtis. (2021). Disturbance-accelerated succession increases the production of a temperate forest. *Ecological Applications* doi: 10.1002/eap.2417
- Gough, C. M., J. W. Atkins, B. Bond-Lamberty, E. A. Agee, K. R. Dorheim, R. T. Fahey, M. S. Grigri, L. T. Haber, K. C. Mathes, S. C. Pennington, A. N. Shiklomanov, and J. M. Tallant. (2020). Forest Structural Complexity and Biomass Predict First-Year Carbon Cycling Responses to Disturbance. *Ecosystems* 24: 699-712.
- Gough, C. M., G. Bohrer, and P. S. Curtis. 2016. AmeriFlux US-UMd UMBS Disturbance, Dataset, <https://ameriflux.lbl.gov/>.
- Gough, C. M., B. S. Hardiman, L. E. Nave, G. Bohrer, K. D. Maurer, C. S. Vogel, K. J.

- Nadelhoffer, and P. S. Curtis. (2013). Sustained carbon uptake and storage following moderate disturbance in a Great Lakes forest. *Ecological Applications* 23:1202–1215.
- Gough, C. M., G. Bohrer, and P. S. Curtis. (1999). AmeriFlux US-UMB Univ. of Mich. Biological Station, Dataset, <https://ameriflux.lbl.gov/>.
- Goulden, M. L., A. M. S. Mcmillan, G. C. Winston, A. V. Rocha, K. L. Manies, J. W. Harden, and B. P. Bond-Lamberty. (2011). Patterns of NPP, GPP, respiration, and NEP during boreal forest succession. *Global Change Biology*, 17:855–871.
- Hanson, P. J., and A. P. Walker. (2020). Advancing global change biology through experimental manipulations: Where have we been and where might we go? *Global Change Biology* 26:287–299.
- Harmon, M. E., B. Bond-Lamberty, J. Tang, and R. Vargas. (2011). Heterotrophic respiration in disturbed forests: A review with examples from North America. *Journal of Geophysical Research: Biogeosciences* 116. doi: 10.1029/2010JG001495.
- Harrison, G. W. (1979). Stability under Environmental Stress: Resistance, Resilience, Persistence, and Variability. *The American Naturalist* 113:659–669.
- Hedges, L. V., J. Gurevitch, and P. S. Curtis. (1999). The Meta-Analysis of Response Ratios in Experimental Ecology. *Ecology* 80:1150–1156.
- Hicke, J. A., C. D. Allen, A. R. Desai, M. C. Dietze, R. J. Hall, E. H. T. Hogg, D. M. Kashian, D. Moore, K. F. Raffa, R. N. Sturrock, and J. Vogelmann. (2012). Effects of biotic disturbances on forest carbon cycling in the United States and Canada. *Global Change Biology* 18:7–34.
- Hillebrand, H., and C. Kunze. (2020). Meta-analysis on pulse disturbances reveals differences in functional and compositional recovery across ecosystems. *Ecology Letters* 23:575–585.

- Hillebrand, H., S. Langenheder, K. Lebret, E. Lindström, Ö. Östman, and M. Striebel. (2018). Decomposing multiple dimensions of stability in global change experiments. *Ecology Letters* 21:21–30.
- Holling, C. S. (1973). Resilience and Stability of Ecological Systems. *Annual Review of Ecology, Evolution, and Systematics* 4:1–23.
- Johnstone, J. F., C. D. Allen, J. F. Franklin, L. E. Frelich, B. J. Harvey, P. E. Higuera, M. C. Mack, R. K. Meentemeyer, M. R. Metz, G. L. W. Perry, T. Schoennagel, and M. G. Turner. (2016). Changing disturbance regimes, ecological memory, and forest resilience. *Frontiers in Ecology and the Environment* 14:369–378.
- Kashian, D. M., W. H. Romme, D. B. Tinker, M. G. Turner, and M. G. Ryan. (2013). Postfire changes in forest carbon storage over a 300-year chronosequence of *Pinus contorta*-dominated forests. *Ecological Monographs* 83:49–66.
- Kéfi, S., V. Domínguez-García, I. Donohue, C. Fontaine, E. Thébault, and V. Dakos. (2019). Advancing our understanding of ecological stability. *Ecology Letters* 22:1349–1356.
- Keller, M., D. S. Schimel, W. W. Hargrove, and F. M. Hoffman. (2008). A continental strategy for the National Ecological Observatory Network. *Frontiers in Ecology and the Environment* 6:282–284.
- Litton, C. M., J. W. Raich, and M. G. Ryan. (2007). Carbon allocation in forest ecosystems. *Global Change Biology* 13:2089–2109.
- Lu, W., J. Xiao, X. Cui, F. Xu, G. Lin, and G. Lin. (2019). Insect outbreaks have transient effects on carbon fluxes and vegetative growth but longer-term impacts on reproductive growth in a mangrove forest. *Agricultural and Forest Meteorology* 279.
- McRoberts, R. E., W. A. Bechtold, P. L. Patterson, C. T. Scott, and G. A. Reams. (2005). The

- enhanced Forest Inventory and Analysis program of the USDA Forest Service: Historical perspective and announcement of statistical documentation. *Journal of Forestry* 103:304–308.
- Murphy, G. E. P., and T. N. Romanuk. (2014). A meta-analysis of declines in local species richness from human disturbances. *Ecology and Evolution* 4:91–103.
- Nave, L. E., C. M. Gough, K. D. Maurer, G. Bohrer, B. S. Hardiman, J. Le Moine, A. B. Munoz, K. J. Nadelhoffer, J. P. Sparks, B. D. Strahm, C. S. Vogel, and P. S. Curtis. (2011). Disturbance and the resilience of coupled carbon and nitrogen cycling in a north temperate forest. *Journal of Geophysical Research: Biogeosciences* 116. doi: 10.1029/2011JG001758
- Nave, L. E., E. D. Vance, C. W. Swanston, and P. S. Curtis. (2010). Harvest impacts on soil carbon storage in temperate forests. *Forest Ecology and Management* 259:857–866.
- Odum, E. P. 1969. The strategy of ecosystem development. *Science* 164:262–270.
- Pastorello, G., C. Trotta, E. Canfora, H. Chu, D. Christianson, Y. W. Cheah, C. Poindexter, J. Chen, A. Elbashandy, M. Humphrey, P. Isaac, et al. (2020). The FLUXNET2015 dataset and the ONEFlux processing pipeline for eddy covariance data. *Scientific data* 7. doi: 10.1038/s41597-020-0534-3
- Peterson, G. D., C. R. Allen, C. S. Holling, and G. Peterson. (1998). Ecological Resilience, Biodiversity, and Scale. *Ecosystems* 1:6-18.
- Radchuk, V., F. De Laender, J. S. Cabral, I. Boulangeat, M. Crawford, F. Bohn, J. De Raedt, C. Scherer, J. C. Svenning, K. Thonicke, F. M. Schurr, V. Grimm, and S. Kramer-Schadt. (2019). The dimensionality of stability depends on disturbance type. *Ecology Letters* 22:674–684.
- Rustad, L. E., and J. L. Campbell. (2012). A novel ice storm manipulation experiment in a

- northern hardwood forest. *Canadian Journal of Forest Research* 42:1810–1818.
- Seidl, R., M. J. Schelhaas, W. Rammer, and P. J. Verkerk. (2014). Increasing forest disturbances in Europe and their impact on carbon storage. *Nature Climate Change* 4:806–810.
- Selsted, M. B., L. van der Linden, A. Ibrom, A. Michelsen, K. S. Larsen, J. K. Pedersen, T. N. Mikkelsen, K. Pilegaard, C. Beier, and P. Ambus. (2012). Soil respiration is stimulated by elevated CO₂ and reduced by summer drought: Three years of measurements in a multifactor ecosystem manipulation experiment in a temperate heathland (CLIMAITE). *Global Change Biology* 18:1216–1230.
- Shiklomanov, A. N., B. Bond-Lamberty, J. W. Atkins, and C. M. Gough. (2020). Structure and parameter uncertainty in centennial projections of forest community structure and carbon cycling. *Global Change Biology* 26:6080–6096.
- Sommerfeld, A., C. Senf, B. Buma, A. W. D'Amato, T. Després, I. Díaz-Hormazábal, S. Fraver, L. E. Frelich, Á. G. Gutiérrez, S. J. Hart, B. J. Harvey, H. S. He, T. Hlásny, A. Holz, T. Kitzberger, D. Kulakowski, D. Lindenmayer, A. S. Mori, J. Müller, J. Paritsis, G. L. W. Perry, S. L. Stephens, M. Svoboda, M. G. Turner, T. T. Veblen, and R. Seidl. (2018). Patterns and drivers of recent disturbances across the temperate forest biome. *Nature Communications* 9. doi: 10.1038/s41467-018-06788-9
- Stuart-Haëntjens, E., H. J. De Boeck, N. P. Lemoine, P. Mänd, G. Kröel-Dulay, I. K. Schmidt, A. Jentsch, A. Stampfli, W. R. L. Anderegg, M. Bahn, J. Kreyling, T. Wohlgemuth, F. Lloret, A. T. Classen, C. M. Gough, and M. D. Smith. (2018). Mean annual precipitation predicts primary production resistance and resilience to extreme drought. *Science of the Total Environment* 636:360–366.
- Stuart-Haëntjens, E. J., P. S. Curtis, R. T. Fahey, C. S. Vogel, and C. M. Gough. (2015). Net

primary production of a temperate deciduous forest exhibits a threshold response to increasing disturbance severity. *Ecology* 96:2478–2487.

Sun, Q., W. S. Meyer, G. R. Koerber, and P. Marschner. (2020). Rapid recovery of net ecosystem production in a semi-arid woodland after a wildfire. *Agricultural and Forest Meteorology*, 291.

Turner, M. G., W. H. Romme, R. H. Gardner, R. V. O'Neill, and T. K. Kratz. (1993). A revised concept of landscape equilibrium: Disturbance and stability on scaled landscapes. *Landscape Ecology* 8:213–227.

Vitousek, P. (1982). Nutrient cycling and nutrient use efficiency. *American Naturalist* 119:553–572.

Williams, C. A., G. J. Collatz, J. Masek, C. Huang, and S. N. Goward. (2014). Impacts of disturbance history on forest carbon stocks and fluxes: Merging satellite disturbance mapping with forest inventory data in a carbon cycle model framework. *Remote Sensing of Environment*, 151:57–71.

Tables and Figures

Table 1.1: Multidimensional stability metrics for UMBS gross primary production (GPP), ecosystem respiration (R_e), soil respiration (R_s) and net ecosystem production (NEP) from the log response ratios of treatment and control estimates (Figure 1.1). R_s resistance could not be calculated because data were not available the year following disturbance. To account for pre-treatment site differences, the response ratios of control and treatment C fluxes were normalized to pre-disturbance values.

C flux	Resistance (r_s)	Resilience (r_l)	Temporal stability (s_t)	Recovery (r_v)
GPP	0.039 (± 0.00002)	-0.011 (±0.002)	19.1 (±1.65)	-0.073 (±0.0025)
NEP	-0.128 (±0.01)	0.057 (±0.005)	2.3 (±0.25)	0.367 (±0.023)
R_e	0.073 (±0.001)	-0.027 (±0.003)	9.3 (±0.6)	-0.218 (±0.0065)
R_s	NA	0.015 (±0.013)	8.1 (±1.0)	0.000 (±0.1)

Table 1.2: Critical knowledge gaps in ecology that could benefit from a multidimensional

stability analytical framework.

Knowledge gaps	Reference
• Do plant community composition and structure correlate with functional stability?	(Fraterrigo and Rusak 2008, Johnstone et al. 2016)
• How does the stability of ecosystem functions, such as primary production and nitrogen cycling, feedback to alter compositional and structural stability?	(Nave et al. 2011, Gough et al. 2020)
• Which dimensions of stability are correlated with one another and are therefore consistent trade-offs among stability dimensions?	(Radchuk et al. 2019, Domínguez-García et al. 2019)
• How can management cultivate ecosystems with more robust multidimensional stability profiles in an era of rapid global change?	(Führer 2000, Albrich et al. 2018, Egli et al. 2019)
• How does evolution shape functional stability across biomes?	(Buma et al. 2013, Stuart-Haëntjens et al. 2018)

Box 1. Glossary of terms

Deconstructing “multidimensional stability framework” (MDSF)

Multidimensional: Necessarily characterized by multiple aspects or response behaviors, e.g., with respect to functional change following disturbance.

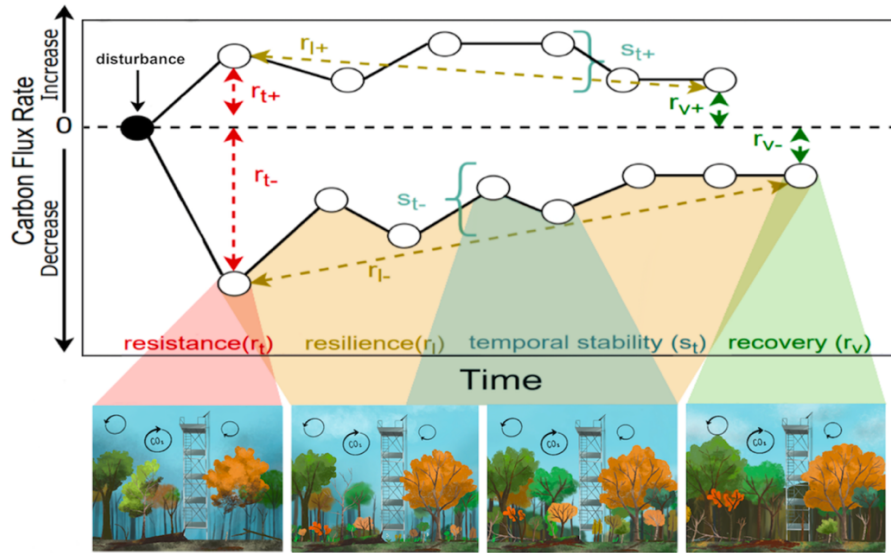
Stability: The magnitude, direction, and rate of structural or functional change following disturbance(s).

Framework: Here, a conceptual foundation *and* analytical approach for assessing structural and functional responses to disturbance.

Other terms

Structure: Physical arrangement, quantity and composition of vegetation in an ecosystem. Examples include leaf area index.

Function: Physical, chemical and biological processes that move energy and material through ecosystem to sustain life. Net primary production, nutrient and water cycling are examples.



Dimension	Equation	Definition
<i>resistance</i> (r_t)	$r_t = \ln \left(\frac{F_{disturb.}}{F_{control}} \right)$	Magnitude of initial response
<i>resilience</i> (r_i)	$\ln \left(\frac{F_{disturb.}}{F_{control}} \right) = i + r_i * t$	Rate of return to pre-disturbance function
<i>temporal stability</i> (s_t)	$s_t = \left(\frac{1}{SE\ of\ resid} \right)$	Variation around resilience slope
<i>recovery</i> (r_v)	$r_v = \ln \left(\frac{F_{disturb.}}{F_{control}} \right)$	Degree of return to pre-disturbance

Figure 1.1: A multidimensional stability framework (MDSF) with four distinct dimensions of stability adopted from Hillebrand et al. 2018 and revised to capture dynamic C cycling responses to disturbance. Conceptual figure shows two example C flux stability profiles following disturbance, one increasing (presented with positive stability dimension labels, e.g. r_{s+}) and one decreasing (presented with negative stability dimension labels, e.g. r_{s-}) immediately following disturbance. Illustration panels provide snapshots of the various stages of disturbance response corresponding with different stability dimensions. Table details mathematical and written definitions of each dimension. “ F ” represents the C flux rate from the y-axis, “ t ” represents time from the x-axis and “ i ” represents the intercept of the resilience regression line.

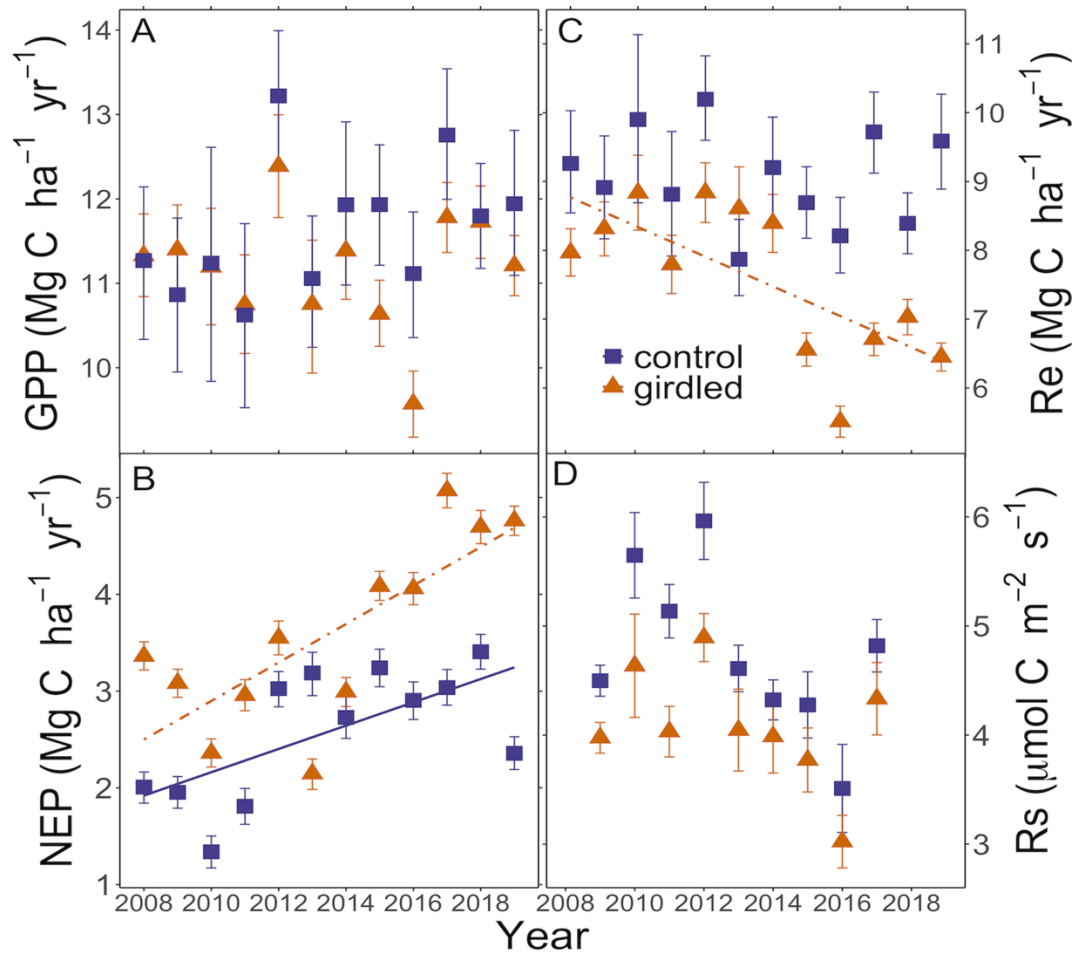


Figure 1.2: Time-series (2008-2019) of disturbance treatment via stem girdling (US-UMd) and control (US-UMB) forests analyzed with simple linear regression. A) Annual gross primary production (GPP) \pm uncertainty: Girdled (p-value: n.s.), Control (p-value: n.s) B) Annual net ecosystem production (NEP) \pm uncertainty: Girdled (p-value < 0.01 , Adjusted $R^2 = 0.53$), Control (p = 0.02, Adjusted $R^2 = 0.36$) C) Annual ecosystem respiration (R_e) \pm uncertainty: Girdled (p-value = 0.01, Adjusted $R^2 = 0.45$), control (p-value: n.s.) and D) Average growing season soil respiration (R_s) \pm plot-level standard error, Girdled (p-value: n.s.), Control (p-value: n.s). The derivation of C fluxes and their uncertainty is detailed in Gough et al. 2021.

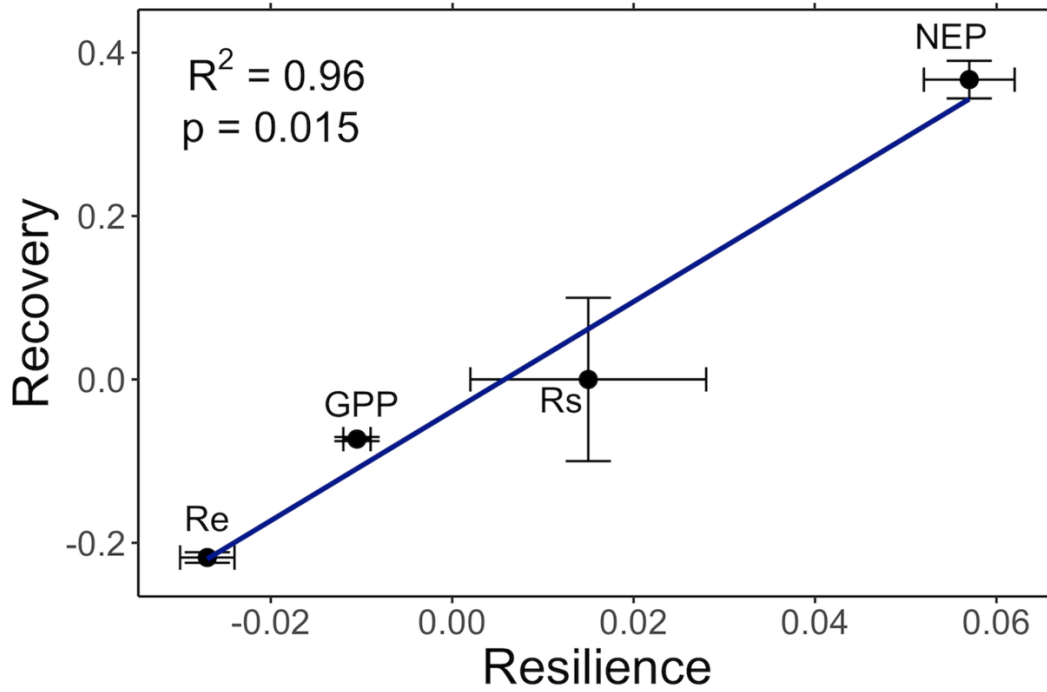


Figure 1.3: Linear regression showing calculated gross primary production (GPP), net ecosystem production (NEP), ecosystem respiration (R_e) and soil respiration (R_s) recovery as a function of C flux resilience from US-UMB and US-UMd flux tower sites.

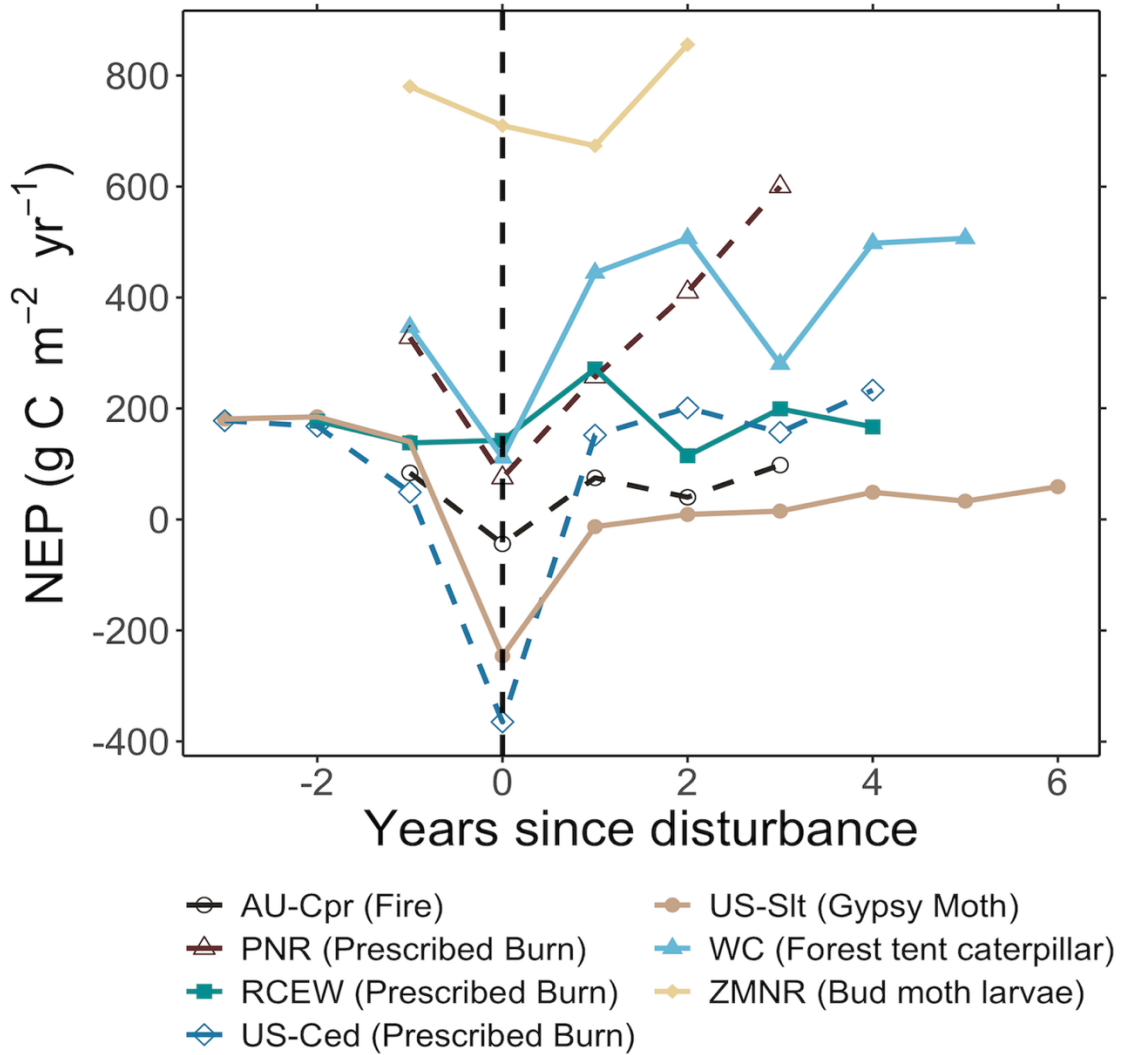


Figure 1.4: Time-series of net ecosystem production (NEP) in years since disturbance (yr 0 = yr of disturbance, indicated with vertical dashed line) for seven forested sites that experienced either a fire (prescribed or natural) or defoliating insect disturbance. See Appendix Table S1.1 for site information.

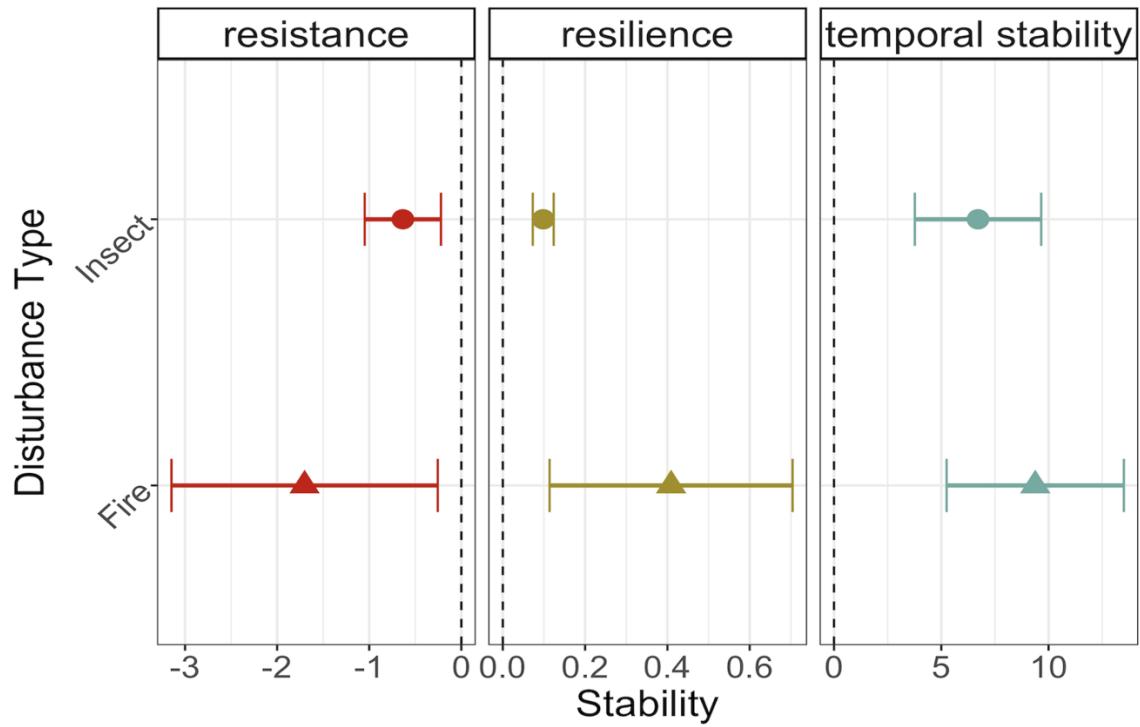


Figure 1.5: Comparison of average net ecosystem production (NEP) stability (resistance, resilience, temporal stability) between fire (n = 4) and insect (n = 3) disturbances presented in figure 1.4.

Appendix

Table S1.1: Description of sites selected in meta-analysis. Search terms in Web of Science: “net ecosystem production*” AND “insect” and “net ecosystem product*” AND “fire”. Selection criteria: Either fire or insect disturbance, directly measures impact of disturbance on NEP in woody ecosystem and contains at least 4 years of data with at least 1 year pre-disturbance.

Site Name in Reference	Latitude/Longitude	Vegetation Type	Disturbance Type	Year of Disturbance	Years Measured	Reference
Willow Creek	45°8'N, 90°1'W	Northern Hardwood	Forest Tent Caterpillar	2001	2000-2006	(Amiro et al. 2010)
Silas Little Experimental (US-Slt)	39°54'N, 74°35'W	Oak-Dominant	Gypsy Moth	2007	2004-2016	(Clark et al. 2018)
Forest New Jersey Pinelands National Reserve	39°45'N, 74°45'W	Pine-Oak Dominant	Prescribed Burn	2008	2007-2011	(Clark et al. 2014)
US-Ced Cedar Bridge Fire Tower (US-Ced)	39°49'N, 74°22'W	Pitch-pine Dominant	Prescribed Burn	2008	2005-2012	(Clark et al. 2018)
Zhanjiang Mangrove National Nature Preserve	21°57'N, 109°76'E	Mangrove Forest	Budmoth Larvae	2010	2009-2012	(Lu et al. 2019)
Calperum Station (Au-Cpr)	34°4'S, 140°71'E	Multi-stem Eucalyptus Woodland	Fire	2014	2013-2017	(Sun et al. 2020)
Reynolds Creek Experimental Watershed	43°7'N, 116°43'W	Big Sagebrush	Prescribed Burn	2007	2006-2012	(Fellows et al. 2018)

Chapter 2: Sustained three-year declines in forest soil respiration are proportional to disturbance severity

Kayla C. Mathes^{1*}, Stephanie Pennington², Carly Rodriguez³, Ben Bond-Lamberty², Jeff W. Atkins^{1,4} Christoph S. Vogel⁵, Christopher M. Gough¹

¹Department of Biology, Virginia Commonwealth University, Box 842012, 1000 West Cary St.,
Richmond, VA 23284

²Joint Global Change Research Institute, Pacific Northwest National Laboratory, 5825
University Research Ct, College Park, MD 20740

³Department of Natural and Environmental Sciences, Western Colorado University, 1 Western
Way, Gunnison, CO 81231

⁴United States Department of Agriculture Forest Service, Southern Research Station, P.O. Box
700 New Ellenton, SC, 29809

⁵University of Michigan Biological Station, 9133 Biological Rd, Pellston, MI 49769

*Corresponding author: Kayla C. Mathes

In review for: *Ecosystems*

(Revised for resubmission following a minor revision decision on March 15, 2023)

Abstract

Soil respiration (R_s) is the largest outward flux of carbon (C) from terrestrial ecosystems, accounting for more than half of total temperate forest C loss. Evaluating the drivers of this globally important flux, as well as identifying autotrophic (R_a) and heterotrophic (R_h) responses, is critical in the era of rapid global change because small changes could result in disproportionately large impacts to ecosystem C balance. We assessed four years of R_s and R_h from the Forest Resilience Threshold Experiment (FoRTE) to better understand how soil C fluxes respond to a disturbance simulating phloem-disrupting insects. This replicated experiment spanning multiple landscape ecosystems contains four disturbance severities of 0, 45, 65 and 85% gross defoliation as well as two disturbance types targeting the upper and lower canopy. We found an immediate and sustained decline in R_s following phloem-disruption that persisted for three years and was proportional to severity. Proportional declines in basal soil respiration and fine-root production with increasing disturbance severity, and stable R_h lead us to conclude that R_a drove the suppression of R_s into the 3rd year following disturbance. These responses were conserved across four landscape ecosystems, suggesting the mechanisms causing R_s to decline following phloem-disruption were similar despite large differences in composition and productivity. The 3-year reduction of C losses through R_s and, contrastingly, sustained C storage through wood production suggests ecosystem C balance may have remained relatively stable in the first few years following disturbance, even at the highest severity.

Keywords: carbon, disturbance, ecosystems, phloem-disruption, resistance, soil respiration.

Highlights

- R_s declined proportionally to disturbance severity following phloem-disruption.
- Autotrophic respiration drove sustained declines in R_s for 3 years post-disturbance.
- Contrasts in R_s and production trends suggest sustained C balance even after severe disturbance.

1. Introduction

Disturbance regimes are changing in North America's upper Great Lakes region (Gough et al. 2016) resulting in an uncertain future for terrestrial carbon (C) cycling processes, including soil respiration (R_s , the soil-to-atmosphere CO_2 flux) (Cohen et al. 2016, Sommerfeld et al. 2018). R_s , the largest terrestrial C efflux, contributes more than half of total temperate forest ecosystem respiration (Binkley et al. 2006, Bond-Lamberty et al. 2018, Lei et al. 2021) and even small disturbance-prompted shifts in this large flux can transition ecosystem C balance from sink to source (Amiro 2001). Regionwide, disturbances caused by pests or pathogens are expanding and becoming more frequent, producing gradients of tree mortality (i.e. *disturbance severity, sensu* (Stuart-Haëntjens et al. 2015) across forested landscapes (Ayres and Lombardero 2000, Flower et al. 2013, Seidl et al. 2017, Wilson et al. 2019). While the immediate effects of severe, stand-replacing disturbances on R_s are well-understood (Frey et al. 2006, Hu et al. 2017, Dietrich and MacKenzie 2018, Bai et al. 2020), longer-term C cycling responses to low-to-moderate disturbance severity gradients are less clear despite their increasing prevalence. Moreover, theory and observations suggest that the components of R_s , autotrophic (R_a) and heterotrophic (R_h) respiration, could respond differently to phloem-disrupting disturbance because these disturbances modify plant and microbial processes through different mechanisms (Harmon et al.

2011). Rates of R_a are dependent upon the allocation of recently fixed photosynthate to roots (Högberg et al. 2001, Gaumont-Guay et al. 2008), whereas R_h is strongly coupled with the quantity of detritus produced through disturbance (Harmon et al. 2011, Mayer et al. 2017). Because detritus-fueled R_h may determine whether disturbance transitions a system from C sink to source, assessing component fluxes is critical to understanding how disturbances of different severities and sources impact ecosystem C balance (Bond-Lamberty et al. 2004).

While gradients of disturbance severity are widespread on forested landscapes, prior observations of R_s focus on single levels of disturbance severity and first-year responses. For example, researchers have used phloem-disruption via stem-girdling or chilling as a methodology to examine below-ground processes in the absence of carbohydrate transport, showing major declines in bulk R_s within days or weeks following disturbance (Högberg et al. 2001, Bhupinderpal-Singh et al. 2003, Binkley et al. 2006). While a breadth of literature has produced a robust understanding of R_s response at the highest end of disturbance severity immediately following phloem-disruption, R_s responses to phloem-disruption over multiple years *and* multiple severity levels are not known. Addressing this knowledge gap is timely and critical because disturbances from phloem-disrupting insects are increasing in Northern American forests (Edgar and Westfall 2022). Patterns of R_s response to other disturbance types, such as fire, herbivory and drought, particularly at moderate severity levels, have been highly variable, with R_s increasing (Zhao et al. 2018), decreasing (Sun et al. 2014), or remaining the same (Masyagina et al. 2006). In addition to the variability present among disturbance types, long-term field experiments and modeling studies suggest soil C cycling processes may be dynamic for years to decades following disturbance (Harmon et al. 2011, Cooperdock et al. 2020, Xu et al.

2022). Therefore, investigating multi-year responses of R_s to a breadth of severities through systematic experimentation is critical to advancing real-world mechanistic understanding of disturbance responses over time (Hicke et al. 2012).

We used a large-scale, replicated phloem-disrupting experimental manipulation of disturbance severity and type called the Forest Resilience Threshold Experiment (FoRTE) to characterize 3-year responses in R_s and R_h , focusing on the initial “resistance” phase of disturbance response. We define resistance as the initial direction and magnitude of change in functioning, here R_s and R_h , following disturbance (*sensu* Mathes and others 2021). Our specific objectives are to: **O1**) Characterize 3-year absolute changes in R_s and R_h and quantify normalized R_s and R_h resistance as a function of disturbance severity and disturbance type; **O2**) Determine whether R_s and R_h respond similarly to disturbance severity and type treatments; **O3**) Calculate temperature sensitivity of R_s (Q10) and basal respiration rates (BR) and assess whether these metrics change across the disturbance severity gradient and between disturbance types. We hypothesize that: 1) R_s declines will be immediate and proportional to increasing disturbance severity, and correlate with declines in fine-root production; 2) in contrast, R_h will exhibit a lagged and gradual increase with increasing disturbance severity over time as detritus increases; and 3) R_s will decline more in the disturbance type targeting smaller canopy trees because the higher root:shoot the small diameter trees will cause a proportionally larger reduction in root mass and respiration, and thus soil respiration (Ledo and others 2018). We present both absolute and normalized R_s and R_h responses to disturbance treatments because they offer complementary assessments of disturbance response; the former expresses the absolute magnitude of change in fluxes following disturbance, and the latter, an effect size, presents the treatment response relative to a control,

allowing for a normalized comparison of fluxes derived and expressed using different methods and units, respectively (Mathes et al. 2021).

2. Methods

2.1 Study Site and Experimental Design

Our research site is the University of Michigan Biological Station (UMBS) near Pellston, MI, USA (45.56 N, 84.67 W). The mean annual air temperature and precipitation are 5.5°C and 817 mm, respectively (Gough et al. 2021a). Our study sites are ~ 110-yr-old temperate mixed hardwood forests with variation in vegetation types and site productivity attributed to underlying glacial landforms, notably outwash plains and terminal moraines, which create distinct topography, microclimate and soil textures (Pearsall et al. 1995). The outwash sites are transitioning from a big-toothed aspen (*Populus grandidentata*) and paper birch (*Betula papyrifera*) dominated canopy to red maple (*Acer rubrum*), Eastern white pine (*Pinus strobus*) and Northern red oak (*Quercus rubra*) dominated canopy and sub-canopy. The terminal moraine sites are transitioning from *P. grandidentata* and *B. papyrifera* to sugar maple (*Acer saccharum*), American beech (*Fagus grandifolia*) and striped maple (*Acer pensylvanicum*) dominated canopy and subcanopy. Soils are spodosols ranging from well-drained loam on the more productive moraine landforms to excessively drained sand on the outwash plain (Pearsall et al. 1995).

We initiated FoRTE in 2019 to identify the mechanisms underpinning forest C cycling stability across a range of disturbance severities and sources (Gough et al. 2021a). While our analysis focuses on soil respiration, prior analyses from FoRTE emphasized aboveground C cycling processes (Grigri et al. 2020, Atkins et al. 2021, Niedermaier et al. 2022), modeled responses to

the FoRTE treatments (Dorheim et al. 2022) and structural and compositional change (Gough et al. 2021a), with a key finding demonstrating that C uptake and allocation to biomass was sustained in the first 3 years after disturbance, even at the highest severity level (Grigri et al. 2020, Gough et al. 2021a, Niedermaier et al. 2022). Following pre-disturbance data collection in 2018, we stem girdled a total of ~3600 canopy trees (>8 cm diameter at breast height, DBH) in May 2019. The girdling treatment was implemented by scoring the full circumference of the stem ~ 15-20 cm apart and completely through the phloem-tissue with a chainsaw, fully encircling the tree. The bark and phloem tissues between the circular cuts were then removed using a pry bar. The experiment was replicated in four different ecosystem types that are representative of upper Great Lakes regional variation in forest productivity, plant community composition, topography and soil microclimate (Nave et al. 2019; Gough et al. 2021a). Notably, the four treatment replicates are positioned on ecosystems spanning a two-fold range in biomass and a three-fold range in canopy complexity (Table 2.1).

Each replicate was comprised of four 0.5 ha circular whole plots (n=16) randomly assigned to target levels of gross defoliation, i.e. disturbance severity of 0% (control), 45%, 65% or 85% determined from tree allometric equations. Each whole-plot was split into two, 0.25 ha split-plots (n = 32) and randomly assigned a disturbance type affecting the canopy from the “top-down” or “bottom-up” (Atkins et al. 2020). In the “top-down” treatment, the largest DBH tree within a subplot was girdled first, regardless of species, followed by sequentially smaller trees until the targeted severity (i.e., gross defoliation) level was reached. “Bottom-up” treatments, conversely, followed ascending DBH (>8 cm) order. (Figure 2.1A: FoRTE map). These treatment types simulate the structural outcomes of disturbance agents targeting larger and smaller tree size

classes, respectively (Atkins et al. 2020). One circular 0.1 ha subplot was nested in each disturbance severity x type treatment split-plot (n = 32).

2.2. Aboveground biomass and vegetation area index (VAI)

Total aboveground wood biomass was calculated from a full census of canopy trees in all subplots during summer of 2018. Diameter at breast height (DBH) was measured for all trees > 8 cm using a tape and biomass was calculated using species and site-specific allometric equations (Gough et al. 2021a). Allometries were also used to estimate the projected leaf area of each censused tree and to assign girdled or ungirdled status to each individual to achieve targeted levels of 0, 45, 65 and 85% gross defoliation and the “top-down” and “bottom-up” treatments.

To evaluate changes in canopy structure following disturbance, we annually sampled the vegetation area index (VAI) of each subplot using LiDAR during peak leaf out. VAI is conceptually similar to LAI, but additionally includes lateral branches. A complete description of VAI determination is detailed in (Gough et al. 2022); briefly, we employed a terrestrial portable canopy LiDAR (PCL) system that uses an upward-facing pulsed-laser to map the location and density of vegetation. Raw LiDAR hit data were binned into horizontal and vertical grids and VAI was estimated using the *forestr* package (Atkins et al. 2018). VAI was sampled in each of the 32 subplots once a year during peak growing-season from 2018-2021.

2.3 Bulk Soil Respiration (R_s) and soil micrometeorology

We measured *in situ* bulk soil respiration (R_s , $\mu\text{molCO}_2 \text{ m}^{-2} \text{ s}^{-1}$) for four years, one year prior and three years following disturbance. Four measurement campaigns were taken before disturbance,

between July 2018 and May 2019, and 14 were taken between May 2019 and November 2021, after the stem-girdling disturbance was implemented. Each of the 32 subplots contained five permanent, 10 cm diameter PVC collars, for a total of 160 collars experiment-wide, installed 4 cm deep and leaving 1 cm above the soil surface. Collars positioned along opposite cardinal axes were spaced 10 m apart, with one additional collar installed at the subplot center (Figure 2.1B). R_s measurements were made at every collar 3 to 7 times a year using a LI-6400 portable gas analyzer with a 10 cm diameter cuvette (LI-COR Inc, Lincoln, NE, USA). At each measurement location, two R_s values were recorded and averaged for analysis. Measurement campaigns were completed within three days under climatologically similar conditions. The settings during measurements were as follows: 400 ppm target CO_2 concentration with measurement range from 390 to 410 ppm ($\Delta = 10$), 10 second gap between drawdown and measurements (Dead Time), 20 second minimum measurement time, 120 second maximum measurement time, 80 cm^2 soil surface area within chamber, 50-200 ($\mu mol s^{-1}$) drawdown flow rate during dormant season measurements and 200-500 ($\mu mol s^{-1}$) drawdown flow rate during growing season measurements. To minimize the confounding of treatment and time-of-day, subplot sampling order within a replicate, as well as order of the replicates, were randomized for each measurement campaign. R_s measurements were not taken within 24 hours of heavy precipitation. R_s measurements were paired with adjacent measurements of 7 cm depth soil temperature (T_s , $^{\circ}C$) using a LI-6400 thermocouple probe and 20 cm integrated soil volumetric water content % (VWC) using a CS620 soil moisture probe (Campbell Scientific, Inc, Logan, UT, USA).

2.4 Partitioning R_s : Soil heterotrophic respiration (R_h)

The heterotrophic respiration of surface soils (R_h , $\mu\text{mol CO}_2 \text{ g}^{-1} \text{ sec}^{-1}$) was estimated from incubated root-free soils (Curtis et al. 2005) using a method previously applied at our site and shown through independent cross-validation to produce ecologically plausible values (Gough et al. 2007). Soils were collected from four, 1 m^2 sampling squares located on the north and south ends of each subplot margins ($n = 128$ experiment-wide; Figure 2.1C) annually between 2019 and 2021. Once a year in July or August, soils from each sampling location were excavated to 10 cm depth, excluding the freshest litter layer (O_i horizon) but including partially and fully decomposed organic layers (O_e and O_a horizons) and A horizon. Soils were collected with a 10 cm diameter metal corer from three randomly selected points within each 1 m^2 sampling location and then pooled and manually homogenized. Soil temperature (T_s) at 7 cm depth was measured concurrently. Immediately following collection, soils were refrigerated at 4°C for 24 hours, sieved to remove roots and fragments, and root-free soil placed in a 950 cm^3 glass jar, leaving 350 cm^3 of headspace. Soil filled glass jars were weighted, capped with a 1 mm ventilation hole and incubated for 2 weeks at the average T_s recorded within a replicate on the day of collection, which ranged from 14.8 to 21.6°C . Following incubation, unadjusted CO_2 efflux ($\mu\text{mol CO}_2 \text{ m}^{-2} \text{ sec}^{-1}$) was measured with a LI-6400 portable gas analyzer (LI-COR Inc, Lincoln, NE, USA) and custom cuvette system fitted to soil filled glass jars. Prior to measurements, we degassed soils on a benchtop by removing the jar lid for 75 mins (Figure S2.1). Next, four sequential CO_2 efflux measurements were taken per soil filled jar and the last two were retained for analysis to ensure stability. We then dried a soil subsample from each jar at 60°C for 48 hours to determine soil dry mass (g). R_h ($\mu\text{mol CO}_2 \text{ g}^{-1} \text{ sec}^{-1}$) was estimated by converting fixed area based efflux measurements ($\mu\text{mol CO}_2 \text{ m}^{-2} \text{ sec}^{-1}$) to soil sample-specific dry mass adjusted estimates of R_h .

2.5 R_s temperature response curves (Q10 and basal R_s rates)

To quantify R_s temperature response curves, we used a two parameter exponential equation model fit separately to data from each subplot (Equation 1, Meyer et al. 2018) and interpreted temperature sensitivity from Q10 values (Equation 2) and basal R_s rates (BR) at 10 °C. We analyzed differences between average Q10 values and BR across disturbance severities and between disturbance types.

$$\text{Equation 1: } R_{s_t} = a * \exp^{b * T_s}$$

$$\text{Equation 2: } Q10 = \exp^{b * T_s}$$

2.6 Annual fine-root production

We measured fine-root production annually from 2019 to 2021 using root in-growth cores installed at the beginning of each growing season (May-June) and extracted at the end of the growing season (November). Four, 5 cm diameter hard plastic mesh cores with 2 mm holes were installed to 30 cm soils depth in each subplot (n = 128) and were spatially paired with R_s measurements. Cores were filled with sieved soils from adjacent forest plots with physical and chemical properties comparable to those found in the FoRTE plots (Pearsall et al. 1995). Extracted cores were stored at 4° C until processing. The four cores from each subplot were pooled and homogenized, and then sieved to remove roots, washed, dried at 60 °C for 48 hours and weighed to determine dry mass. To adjust for ash-free mass, a root subsample (n = 12) was burned in a muffle furnace at 500 °C for 12 hours and an ash-free adjustment was applied to all samples. Root production was scaled and converted to carbon mass (kg C m⁻² yr⁻¹) using a site-specific C fraction of 0.49 (Gough et al. 2008).

2.7 Quantifying R_s and R_h resistance values

To compare normalized measures of R_s and R_h resistance, we adopted a framework described in (Mathes et al. 2021) and (Hillebrand et al. 2018) (Equation 3). This approach allows us to directly compare patterns and changes in fluxes with variable units and magnitudes that may be obscured when only assessing absolute values. Resistance is a dimension of stability quantitatively describing the magnitude of initial response to disturbance normalized against a control and expressed on a natural log scale.

$$\text{Equation 3: } \textit{resistance} = \ln\left(\frac{\textit{Disturbance } R_x}{\textit{Control } R_x}\right)$$

Disturbance R_x is the respiratory flux (R_s or R_h) in a disturbed plot or sample and *Control R_x* the respiratory flux in the control plot or sample. *Resistance* values that are < 0 represent a respiratory (i.e., functional) decline relative to the control, *resistance* values $= 0$ represent no change, and *resistance* values > 0 represent functional increase.

2.8 Statistical analysis

2.8.1 Analysis of absolute values

To analyze the effect of disturbance severity and type on R_s and R_h (**O1** and **O2**) we used a repeated measures split-split plot fully-replicated ANOVA model with alpha values set to 0.05 (Gough et al. 2021a). We used replicate (i.e., landscape ecosystem) as the blocking factor, disturbance severity as the whole-plot factor, type as the split-plot factor and year as the split-split plot factor. We tested models with VWC and T_s as covariates and chose the best fit model based on the Akaike information criterion (AIC). The best fit model for R_s included neither T_s or VWC as covariates and for R_h included untransformed VWC as a covariate. All model

assumptions were met without transformation for R_s and with a log-transformation of R_h data. To minimize spatial auto correlation, the experimental unit was the subplot average over 5 collars for R_s and the subplot average over the 4 soil sampling plots for R_h . Pairwise analyses ($\alpha = 0.05$) were performed on all significant main effects and interaction using Fisher's Least Significant difference (LSD) test (See Tables S2.1 and S2.2 for full ANOVA models and post-hoc output). Interactions were only included in post-hoc analyses if at least one component main effect was significant and there were *a priori* ecological expectations.

To analyze the effect of disturbance severity and type on the Q10 and BR values for the temperature sensitivity of R_s (**O3**), we ran the same split-plot, fully replicated ANOVA as described above, except year was not included in the model (See Tables S2.3 and S2.4 for full ANOVA models and post-hoc output). Finally, the same split-split plot ANOVA was also run to characterize VAI response to disturbance severity and type over time. (See Tables S2.5 for full ANOVA models and post-hoc output). All analyses were performed in R (R Core Team 2022), the split-split plot ANOVA design was made in the package "stats" (R Core Team 2022), the LSD test was conducted using the package "agricolae" (de Mendiburu 2021) and all figures were made in the package "ggplot2" (Wickham 2016).

To analyze the relationship between R_s and annual fine-root production (H2), we ran a multivariate linear regression analysis with R_s as a function of fine-root production, disturbance severity and time (year). Severity and time were included as covariates to assess whether the relationship changed over time and was different across the severity treatments. All model assumptions were met with a log transformation of fine-root production. Pair-wise analyses of

significant interactions were performed using Tukey’s Honestly Significant Difference (HSD) test to compare slopes of R_s as a function of fine-root production across severities (See Tables S2.6 for regression and post-hoc output). Multiple linear regression was performed using R package “stats” (R Core Team 2022) and Tukey’s HSD tests were performed using package “emmeans” (Lenth 2022).

2.8.2 Analysis of R_s and R_h resistance values

To quantify the relationship between R_s and R_h resistance and disturbance severity (**O1** and **O2**), we conducted multiple linear regression analyses with R_s or R_h resistance as a function of severity and time (year). Regression analysis and post-hoc test were performed as described above. All model assumptions were met without transformation (See Tables S2.7 and S2.8 for regression and post-hoc output).

3. Results

3.1 Aboveground biomass and vegetation area index (VAI)

The amount of remaining ungirdled biomass following the treatment implementation was generally proportional to the targeted treatment levels of gross defoliation (i.e., disturbance severity) (Figure 2.2A). In contrast, declines in VAI with increasing disturbance severity lagged girdling and were not directly proportional in magnitude (i.e., 1:1) to gross defoliation (Figure 2B) because of the gradual rate of mortality and associated defoliation that occurs following phloem-disruption (Stuart-Haëntjens et al. 2015). Significant differences in VAI emerged in 2019 between the control and at 85% severity, but were not present among all severities until 2021 (Figure 2.2B; $F = 2.045$, $p = 0.047$).

3.2 Seasonality and range of soil respiration (R_s) and microclimate data

Across all disturbance treatments, mean R_s , T_s and VWC values varied seasonally and were within the range of previously recorded values from our site (Clippard et al. 2022). Mean subplot R_s varied by more than an order of magnitude, from 0.5 to 14.3 $\mu\text{mol CO}_2 \text{ m}^{-2} \text{ sec}^{-1}$, with low values occurring during the cooler dormant season. Summertime T_s ranged from 10.1 and 24.7 °C, declining to an average of 4.2°C during the dormant season. VWC displayed the opposite seasonal pattern, reaching high values of 22% during the dormant season and minimum values as low as 3% during the summer (Figure 2.3). Pre-treatment (2018) control R_s was significantly lower than subsequent years, which was driven by low summertime VWC (Figure S2.2).

3.3 Soil respiration (R_s) and disturbance severity

A pattern of declining R_s with increasing severity emerged the year of the girdling disturbance (2019) and persisted for three consecutive years (Figure 2.4). Declines in R_s were temporally aligned with the onset of the girdling and proportional to the targeted levels of gross defoliation (Figure 2.2A), but preceded declines in total VAI across all severities by two years (Figure 2.2B). We did not observe differences among disturbance severity treatments prior to girdling in 2018. However, the girdling treatment in 2019 prompted a significant decrease in R_s with increasing severity and this pattern held through 2021 ($F = 4.42$, $p < 0.001$). From 2019 to 2021, control R_s values were consistently higher than those observed in the disturbance severity treatments, with mean R_s in the 85% disturbance severity treatment averaging 35% less than the control (Figure 2.4).

3.4 Soil respiration (R_s) and disturbance type

In contrast to disturbance severity, we observed no significant differences in R_s between top-down and bottom-up disturbance types before (2018) or after (2019-2021) stem girdling (Figure 2.5). Within-year pairwise treatment comparisons revealed no significant differences ($F = 0.924$, $p = 0.42$), indicating that the stem size distribution of girdled trees had no effect on R_s in the first three years following disturbance.

3.5 R_s temperature response curves, Q_{10} and basal R_s rates

The step-down pattern of R_s with increasing disturbance severity was caused by a reduction in basal soil respiration (BR) rather than change in temperature sensitivity. Post-disturbance R_s exhibited similar exponential increases with temperature (i.e., temperature sensitivities) across disturbance severities ($F = 1.847$, $p = 0.21$, Figure 2.6A,C) and disturbance types ($F = 1.343$, $p = 0.27$, Figure 2.6B,D), with Q_{10} averaging 2.24. However, BR and R_s displayed similar significant declines ($F = 4.418$, $p = 0.04$, Figure 2.6E) with increasing disturbance severity, from 3.59 to 2.42 $\mu\text{mol CO}_2 \text{ m}^{-2} \text{ sec}^{-1}$ at 10°C, and was similar between the top-down and bottom-up treatments ($F = 0.17$, $p = 0.690$, Figure 2.6F).

3.6 Heterotrophic respiration (R_h) and disturbance severity and type

Mean R_h was lowest in the 65% disturbance severity and top-down treatments, departing somewhat from the trends of total R_s . R_h ranged from 0.0017 to 0.012 $\mu\text{mol CO}_2 \text{ g}^{-1} \text{ sec}^{-1}$ with a grand mean of 0.004 $\mu\text{mol CO}_2 \text{ g}^{-1} \text{ sec}^{-1}$ between 2019-2021. R_h was significantly lower in the 65% treatment (Figure 2.7A, $F = 4.369$, $p = 0.042$) and we did not find a year x treatment

interaction, indicating that the relationship between R_h and disturbance severity was consistent across years. A significant, but quantitatively small difference of 8.7% between the top-down and bottom-up treatments was also present following disturbance (Figure 2.7B, $F = 6.837$, $p = 0.024$), however the difference was too small and noisy to significantly influence total R_s .

3.7. Fine-root production and R_s

We observed a significant positive relationship between R_s and fine-root production in stem-girdled but not control plots (Figure 2.8, $R^2 = 0.50$, $p\text{-value} < 0.001$). The slope of the fine root production- R_s relationship was shared among post-disturbance years and levels of disturbance severity. However, the slopes between control and disturbance plots (all severities) were significantly different from each other (Figure 2.8, $F = 2.2$, $p\text{-value} = 0.03$), suggesting disturbance-induced declines in fine-root production drove reductions in R_s .

3.8 Soil respiration (R_s and R_h) resistance

A comparison of normalized R_s and R_h resistance values underscores their contrasting relative response to increasing disturbance severity, further suggesting that autotrophic rather than heterotrophic respiration primarily drove declines in total soil CO_2 efflux. R_s resistance exhibited a temporally consistent decline across the disturbance severity gradient following stem girdling from 2019-2021, showing as much as 37% decrease in the highest severity as compared to the control (Figure 2.9A). Contrastingly, R_h resistance, while variable, did not change significantly across disturbance severity treatments (Figure 2.9B), only showing a 7% decline in the highest severity. This result suggests that 3-year declines in R_s primarily were driven by consistently suppressed autotrophic respiration.

4. Discussion

Our analysis provides new mechanistic insight into how forest R_s responds to a range of disturbance severities caused by phloem-disruption. With complementary analyses of absolute measurements and normalized resistance values, we observed an immediate and strikingly sustained 3-yr decline in R_s with increasing disturbance severity, indicating that disturbance effects were relatively long-lasting and proportional to targeted gross defoliation levels but lagged behind changes in VAI. The temporal mismatch in R_s and VAI responses to girdling was likely associated with the immediate elimination of photosynthate allocation to roots (Högberg et al. 2001), but slower and more gradual defoliation. Basal soil respiration (BR), but not R_h or Q_{10} , decreased with increasing disturbance severity and declines in fine-root production drove declines in R_s , suggesting that a reduction in autotrophic rather than heterotrophic respiration or temperature sensitivity drove R_s responses to phloem-disruption. In contrast to disturbance severity, the top-down and bottom-up disturbance types exhibited comparable R_s . These findings extend knowledge derived from short-term (e.g., 1-year) observations and studies encompassing a narrower range of disturbance severities or forest types (Högberg et al. 2001, Nave et al. 2011, Bloemen et al. 2014), demonstrating that the targeted disturbance severity consistently reduced R_s through its sustained, proportional effect on autotrophic respiration.

Our results indicate that declines from phloem-disruption are generally proportional to the degree of disturbance severity expressed as gross defoliation and similar across disturbance types, a finding that contrasts with the response of aboveground production. Our observation that phloem-disrupting disturbance initially reduces R_s is consistent with numerous studies conducted in a variety of forest types (Bhupinderpal-Singh et al. 2003, Andersen et al. 2005, Binkley et al.

2006, Frey et al. 2006, De Schepper et al. 2011). Similar to our results, a pattern of declining R_s with increasing tree mortality was observed in a Northern temperate forest manipulated via stem-girdling (Levy-Varon et al. 2012). Additionally, our findings align with studies that report declines in R_s are greater from severe disturbance caused by fire (Kelly et al. 2021) and harvesting (Bai et al. 2020). Building on these studies, our replicated experiment further demonstrates that patterns of declining R_s with increasing disturbance severity are consistent among forest ecosystems varying substantially in composition, productivity, soils, and landform. Such consistency across ecosystems suggests that a common physiological basis underlies changes in R_s following phloem-disruption, regardless of tree species composition. Notably, we did not observe signs of recovery in R_s over time despite finding increases in subcanopy growth and relatively stable total aboveground primary production (Grigri et al. 2020, Niedermaier et al. 2022). The opposing responses of C uptake (i.e., primary production) and loss (i.e., R_s) suggest that surviving vegetation may have invested less in metabolically active fine root biomass as competition for limiting resources declined after disturbance (Bae et al. 2015, Kang et al. 2016).

Declines in R_s emerged within the first two months of phloem-disruption and persisted through the third year, underscoring a rapid and sustained disturbance response. This rapid R_s response to phloem-disruption is consistent with experiments observing almost immediate changes in soil CO_2 efflux after disturbance (Scott-Denton et al. 2006, Subke et al. 2011). Additionally, our 3-yr analysis demonstrates that disturbance effects can persist for years, a duration that is consistent with a landscape-level single severity phloem-disrupting disturbance at our site (Gough et al. 2021b), model simulations of the FoRTE treatments (Dorheim et al. 2022), and the 6 to 7 year recovery time following a phloem-disrupting insect disturbance elsewhere (Moore et al. 2013).

However, this sustained decline is longer than the 1-yr recovery in R_s following experimental stem-girdling in a temperate deciduous forest (Levy-Varon et al. 2014). Simulations of the FoRTE disturbance suggest that climatic and biotic variables such as precipitation, humidity and forest productivity influence the pattern and timing of C cycling disturbance response (Dorheim et al. 2022). In contrast, our observations demonstrate that landscape ecosystems with primary production values varying by a factor of four (Gough et al. 2021a) exhibit similar initial responses to disturbance.

Our analysis suggests autotrophic rather than heterotrophic respiration predominantly drove declines in R_s following phloem-disruption. Girdling immediately eliminates photosynthate transport to roots causing declines in root metabolism and, consequently, R_s (Högberg and Högberg 2002, Chen et al. 2010). While we expected to observe a gradual rise in R_h as root detritus increased (Subke et al. 2011), three lines of evidence instead point to a sustained 3-yr reduction in autotrophic respiration. First, R_h declined slightly or was stable with increasing severity during the three years following disturbance, implying that disturbance-fueled decomposition was minimal, or that it was offset by reduced heterotrophic respiration of root exudates. In contrast, studies of stand-replacing disturbances reveal that a large and rapid influx of organic substrate (Ekberg et al. 2007) and extreme shifts in soil microclimate (Mayer et al. 2017) can cause immediate increases in R_h . Relatively stable R_h during the first three years of our experiment could suggest that, unlike stand-replacing events, the amount of disturbance-induced substrate was not significant enough to cause an immediate microbial priming effect. Furthermore, since declines in VAI lag the onset of phloem-disrupting disturbances, microclimatic changes that may impact R_h were not as pronounced. Our results are consistent

with the lagged increase in R_h predicted by model runs of the FoRTE study (Dorheim et al. 2022) and by theory (Harmon et al. 2011). Second, declines in R_s with increasing disturbance severity were accompanied by parallel reductions in basal respiration (BR) rather than temperature sensitivity (Q_{10}), implying labile rather than more recalcitrant C substrate limited total R_s after stem-girdling. BR rates are particularly sensitive to changes in labile C supply, including the quantity of recently fixed non-structural C allocated to roots, while temperature sensitivity is generally more limited by the degree of organic matter recalcitrance (Bhupinderpal-Singh et al. 2003, Sampson et al. 2007, Yan et al. 2021). Finally, consistent with studies showing declines in fine-root production in windthrow (Ivanov et al. 2022) and fire disturbances (Yuan and Chen 2013), variation in fine-root production was a predictor of R_s in the disturbed plots but not the control, suggesting loss of autotrophic activity drove declines in R_s following phloem-disruption. Our findings offer useful empirical support for models, theory, and short-term studies, suggesting that the influence of phloem-disruption on the autotrophic component of respiration can be long-lasting, despite an imminent influx of disturbance-generated detritus.

Contrary to our hypothesis, we found no significant differences in R_s between disturbance types targeting either upper or lower canopy trees. We anticipated higher root:shoot in smaller stems (Ledo et al. 2018) would result in a proportionally greater effect on autotrophic fluxes in the bottom-up treatment. Instead, we observed a small, but significant, increase in R_h in the bottom-up treatment, suggesting that greater fine-root mortality could be gradually enhancing R_h and offsetting the reduction in autotrophic contributions (Ekberg et al. 2007). Moving forward, we expect canopy structural changes, which lag behind phloem-disruption (Gough et al. 2021b), will impart different effects on soil microclimate in the top-down and bottom-up disturbance types,

causing R_s to diverge over the long-term. That top-down and bottom-up disturbance types have not diverged in the first three years following disturbance, in advance of peak canopy structural changes, highlights the need for long-term observations of disturbance response (Buma 2015).

Expressing R_s and R_h responses to disturbance in relative terms (i.e., as resistance) made these fluxes – expressed in different units and spanning a large absolute range – more comparable, while revealing some limitations. Mathes and others (2021) recommended the use of relative, normalized, and systematic expression of disturbance response as a way of placing functional responses derived via different approaches and expressed using different units on equivalent scales. In our study system, we anticipated large absolute differences in fluxes among the different landscape ecosystems. However, a surprisingly uniform response to disturbance across landscape ecosystems varying substantially in productivity, composition, and soils made such normalization less imperative to revealing trends. Nevertheless, the adoption of normalized approaches to characterizing disturbance response may prove useful when magnitudes of response are different or when comparing functional responses across disparate sites, experiments, and biomes (Hillebrand et al. 2018, Mathes et al. 2021).

Finally, we acknowledge several study limitations. First, the rapid implementation of our disturbance experiment does not simulate the more temporally gradual effects of phloem-disrupting insects (Duan et al. 2022). In addition, many prevalent phloem-disrupting insects are host-specific (Busby and Canham 2011, Borkhuu et al. 2015) and species-specific physiology, functional traits and evolutionary mechanisms of resistance might become important factors driving functional responses in some circumstances (Seidl et al. 2017). However, that we

observed consistent disturbance responses across four different landscape ecosystems suggests severity was a more important driver of R_s than the composition of disturbed individuals. Additionally, the spatial distribution of tree mortality is often affected by tree vigor and density, and compounding press disturbances, such as prolonged drought (Bentz et al. 2010). Second, we inferred the behavior of autotrophic respiration from indirect measures that are made with high uncertainty (Bond-Lamberty and others 2004). Partitioning R_s into autotrophic and heterotrophic components remains notoriously challenging (Savage et al. 2018). While the method we used to estimate R_h yields estimates comparable to those derived via independent approaches (Gough et al. 2007), soil sieving eliminates physical structure and disrupts root-microbial interactions, creating artificial biological and physical conditions that limit the inference to field measurements. Third, we did not measure R_s continuously, omitting nighttime R_s as well as the peak dormant season. Finally, while our study captured 3-year responses, our analysis extends through only the initial resistance stage of disturbance response and we anticipate substantial changes in R_s and its source components as canopy structure and microclimate shift, and mortality results in a large influx of detritus. Complete disturbance response cycles—from initial response through recovery – may occur over decades (Amiro et al. 2010, Dorheim et al. 2022), highlighting the need for long-term ecological observations.

5. Conclusions

The findings from our large-scale replicated manipulation of disturbance severity and type supports several conclusions. First, our results of declining R_a with stable R_h in addition to findings showing stable NPP across the same disturbance continuum (Grigri et al. 2020, Niedermaier et al. 2022) suggests that net ecosystem production (NEP) was sustained— at least

initially – even at high levels of phloem-disruption. Placing our instantaneous R_s measurements in terms of cumulative R_s at our site (Curtis et al. 2005), our observed 37% decline in R_s at the highest disturbance severity would translate to a loss of approximately $300\text{g C m}^{-2}\text{y}^{-1}$. This is comparable to total annual NEP at our site (Gough et al. 2021b), suggesting the magnitude of R_s decline significantly changed ecosystem C balance. Second, our 3-yr study, leveraging both absolute flux and relative resistance analyses, demonstrates that the effects of phloem-disruption on R_s can be relatively long-lasting, underscoring the importance of multi-year observations. Third, we conclude that R_s responses to disturbance are conserved across different forest ecosystems on our upper Great Lakes landscape, suggesting a common physiological response to phloem-disruption regardless of canopy composition. Finally, while this study assesses several years following a disturbance event, future work should prioritize synthesizing patterns and mechanisms of R_s recovery to the breadth of disturbance severities and types as well as disentangling variable outcomes of R_s disturbance response. Such synthetic, longer-term work will be critical for improving ecological forecasting of ecosystem C balance in an era of increasing and ever changing disturbance regimes.

Data availability statement:

Data used in this analysis are available via the R FoRTE data package (*fortedata*):

<https://github.com/FoRTEexperiment/fortedata>. Statistical analysis, workflow and code used to visualize results are available via: https://github.com/kaylamathes/FoRTE_Rs.

Acknowledgements: We thank the University of Michigan Biological Station for hosting our work and supporting our team members.

Funding: This work was funded by the National Science Foundation, Division of Environmental Biology (Award 1655095).

Literature Cited

- Amiro BD. 2001. Paired-tower measurements of carbon and energy fluxes following disturbance in the boreal forest. *Glob Chang Biol* 7:253–68.
- Amiro BD, Barr AG, Barr JG, Black TA, Bracho R, Brown M, Chen J, Clark KL, Davis KJ, Desai AR, and others. 2010. Ecosystem carbon dioxide fluxes after disturbance in forests of North America. *J Geophys Res Biogeosci* 115.
- Andersen CP, Nikolov I, Nikolova P, Matyssek R, Häberle KH. 2005. Estimating ‘autotrophic’ belowground respiration in spruce and beech forests: Decreases following girdling. *Eur J For Res* 124:155–63.
- Atkins JW, Agee E, Barry A, Dahlin KM, Dorheim K, Grigri MS, Haber LT, Hickey LJ, Kamoske AG, Mathes K, and others. 2021. The fortedata R package: Open-science datasets from a manipulative experiment testing forest resilience. *Earth Syst Sci Data* 13:943–52.
- Atkins JW, Bohrer G, Fahey RT, Hardiman BS, Morin TH, Stovall AEL, Zimmerman N, Gough CM. 2018. Quantifying vegetation and canopy structural complexity from terrestrial LiDAR data using the forestR package. *Methods Ecol Evol* 9:2057–66.
- Atkins JW, Bond-Lamberty B, Fahey RT, Haber LT, Stuart-Haëntjens E, Hardiman BS, LaRue E, McNeil BE, Orwig DA, Stovall AEL, and others. 2020. Application of

- multidimensional structural characterization to detect and describe moderate forest disturbance. *Ecosphere* 11.
- Ayres MP, Lombardero MJ. 2000. Assessing the consequences of global change for forest disturbance from herbivores and pathogens. *Science of the Total Environment* 262:263–86.
- Bae K, Fahey TJ, Yanai RD, Fisk M. 2015. Soil Nitrogen Availability Affects Belowground Carbon Allocation and Soil Respiration in Northern Hardwood Forests of New Hampshire. *Ecosystems* 18:1179–91.
- Bai S, Qiu W, Zhang H, Wang Y, Berninger F. 2020. Soil respiration following Chinese fir plantation clear-cut: Comparison of two forest regeneration approaches. *Science of the Total Environment* 709:135980.
- Bentz BJ, Régnière J, Fettig CJ, Hansen EM, Hayes JL, Hicke JA, Kelsey RG, Negrón JF, Seybold SJ. 2010. Climate Change and Bark Beetles of the Western United States and Canada: Direct and Indirect Effects. *Bioscience* 60:602–13.
- Bhupinderpal-Singh, Nordgren A, Löfvenius MO, Högberg MN, Mellander PE, Högberg P. 2003. Tree root and soil heterotrophic respiration as revealed by girdling of boreal Scots pine forest: Extending observations beyond the first year. *Plant Cell Environ* 26:1287–96.
- Binkley D, Stape JL, Takahashi EN, Ryan MG. 2006. Tree-girdling to separate root and heterotrophic respiration in two Eucalyptus stands in Brazil. *Oecologia* 148:447–54.
- Bloemen J, Agneessens L, Van Meulebroek L, Aubrey DP, McGuire MA, Teskey RO, Steppe K. 2014. Stem girdling affects the quantity of CO₂ transported in xylem as well as CO₂ efflux from soil. *New Phytologist* 201:897–907.

- Bond-Lamberty B, Bailey VL, Chen M, Gough CM, Vargas R. 2018. Globally rising soil heterotrophic respiration over recent decades. *Nature* 560:80–3.
- Bond-Lamberty B, Wang C, Gower ST. 2004. A global relationship between the heterotrophic and autotrophic components of soil respiration? *Glob Chang Biol* 10:1756–66.
- Borkhuu B, Peckham SD, Ewers BE, Norton U, Pendall E. 2015. Does soil respiration decline following bark beetle induced forest mortality? Evidence from a lodgepole pine forest. *Agric For Meteorol* 214–215:201–7.
- Buma B. 2015. Disturbance interactions: Characterization, prediction, and the potential for cascading effects. *Ecosphere* 6:1–15.
- Busby PE, Canham CD. 2011. An exotic insect and pathogen disease complex reduces aboveground tree biomass in temperate forests of eastern North America. *Canadian Journal of Forest Research* 41:401–11.
- Chen D, Zhang Y, Lin Y, Zhu W, Fu S. 2010. Changes in belowground carbon in *Acacia crassicarpa* and *Eucalyptus urophylla* plantations after tree girdling. *Plant Soil* 326:123–35.
- Clippard EA, Haruna SI, Curtis PS, Clay C, Bond B, Mathes K, Vogel CS, Gough CM. 2022. Decadal forest soil respiration following stem girdling. *Trees*.
- Cohen WB, Yang Z, Stehman S v., Schroeder TA, Bell DM, Masek JG, Huang C, Meigs GW. 2016. Forest disturbance across the conterminous United States from 1985-2012: The emerging dominance of forest decline. *For Ecol Manage* 360:242–52.
- Cooperdock SC, Hawkes C V., Xu DR, Breecker DO. 2020. Soil Water Content and Soil Respiration Rates Are Reduced for Years Following Wildfire in a Hot and Dry Climate. *Global Biogeochem Cycles* 34:1–18.

- Curtis PS, Vogel CS, Gough CM, Schmid HP, Su HB, Bovard BD. 2005. Respiratory carbon losses and the carbon-use efficiency of a northern hardwood forest, 1999-2003. *New Phytologist* 167:437–56.
- Davis, J. C., J. P. Shannon, M. J. Van Grinsven, N. W. Bolton, J. W. Wagenbrenner, R. K. Kolka, and T. G. Pypker. 2019. Nitrogen cycling responses to simulated emerald ash borer infestation in *Fraxinus nigra*-dominated wetlands. *Biogeochemistry* 145:275–294.
- Dietrich ST, MacKenzie MD. 2018. Comparing spatial heterogeneity of bioavailable nutrients and soil respiration in boreal sites recovering from natural and anthropogenic disturbance. *Front Environ Sci* 6:1–13.
- Dorheim K, Gough CM, Haber LT, Mathes KC, Shiklomanov AN, Bond-Lamberty B. 2022. Climate Drives Modeled Forest Carbon Cycling Resistance and Resilience in the Upper Great Lakes Region, USA. *J Geophys Res Biogeosci* 127:1–15.
- Duan S, He HS, Spetich MA, Wang WJ, Fraser JS, Xu W. 2022. Long-term effects of succession, climate change and insect disturbance on oak-pine forest composition in the U.S. Central Hardwood Region. *Eur J For Res* 141:153–64.
- Edgar CB, Westfall JA. 2022. Timing and extent of forest disturbance in the Laurentian Mixed Forest. *Frontiers in Forests and Global Change* 5:1–15.
- Ekberg A, Buchmann N, Gleixner G. 2007. Rhizospheric influence on soil respiration and decomposition in a temperate Norway spruce stand. *Soil Biol Biochem* 39:2103–10.
- Flower CE, Knight KS, Gonzalez-Meler MA. 2013. Impacts of the emerald ash borer (*Agrilus planipennis* Fairmaire) induced ash (*Fraxinus* spp.) mortality on forest carbon cycling and successional dynamics in the eastern United States. *Biol Invasions* 15:931–44.
- Frey B, Hagedorn F, Giudici F. 2006. Effect of girdling on soil respiration and root composition

in a sweet chestnut forest. *For Ecol Manage* 225:271–7.

Gaumont-Guay D, Black A., Barr A. G., Jassal R. S., Nesic Z. 2008. Biophysical controls on rhizospheric and heterotrophic components of soil respiration in a boreal black spruce stand. *Tree physiology* 28:161–71.

Gough CM, Atkins JW, Bond-Lamberty B, Agee EA, Dorheim KR, Fahey RT, Grigri MS, Haber LT, Mathes KC, Pennington SC, Shiklomanov AN, Tallant JM. 2021a. Forest Structural Complexity and Biomass Predict First-Year Carbon Cycling Responses to Disturbance. *Ecosystems* 24:699–712.

Gough CM, Atkins JW, Fahey RT, Curtis PS, Bohrer G, Hardiman BS, Hickey LJ, Nave LE, Niedermaier KM, Clay C, Tallant JM, Bond-Lamberty B. 2022. Disturbance has variable effects on the structural complexity of a temperate forest landscape. *Ecol Indic* 140.

Gough CM, Bohrer G, Hardiman BS, Nave LE, Vogel CS, Atkins JW, Bond-Lamberty B, Fahey RT, Fotis AT, Grigri MS, and others. 2021b. Disturbance-accelerated succession increases the production of a temperate forest. *Ecological Applications* 31:1–17.

Gough CM, Curtis PS, Hardiman BS, Scheuermann CM, Bond-Lamberty B. 2016. Disturbance, complexity, and succession of net ecosystem production in North America's temperate deciduous forests. *Ecosphere* 7:1–15.

Gough CM, Vogel CS, Harrold KH, George K, Curtis PS. 2007. The legacy of harvest and fire on ecosystem carbon storage in a north temperate forest. *Glob Chang Biol* 13:1935–49.

Gough CM, Vogel CS, Schmid HP, Su HB, Curtis PS. 2008. Multi-year convergence of biometric and meteorological estimates of forest carbon storage. *Agric For Meteorol* 148:158–70.

Grigri MS, Atkins JW, Vogel C, Bond-Lamberty B, Gough CM. 2020. Aboveground wood

- production is sustained in the first growing season after phloem-disrupting disturbance. *Forests* 11:1–19.
- Harmon ME, Bond-Lamberty B, Tang J, Vargas R. 2011. Heterotrophic respiration in disturbed forests: A review with examples from North America. *J Geophys Res Biogeosci* 116:1–17.
- Hicke JA, Allen CD, Desai AR, Dietze MC, Hall RJ, Hogg EHT, Kashian DM, Moore D, Raffa KF, Sturrock RN, Vogelmann J. 2012. Effects of biotic disturbances on forest carbon cycling in the United States and Canada. *Glob Chang Biol* 18:7–34.
- Hillebrand H, Langenheder S, Lebet K, Lindström E, Östman Ö, Striebel M. 2018. Decomposing multiple dimensions of stability in global change experiments. *Ecol Lett* 21:21–30.
- Högberg MN, Högberg P. 2002. Extramatrical ectomycorrhizal mycelium contributes one-third of microbial biomass and produces, together with associated roots, half the dissolved organic carbon in a forest soil. *New Phytologist* 154:791–5.
- Högberg P, Nyberg G, Taylor AFS, Ekblad A, Högn MN, Read DJ, Ottosson-lo M. 2001. Large-scale forest girdling shows that current photosynthesis drives soil respiration. *Nature* 411:789–92.
- Hu T, Sun L, Hu H, Guo F. 2017. Effects of fire disturbance on soil respiration in the non-growing season in a *Larix gmelinii* forest in the Daxing'an Mountains, China. *PLoS One*.
- Ivanov A V., Salo MA, Tolstikova VY, Bryanin S V., Zamolodchikov DG. 2022. Effects of Windfall on Soil Surface Carbon Emission and Fine Root Stocks in the Central Sikhotealin. *Eurasian Soil Science* 55:1405–13.
- Kang H, Fahey TJ, Bae K, Fisk M, Sherman RE, Yanai RD, See CR. 2016. Response of forest

- soil respiration to nutrient addition depends on site fertility. *Biogeochemistry* 127:113–24.
- Kelly J, Ibáñez TS, Santín C, Doerr SH, Nilsson MC, Holst T, Lindroth A, Kljun N. 2021. Boreal forest soil carbon fluxes one year after a wildfire: Effects of burn severity and management. *Glob Chang Biol* 27:4181–95.
- Ledo A, Paul KI, Burslem DFRP, Ewel JJ, Barton C, Battaglia M, Brooksbank K, Carter J, Eid TH, England JR, and others. 2018. Tree size and climatic water deficit control root to shoot ratio in individual trees globally. *New Phytologist* 217:8–11.
- Lei J, Guo X, Zeng Y, Zhou J, Gao Q, Yang Y. 2021. Temporal changes in global soil respiration since 1987. *Nat Commun* 12:1–9.
- Lenth R. 2022. emmeans: Estimated Marginal Means, aka Least-Squares Means_ . .
- Levy-Varon JH, Schuster WSF, Griffin KL. 2012. The autotrophic contribution to soil respiration in a northern temperate deciduous forest and its response to stand disturbance. *Oecologia* 169:211–20.
- Levy-Varon JH, Schuster WSF, Griffin KL. 2014. Rapid rebound of soil respiration following partial stand disturbance by tree girdling in a temperate deciduous forest. *Oecologia* 174:1415–24.
- Masyagina O V., Hirano T, Ji DH, Choi DS, Qu L, Fujinuma Y, Sasa K, Matsuura Y, Prokushkin SG, Koike T. 2006. Effect of spatial variation of soil respiration rates following disturbance by timber harvesting in a larch plantation in northern Japan. *Forest Sci Technol* 2:80–91.
- Mathes KC, Ju Y, Kleinke C, Oldfield C, Bohrer G, Bond-Lamberty B, Vogel CS, Dorheim K, Gough CM. 2021. A multidimensional stability framework enhances interpretation and

- comparison of carbon cycling response to disturbance. *Ecosphere* 12.
- Mayer M, Matthews B, Rosinger C, Sandén H, Godbold DL, Katzensteiner K. 2017. Tree regeneration retards decomposition in a temperate mountain soil after forest gap disturbance. *Soil Biol Biochem* 115:490–8.
- de Mendiburu F. 2021. *_agricolae: Statistical Procedures for Agricultural Research_*. R package .
- Meyer N, Welp G, Amelung W. 2018. The Temperature Sensitivity (Q₁₀) of Soil Respiration: Controlling Factors and Spatial Prediction at Regional Scale Based on Environmental Soil Classes. *Global Biogeochem Cycles* 32:306–23.
- Meyer, G., Black, T. A., Jassal, R. S., Nestic, Z., Coops, N. C., Christen, A., Fredeen, A. L., Spittlehouse, D. L., Grant, N. J., Foord, V. N., & Bowler, R. (2018). Simulation of net ecosystem productivity of a lodgepole pine forest after mountain pine beetle attack using a modified version of 3-PG. *Forest Ecology and Management*, 412, 41–52.
<https://doi.org/10.1016/j.foreco.2018.01.034>
- Moore DJP, Trahan NA, Wilkes P, Quaife T, Stephens BB, Elder K, Desai AR, Negron J, Monson RK. 2013. Persistent reduced ecosystem respiration after insect disturbance in high elevation forests. *Ecol Lett* 16:731–7.
- Nave LE, Gough CM, Maurer KD, Bohrer G, Hardiman BS, le Moine J, Munoz AB, Nadelhoffer KJ, Sparks JP, Strahm BD, and others. 2011. Disturbance and the resilience of coupled carbon and nitrogen cycling in a north temperate forest. *J Geophys Res Biogeosci* 116:1–14.
- Nave LE, Walters BF, Hofmeister KL, Perry CH, Mishra U, Domke GM, Swanston CW. 2019. The role of reforestation in carbon sequestration. *New For (Dordr)* 50:115–37.
- Niedermaier KM, Atkins JW, Grigri MS, Bond-lamberty B, Gough CM. 2022. Structural

- complexity and primary production resistance are coupled in a temperate forest. *Frontiers in Forests and Global Change*. 10.3389/ffgc.2022.941851
- Pearsall DR, Barnes B V, Zogg GR, Lapin M, Ring RR, Ring D. 1995. Landscape ecosystems of the University of Michigan Biological Station. School of Natural Resources & Environment. 66.
- R Core Team. 2022. R: A language and environment for statistical computing.
- Sampson DA, Janssens IA, Curiel Yuste J, Ceulemans R. 2007. Basal rates of soil respiration are correlated with photosynthesis in a mixed temperate forest. *Glob Chang Biol* 13:2008–17.
- Savage KE, Davidson EA, Abramoff RZ, Finzi AC, Giasson MA. 2018. Partitioning soil respiration: quantifying the artifacts of the trenching method. *Biogeochemistry* 140:53–63.
- De Schepper V, Vanhaecke L, Steppe K. 2011. Localized stem chilling alters carbon processes in the adjacent stem and in source leaves. *Tree Physiol* 31:1194–203.
- Scott-Denton LE, Rosenstiel TN, Monson RK. 2006. Differential controls by climate and substrate over the heterotrophic and rhizospheric components of soil respiration. *Glob Chang Biol* 12:205–16.
- Seidl R, Thom D, Kautz M, Martin-Benito D, Peltoniemi M, Vacchiano G, Wild J, Ascoli D, Petr M, Honkaniemi J, and others. 2017. Forest disturbances under climate change. *Nat Clim Chang* 7:395–402. <http://dx.doi.org/10.1038/nclimate3303>
- Sommerfeld A, Senf C, Buma B, D’Amato AW, Després T, Díaz-Hormazábal I, Fraver S, Frelich LE, Gutiérrez AG, Hart SJ, and others. 2018. Patterns and drivers of recent

- disturbances across the temperate forest biome. *Nat Commun* 9:4355.
<https://doi.org/10.1038/s41467-018-06788-9>
- Stuart-Haëntjens EJ, Curtis PS, Fahey RT, Vogel CS, Gough CM. 2015. Net primary production of a temperate deciduous forest exhibits a threshold response to increasing disturbance severity. *Ecology* 96:2478–87.
- Subke JA, Voke NR, Leronni V, Garnett MH, Ineson P. 2011. Dynamics and pathways of autotrophic and heterotrophic soil CO₂ efflux revealed by forest girdling. *Journal of Ecology* 99:186–93.
- Sun L, Hu T, Kim JH, Guo F, Song H, Lv X, Hu H. 2014. The effect of fire disturbance on short-term soil respiration in typical forest of Greater Xing'an Range, China. *J For Res (Harbin)* 25:613–20.
- Wickham H. 2016. *ggplot2: Elegant Graphics for Data Analysis*.
- Wilson DC, Morin RS, Frelich LE, Ek AR. 2019. Monitoring disturbance intervals in forests: a case study of increasing forest disturbance in Minnesota. *Ann For Sci* 76.
- Xu S, Eisenhauer N, Pellegrini AFA, Wang J, Certini G, Guerra CA, Lai DYF. 2022. Fire frequency and type regulate the response of soil carbon cycling and storage to fire across soil depths and ecosystems: A meta-analysis. *Science of the Total Environment* 825:153921.
- Yan Y, Quan Q, Meng C, Wang J, Tian D, Wang B, Zhang R, Niu S. 2021. Varying soil respiration under long-term warming and clipping due to shifting carbon allocation toward below-ground. *Agric For Meteorol* 304–305:108408.
- Yuan ZY, Chen HYH. 2013. Effects of Disturbance on Fine Root Dynamics in the Boreal Forests of Northern Ontario, Canada. *Ecosystems* 16:467–77.

Zhao S, Chen K, Wu C, Mao Y. 2018. Effects of simulated warming on soil respiration to
XiaoPo lake. IOP Conf Ser Earth Environ Sci 113.

Tables

Table 2.1: The vegetation characteristics, landforms and soil textures of treatment replicates in the Forest Resilience Threshold Experiment (FoRTE) before disturbance severity and type treatments were implemented (2018). Species abbreviations are as follows: POGR (*Populus grandidentata*), ACSA (*Acer saccharum*), ACRU (*Acer rubrum*), FAGR (*Fagus grandifolia*), QURU (*Quercus rubra*), PIST (*Pinus strobus*).

	A	B	C	D
Canopy Tree (> 8 cm DBH) composition	POGR (61%) ACSA (17%) ACRU (10%) FAGR (10%)	POGR (58%) ACRU (24%) QURU (9%) FAGR (4%)	QURU (43%) POGR (39%) PIST (6%) ACRU (6%)	QURU (72%) POGR (19%) PIST (4%) FAGR (1%)
Stem Density (Stems ha ⁻¹ , > 8 cm)	865 (32)	888 (46)	910 (55)	796 (81)
Shannon's index of species diversity	1.05 (0.09)	1.05 (0.05)	1.04 (0.11)	0.92 (0.10)
Leaf area index (dimensionless)	4.1 (0.15)	3.6 (0.08)	3.5 (0.10)	2.9 (0.18)
Biomass (kg C ha ⁻¹)	264,6000 (15,800)	229,900 (24,700)	197,000 (13,900)	155,900 (19,000)
Canopy rugosity (m)	28.8 (3.6)	22.3 (2.3)	14.2 (1.7)	8.9 (1.1)
Landform	Moraine	High-elevation outwash over moraine	High-elevation outwash plain	High-elevation outwash plain
Soil Texture	Sandy loam, calcareous	Medium sand, non-calcareous	Sand, calcareous	Sand, calcareous
Drainage	Well drained	Well drained	Excessively drained	Excessively drained

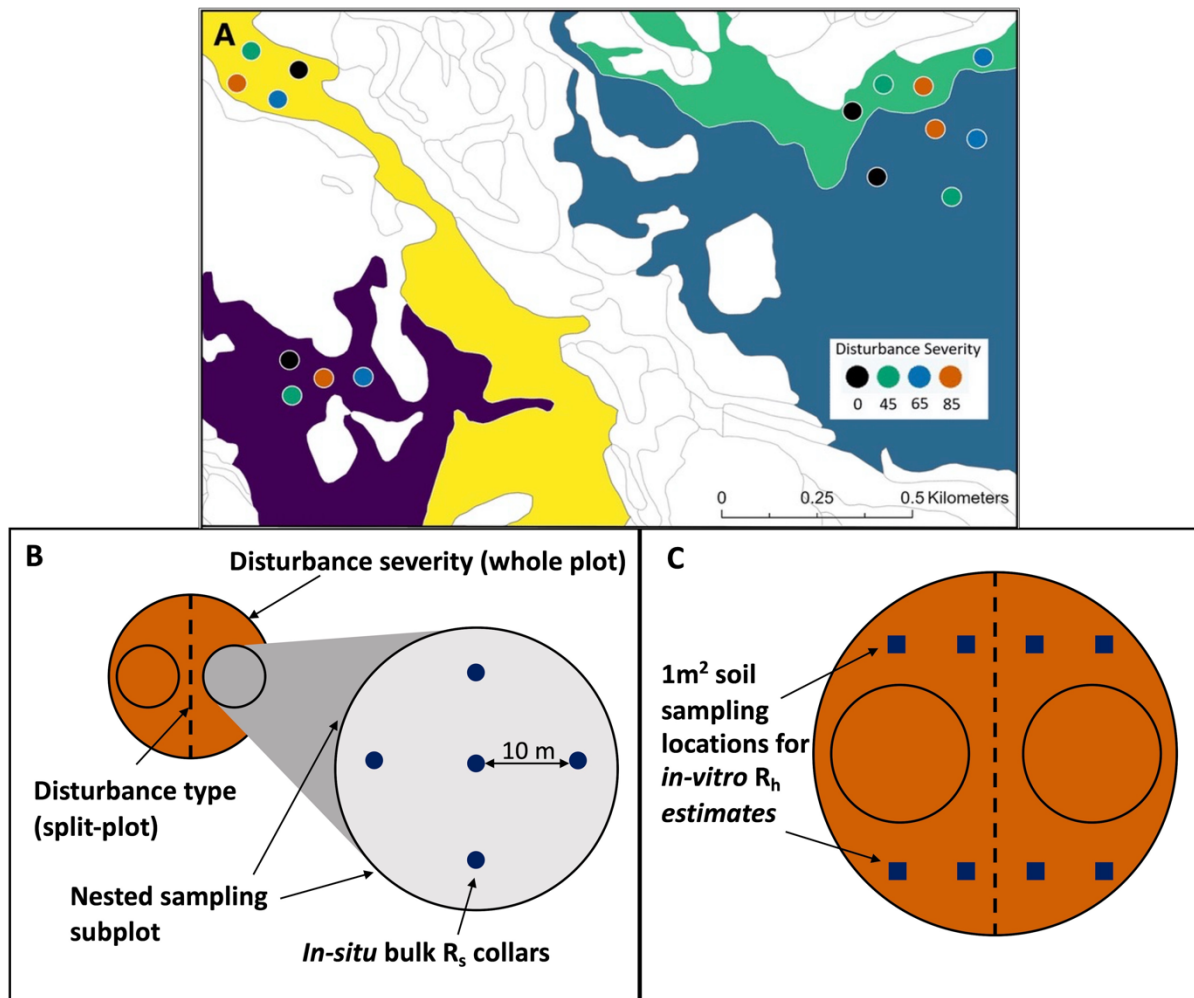


Figure 2.1: Forest Resilience Threshold Experiment (FoRTE) **A)** plot distribution map, **B)** experimental design and layout of *in situ* bulk soil respiration (R_s) collars and **C)** layout of soil sampling locations for *in-vitro* heterotrophic respiration (R_h) estimates.

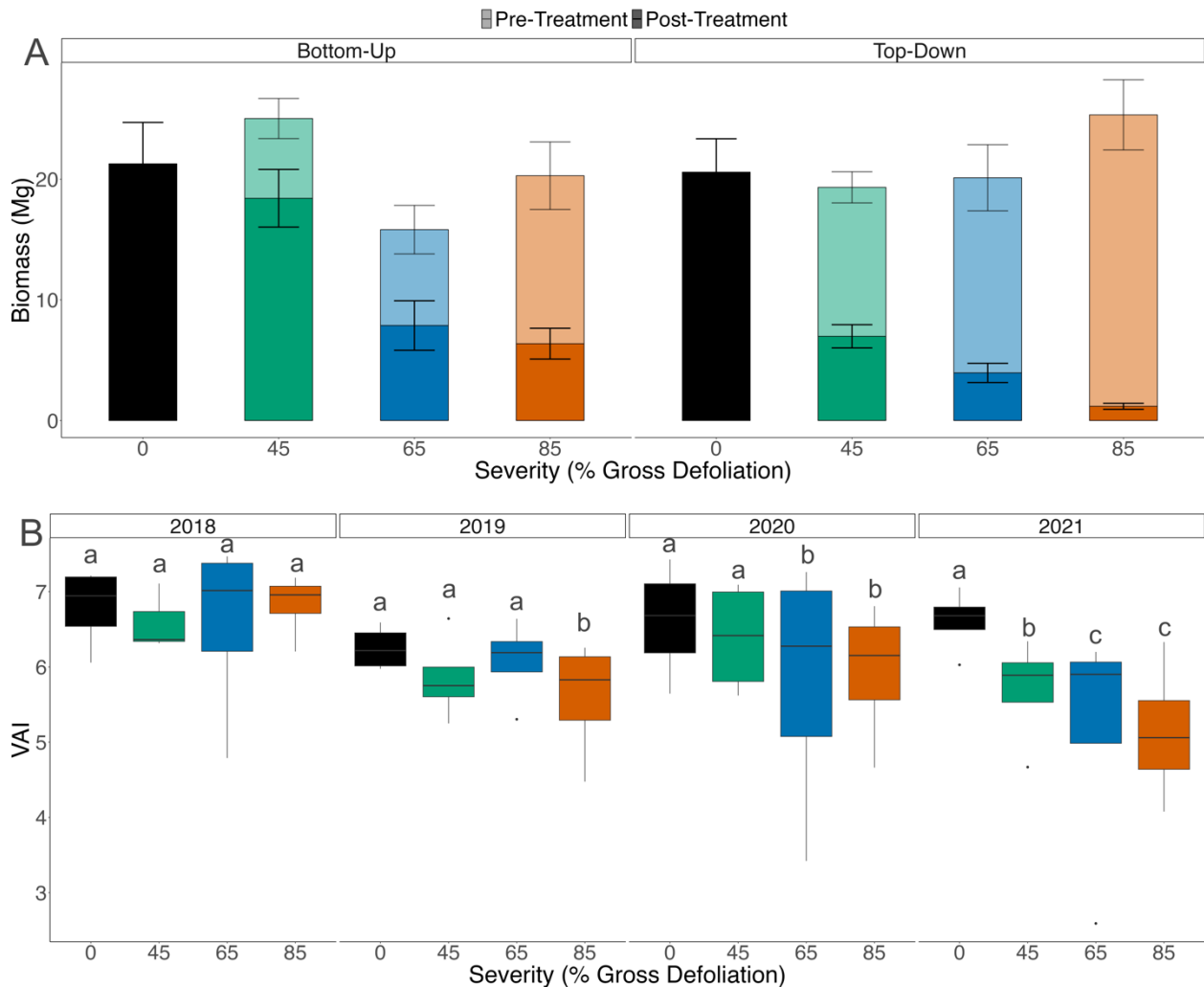


Figure 2.2: A) Mean aboveground wood biomass \pm SE by disturbance severity and disturbance type prior to girdling in 2018 (whole bar) and remaining ungirdled biomass following disturbance treatment applications in 2019 (solid shade only). B) Median, interquartile range (middle 50% of range) and minimum and maximum vegetative area index (VAI) values by disturbance severity for pre-disturbance (2018, gray shading) and post-disturbance (2019-2021) years. Different letters indicate significant within-year differences among disturbance severities ($\alpha = 0.05$, $F = 2.045$, $p = 0.047$).

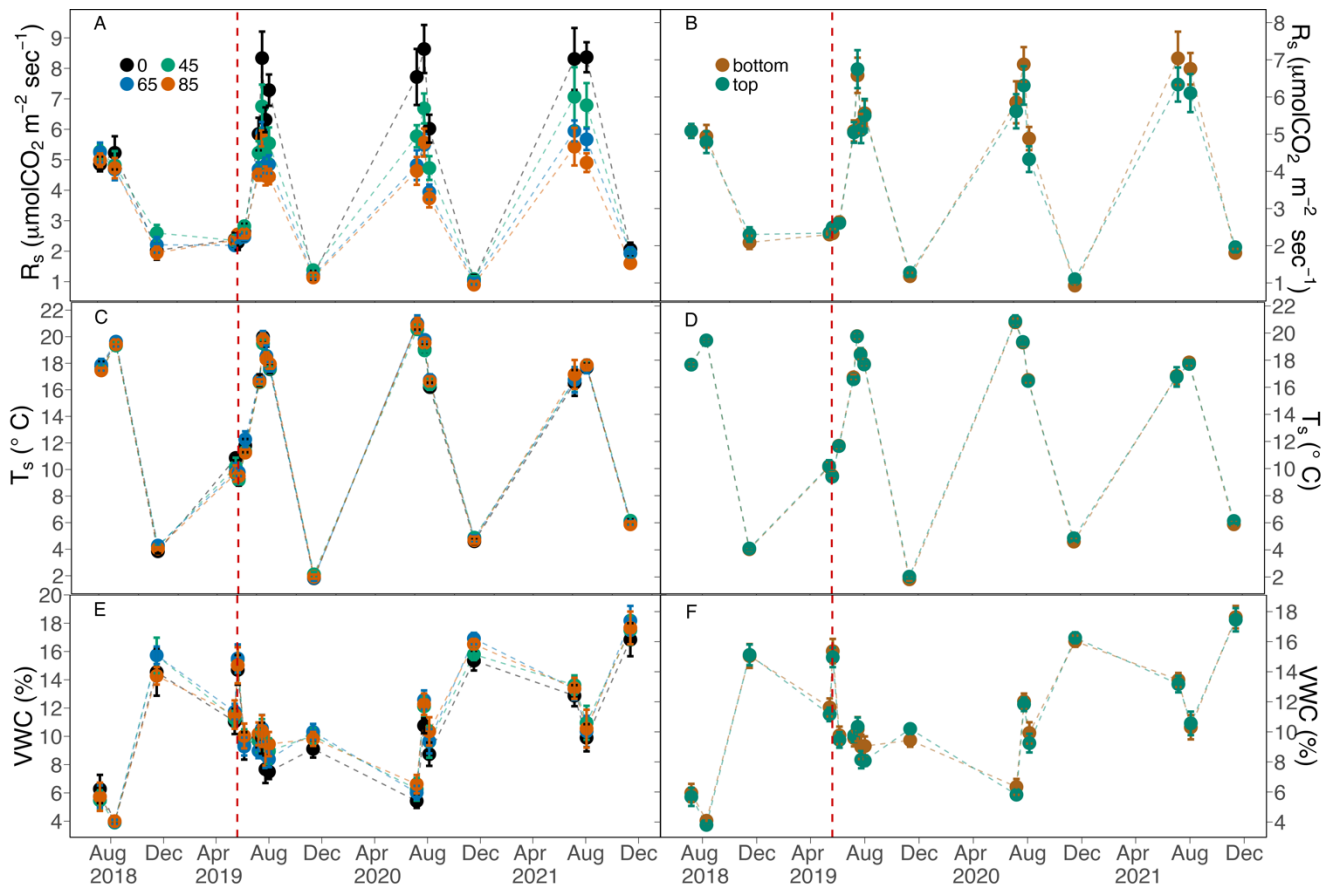


Figure 2.3: Mean (± 1 SE) discrete measurements of soil respiration (R_s ; **A**, **B**), soil temperature (T_s ; **C**, **D**), and volumetric water content (VWC; **E**, **F**) by disturbance severity (left panels) and disturbance type (right panels), 2018-2021. Red vertical dashed line delineates pre- and post-disturbance measurement periods.

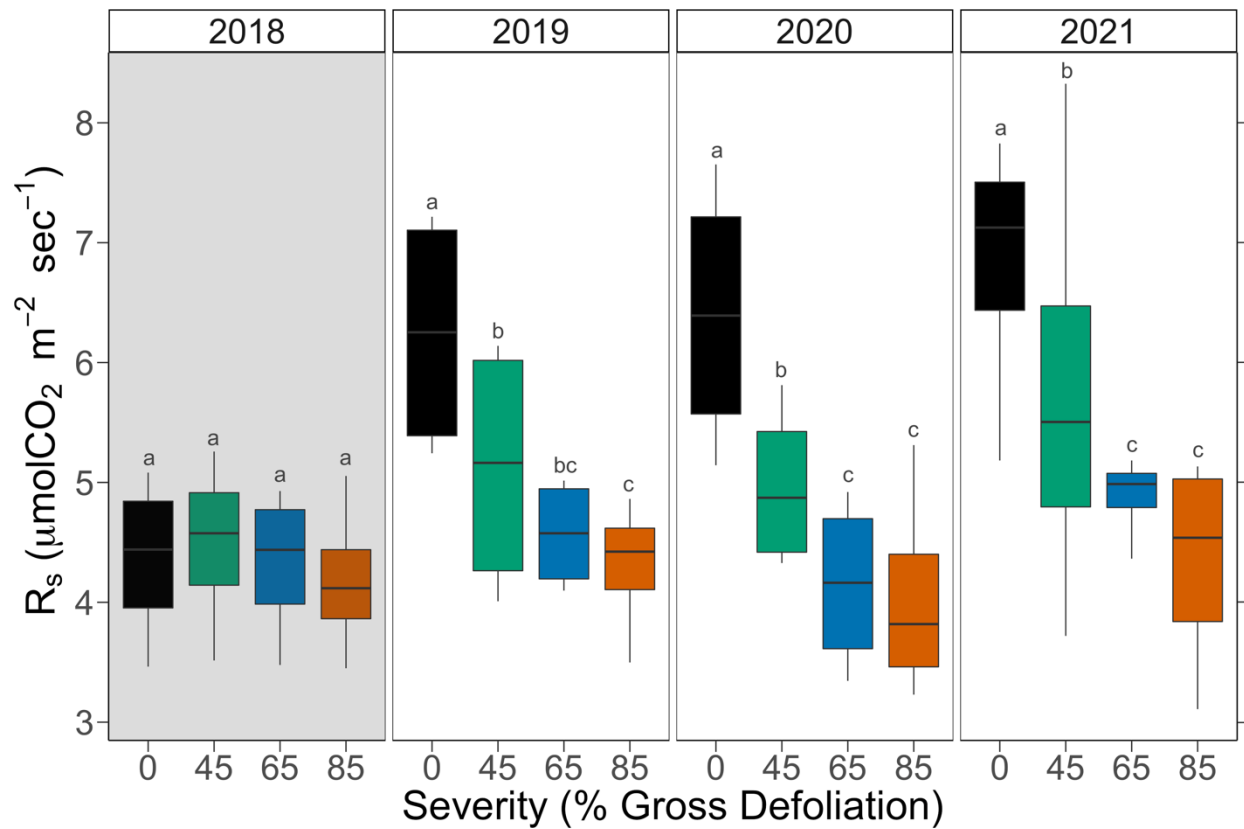


Figure 2.4: Boxplots displaying median, interquartile range (middle 50% of range) and minimum and maximum soil respiration (R_s) values by disturbance severity for pre-disturbance (2018, gray shading) and post-disturbance (2019-2021) years. Different letters indicate significant within-year differences among disturbance severities ($\alpha = 0.05$, $F = 4.42$, $p < 0.001$).

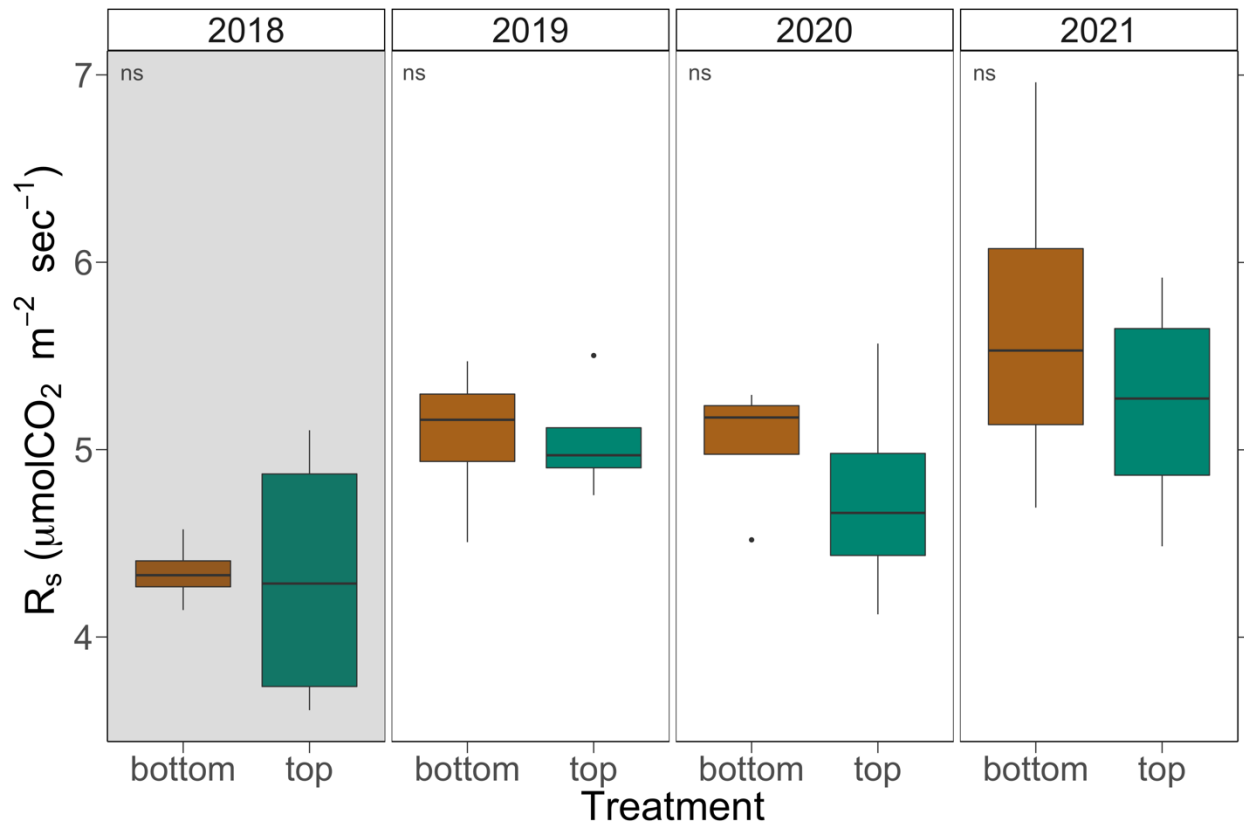


Figure 2.5: Boxplots displaying median, interquartile range (middle 50% of range) and minimum and maximum soil respiration (R_s) values by “top-down” and “bottom-up” disturbance types for pre-disturbance (2018, gray shading) and post-disturbance (2019-2021) years. Within-year comparisons yielded no significant differences ($\alpha = 0.05$, $F = 0.942$, $p = 0.42$).

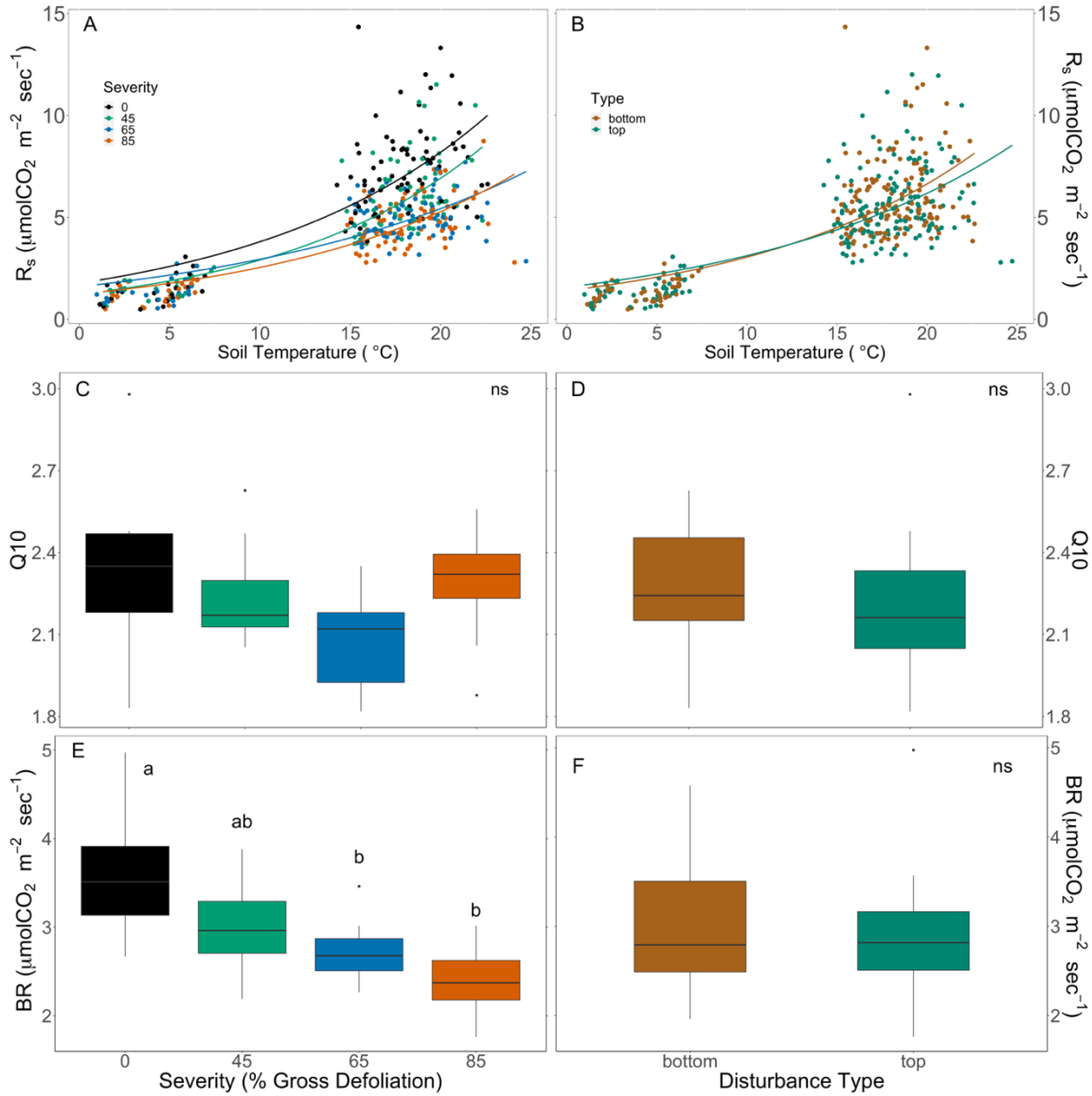


Figure 2.6: Post-disturbance (2019-2021) relationship between soil temperature and R_s using a two-parameter exponential model by **A)** disturbance severity (0,45,65,85% gross defoliation) and **B)** by disturbance type (“top-down” and “bottom-up”). Average Q10 values (increase in R_s for every 10°C in T_s) by **C)** Disturbance severity ($F = 1.847$, $p = 0.21$) and **D)** disturbance type ($F = 1.343$, $p = 0.27$). Average basal R_s rates (BR) at 10°C by **E)** Disturbance severity ($F = 4.418$, $p = 0.04$) and **F)** Disturbance type ($F = 0.17$, $p = 0.690$).

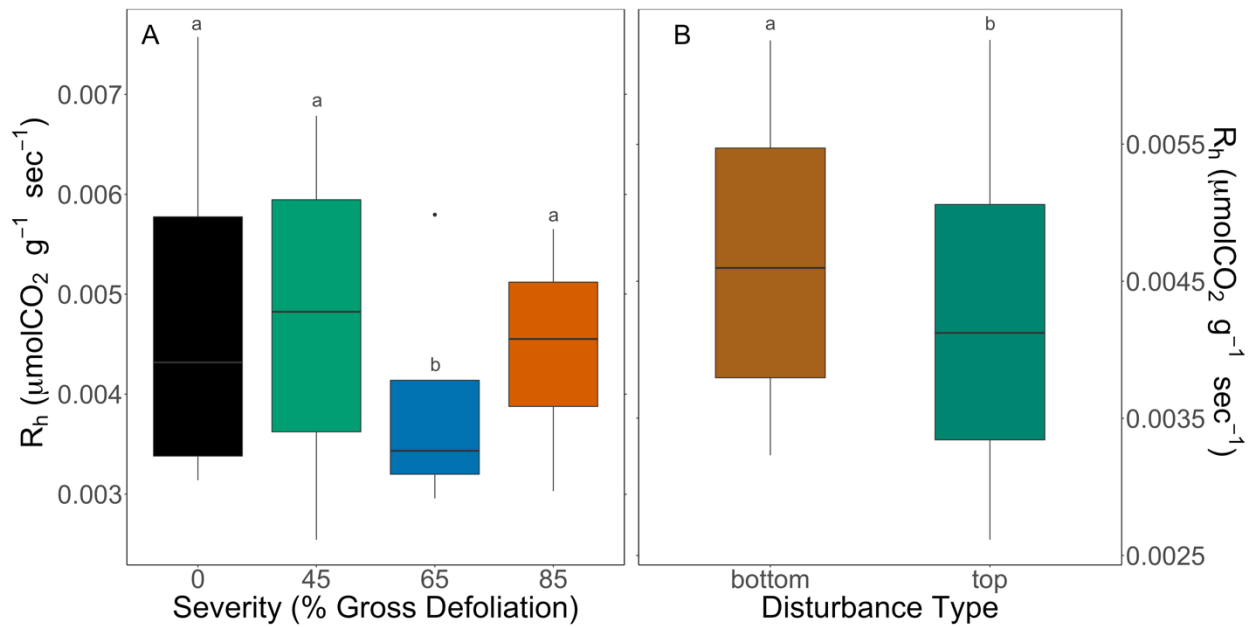


Figure 2.7: Boxplots displaying median, interquartile range (middle 50% of range) and minimum and maximum soil heterotrophic respiration estimates (R_h) of incubated root-free soils (10 cm depth) averaged across all post-disturbance years (2019-2021) by: **A)** disturbance severity ($\alpha = 0.05$, $F = 4.369$, $p = 0.042$) and **B)** “top-down” and “bottom-up” disturbance type ($\alpha = 0.05$, $F = 6.837$, $p = 0.024$). Different letters indicate significant differences among disturbance severities or disturbance type.

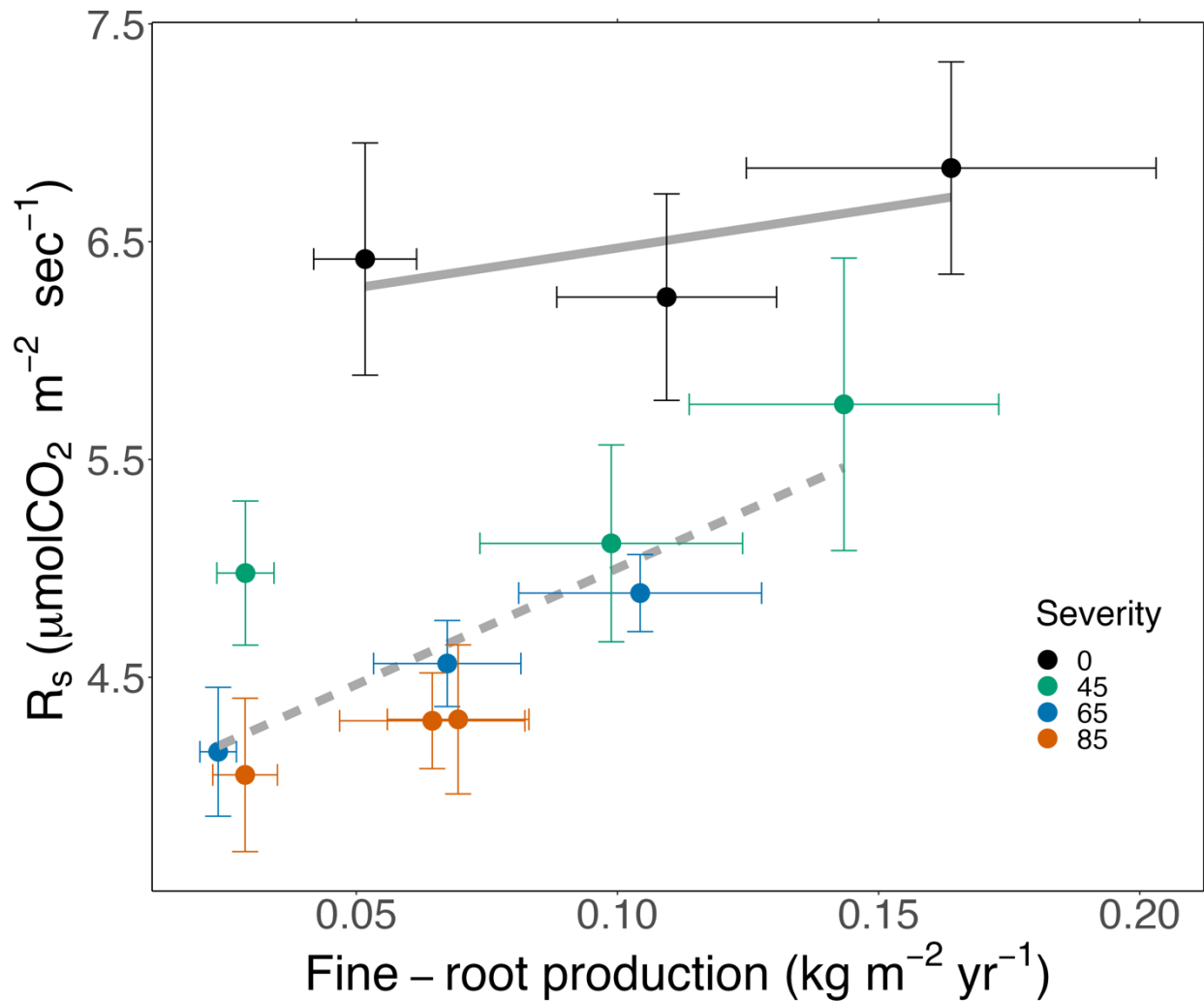


Figure 2.8 Average R_s as a function of fine-root production, 2019-2021 (p -value < 0.001 , Adjusted $R^2 = 0.50$). Solid gray line represents linear relationship between R_s and fine-root production in the control and dotted gray line represents linear relationship between R_s and fine-root production in across disturbance severities. Slopes of the two lines are significantly different from each other (T -value = 2.24, p -value = 0.03).

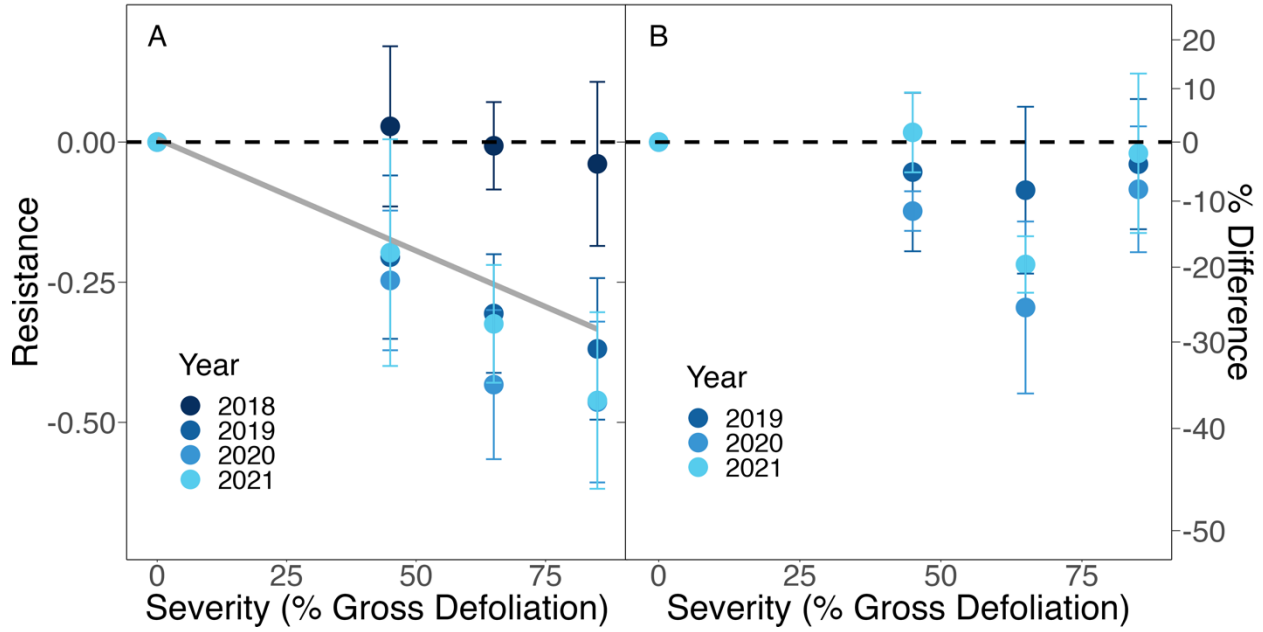


Figure 2.9: **A)** Average R_s resistance and **B)** Average R_h resistance as a function of disturbance severity (% gross defoliation), 2018-2021. Gray line indicates significant linear decline in R_s resistance with increasing disturbance severity between 2019-2021 (p-value: <0.001, Adjusted $R^2 = 0.93$). No significant relationship between R_h resistance and disturbance severity.

Chapter 2 Appendix:

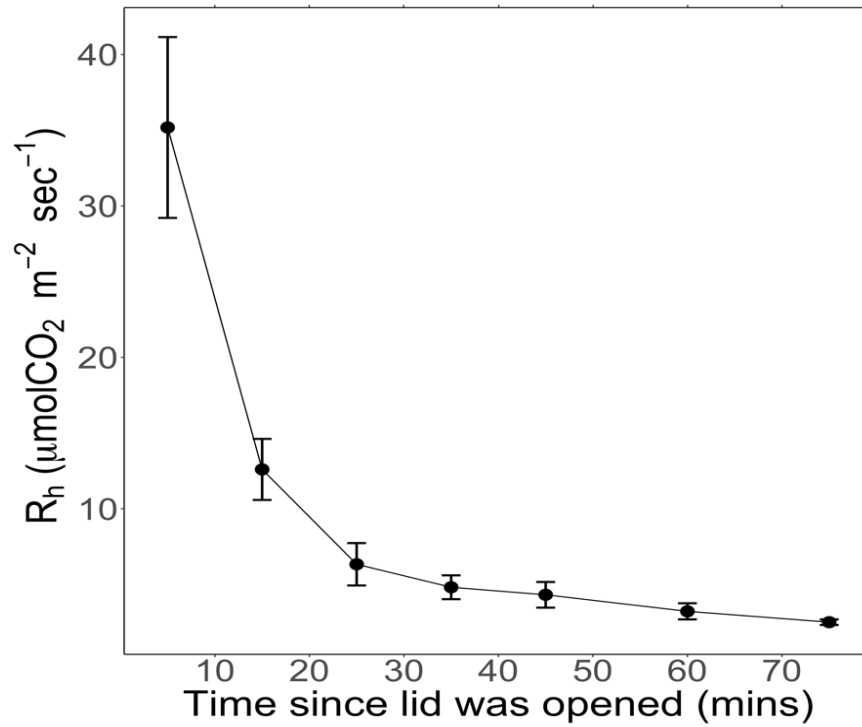


Figure S2.1: Heterotrophic respiration “degassing trial”. Three random samples were selected and efflux ($\mu\text{molCO}_2 \text{ m}^{-2} \text{ s}^{-1}$) was measured at 5-10 minute increments following removal of partially sealed lid to determine time of stabilization in efflux readings following incubation.

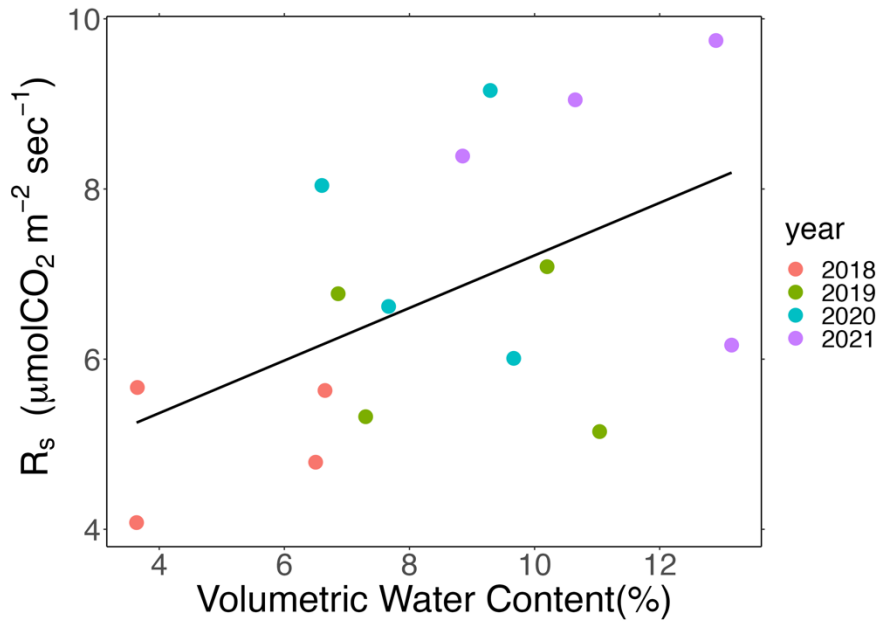


Figure S2.2: Control summertime soil respiration (R_s) as a function of control summertime volumetric water content % (VWC), 2018-2021. Black line indicates significant linear increase in R_s with increasing VWC (p-value: 0.042, Adjusted $R^2= 0.211$). Figure illustrates that low summertime R_s in 2018 was likely driven by low summertime VWC.

Table S2.1a: Summary of ANOVA output for R_s response to experimental disturbance. Split-split plot design with Severity as whole-plot, Type as split-plot, Year as split-split plot and Replicate as blocking factor. Alpha = 0.05. Significance codes: 0.001 = ***, 0.01 = **, 0.05 = *, 0.1 = •.

Source of Variation	Degrees of Freedom	Sum of Squares	Mean Square	F	p-value
Severity	3	58.16	19.387	3.276	0.0728•
Whole Plot Error (Replicate *Severity)	9	53.27	5.919		
Type	1	1.353	1.353	0.641	0.439
Severity*Type	3	5.349	1.783	0.845	0.495
Split-Plot Error (Replicate*Severity*Type)	12	25.326	2.111		
Year	3	20.3	6.767	15.022	<0.001***
Severity*Year	9	17.92	1.991	4.42	<0.001***
Type*Year	3	1.28	0.426	0.946	0.423
Severity*Type*Year	9	2.51	0.278	0.618	0.778
Split-split Plot Error (Replicate*Severity*Type*Year)	72	32.43	0.45		

Table S2.1b: Summary of Least Significant Difference (LSD) for significant Severity*Year interaction (Table S1a) with 95% lower and upper confidence levels. Alpha = 0.05. Levels with the same group letter are not significantly different.

Factor	Mean Square Error	DF Error	Critical Value	LSD
Year	0.703	72	1.993	0.419

Level	R_s	Lower CL	Upper CL	Min	Max	Groups
2018	4.337	4.042	4.633	3.060	6.003	a
2019	5.056	4.760	5.351	3.192	8.616	bc
2020	4.902	4.607	5.198	3.009	8.588	b
2021	5.446	5.151	5.742	2.798	9.007	c

Factor	Mean Square Error	DF Error	Critical Value	LSD
Severity*Year	0.45	72	1.993	0.669

Level	R_s	Lower CL	Upper CL	Min	Max	Groups
0:2021	6.838	6.365	7.311	4.376	9.007	a
0:2019	6.246	5.773	6.718	4.515	8.616	ab
0:2020	6.421	5.947	6.893	4.384	8.588	ab
45:2021	5.753	5.281	6.226	3.653	9.003	bc
45:2019	5.115	4.642	5.588	3.903	7.318	cd
45:2020	4.978	4.506	5.451	4.133	6.58	de
65:2021	4.887	4.414	5.359	4.224	5.59	def
45:2018	4.481	4.008	4.954	3.445	5.301	defg

65:2019	4.563	4.09	5.036	3.932	5.466	defg
0:2018	4.364	3.892	4.838	3.059	6.003	efg
65:2018	4.32	3.848	4.793	3.133	5.437	efg
85:2019	4.3	3.827	4.773	3.192	4.945	fg
85:2021	4.307	3.834	4.779	2.798	5.814	fg
65:2020	4.158	3.685	4.631	3.081	5.486	g
85:2018	4.183	3.71	4.655	3.201	5.275	g
85:2020	4.052	3.579	4.524	3.009	6.034	g

Table S2.2a: Summary of ANOVA output for log transformed R_h response to experimental disturbance. Split-split plot design with Severity as whole-plot, Type as split-plot, Year as split-split plot and Replicate as blocking factor. Alpha = 0.05. Significance codes: 0.001 = ***, 0.01 = **, 0.05 = *, 0.1 = •.

Source of Variation	Degrees of Freedom	Sum of Squares	Mean Square	F	p-value
VWC	1	5.616	5.616	9.965	0.0874•
Error (Replicate)	2	1.127	0.564		
Severity	3	0.5124	0.1708	4.369	0.042*
VWC	1	1.1503	1.1503	29.32	<0.001***
Whole Plot Error (Replicate *Severity)	8	0.313	0.039		
Type	1	0.2252	0.2252	6.837	0.024*
VWC	1	1.0329	1.0329	31.361	<0.001***
Severity* Type	3	0.0584	0.0195	0.591	0.6334
Split-Plot Error (Replicate*Severity* Type)	11	0.3623	0.0329		
Year	2	6.656	3.328	33.663	<0.001***
VWC	1	0.015	0.015	0.151	0.699
Severity*Year	6	0.131	0.022	0.220	0.968
Type *Year	2	0.174	0.087	0.878	0.422
Severity* Type *Year	6	0.063	0.010	0.106	0.995
Split-split Plot Error (Replicate*Severity* Type*Year)	47	4.646	0.099		

Table S2.2b: Summary of Least Significant Difference (LSD) for significant main effects and interactions (Table S2a) with 95% lower and upper confidence levels. Alpha = 0.05. Levels with the same group letter are not significantly different.

Factor	Mean Square Error	DF Error	Critical Value	LSD
Severity	0.0391	8	2.306	0.132

Level	(R_h) log transformed	Lower CL	Upper CL	Min	Max	Groups
0	-5.458	-5.551	-5.364	-6.247	-4.392	a
45	-5.515	-5.608	-5.422	-6.399	-4.466	a
65	-5.651	-5.744	-5.558	-6.403	-4.657	b
85	-5.495	-5.588	-5.401	-6.249	-4.737	a

Factor	Mean Square Error	DF Error	Critical Value	LSD
--------	-------------------	----------	----------------	-----

Type	0.0329	11	2.201	0.0815		
------	--------	----	-------	--------	--	--

Level	(R _h) log transformed	Lower CL	Upper CL	Min	Max	Groups
Bottom-up	-5.481	-5.539	-5.424	-6.403	-4.390	a
Top-down	-5.578	-5.635	-5.520	-6.399	-4.608	b

Factor	Mean Square Error	DF Error	Critical Value	LSD
Year	0.0391	8	2.306	0.132

Level	(R _h) log transformed	Lower CL	Upper CL	Min	Max	Groups
2019	-5.201	-5.313	-5.089	-6.396	-4.390	a
2020	-5.846	-5.957	-5.734	-6.403	-5.038	b
2021	-5.542	-5.654	-5.431	-6.099	-5.059	c

Table S2.3: Summary of ANOVA output for Q10 response to experimental disturbance. Split-plot design with Severity as whole-plot and Type as split-plot, and Replicate as blocking factor. Alpha = 0.05. Significance codes: 0.001 = ***, 0.01 = **, 0.05 = *, 0.1 = •.

Source of Variation	Degrees of Freedom	Sum of Squares	Mean Square	F	p-value
Severity	3	0.3028	0.10093	1.847	0.209
Whole Plot Error (Replicate *Severity)	9	0.4918	0.05465		
Type	1	0.0269	0.02693	1.343	0.2691
Severity*Type	3	0.3489	0.11632	5.799	0.0109 *
Split-Plot Error (Replicate*Severity*Type)	12	0.2407	0.2006		

Table S2.4a: Summary of ANOVA output for Basal soil respiration (BR) response to experimental disturbance. Split-plot design with Severity as whole-plot and Type as split-plot, and Replicate as blocking factor. Alpha = 0.05. Significance codes: 0.001 = ***, 0.01 = **, 0.05 = *, 0.1 = •.

Source of Variation	Degrees of Freedom	Sum of Squares	Mean Square	F	p-value
Severity	3	6.544	2.1814	4.418	0.036 *
Whole Plot Error (Replicate *Severity)	9	4.443	0.4937		
Type	1	0.0384	0.03845	0.167	0.69
Severity*Type	3	0.1774	0.05913	0.256	0.855
Split-Plot Error (Replicate*Severity*Type)	12	2.7686	0.23072		

Table S2.4b: Summary of Least Significant Difference (LSD) for significant main effects (Table S5a) with 95% lower and upper confidence levels. Alpha = 0.05. Levels with the same group letter are not significantly different.

Factor	Mean Square Error	DF Error	Critical Value	LSD
Severity	0.4937	9	2.262	0.795

Level	BR	Lower CL	Upper CL	Min	Max	Groups
0	3.629650	3.067685	4.191616	2.668135	4.973515	a
45	3.016356	2.454391	3.578321	2.189614	3.880921	ab
65	2.731134	2.169169	3.293099	2.264192	3.461719	b
85	2.398683	1.836718	2.960648	1.760931	3.017367	b

Table S2.5a: Summary of ANOVA output for vegetation area index (VAI) response to experimental disturbance. Split-split plot design with Severity as whole-plot, Type as split-plot, Year as split-split plot and Replicate as blocking factor. Alpha = 0.05. Significance codes: 0.001 = ***, 0.01 = **, 0.05 = *, 0.1 = •.

Source of Variation	Degrees of Freedom	Sum of Squares	Mean Square	F	p-value
Severity	3	10.565	2.522	14.34	0.002**
Whole Plot Error (Replicate *Severity)	7	1.719	0.246		
Type	1	1.377	1.3774	1.32	0.277
Severity*Type	3	0.428	0.143	0.137	0.936
Split-Plot Error (Replicate*Severity*Type)	10	10.435	1.043		
Year	3	19.34	6.448	20.33	<0.001***
Severity*Year	9	5.837	0.649	2.045	0.047*
Type*Year	3	1.309	0.436	1.376	0.2575
Severity*Type*Year	9	1.768	0.196	0.62	0.776
Split-split Plot Error (Replicate*Severity*Type*Year)	69	21.88	0.317		

Table S2.5b: Summary of Least Significant Difference (LSD) for significant main effects and interactions (Table S7a) with 95% lower and upper confidence levels. Alpha = 0.05. Levels with the same group letter are not significantly different.

Factor	Mean Square Error	DF Error	Critical Value
Severity	1.121	9	2.262

Level	VAI	Lower CL	Upper CL	Min	Max	Groups
0	6.579	6.1553	7.002	4.893	7.895	a
45	6.125	5.688	6.562	4.107	7.507	ab
65	5.898	5.4678	6.328	2.570	7.541	b
85	5.886	5.463	6.309	3.828	7.528	b

Factor	Mean Square Error	DF Error	Critical Value
--------	-------------------	----------	----------------

Level	VAI	Lower CL	Upper CL	Min	Max	Groups
2018	6.699	6.493	6.904	4.437	7.895	a
2019	5.974	5.773	6.176	3.828	7.016	b
2020	6.182	5.983	6.380	3.122	7.549	b
2021	5.671	5.472	5.869	2.570	7.572	c

Factor	Mean Square Error	DF Error	Critical Value
Severity*Year	0.317	69	1.995

Level	VAI	Lower CL	Upper CL	Min	Max	Groups
85:2018	6.854	6.457	7.251	5.982	7.528	a
0:2018	6.792	6.395	7.189	6.020	7.895	ab
0:2020	6.643	6.246	7.041	4.893	7.549	abc
0:2021	6.611	6.214	7.008	5.912	7.572	abc
45:2018	6.595	6.136	7.054	5.873	7.281	abc
65:2018	6.527	6.131	6.925	4.438	7.510	abc
45:2020	6.359	5.961	6.756	5.389	7.507	abcd
0:2019	6.269	5.872	6.666	5.579	6.875	bcde
65:2019	6.138	5.713	6.562	5.304	7.016	cdef
85:2020	5.917	5.520	6.314	3.936	7.009	def
45:2019	5.915	5.517	6.312	4.750	6.947	def
65:2020	5.808	5.411	6.205	3.122	7.541	def
45:2021	5.749	5.352	6.146	4.107	7.208	ef
85:2019	5.597	5.199	5.994	3.829	7.009	fg
85:2021	5.175	4.778	5.573	4.021	6.345	g
65:2021	5.148	4.751	5.545	2.570	6.546	g

Table S2.6a: Output for regression analysis of R_s as a function of annual fine-root production, disturbance (Disturbance or control) and year (2019, 2020, 2021). Significance codes: 0.001 = ***, 0.01 = **, 0.05 = *, 0.1 = •.

Predictors	Estimates	Standard Error	p-value
(Intercept)	0.0155513	0.0284489	0.599537
Disturbance	-0.0004094	0.0004902	0.427797
Year[2019]	-0.0197044	0.0402328	0.637451
Year[2020]	-0.0198662	0.0402328	0.634731
Year[2021]	-0.0002597	0.0402328	0.995007
Severity*Year[2019]	-0.0040187	0.0006932	0.000406
Severity*Year[2020]	-0.0053648	0.0006932	<0.001***
Severity*Year[2021]	-0.0049425	0.0006932	<0.001***

Residual SE: 0.03088 on 8 df. Adjusted R^2 : 0.9726. F-statistic: 77.15. p-value: <0.001***

Table S2.6b: Estimated marginal means for comparisons of R_s as a function of annual fine-root production and disturbance across three years.

Type	Estimated Marginal Means	SE	df	Lower 95% CI	Upper 95% CI
Disturbance	4.69	0.158	39	5.99	7.26
Control	6.63	0.314	39	4.37	5.01

Table S2.6c: Tukey's Honest Significant Difference test for R_s as a function of annual fine-root production and disturbance across three years.

Contrasts	Estimate	SE	df	t-ratio	p-value
Disturbance-Control	1.94	0.352	39	5.506	<0.001***

Table S2.7a: Output for regression analysis of R_s resistance as a function of year (2018, 2019, 2020, 2021) and disturbance severity (0,45,65,85%). Significance codes: 0.001 = ***, 0.01 = **, 0.05 = *, 0.1 = •.

Predictors	Estimates	Standard Error	p-value
(Intercept)	0.0155513	0.0284489	0.599537
Severity	-0.0004094	0.0004902	0.427797
Year[2019]	-0.0197044	0.0402328	0.637451
Year[2020]	-0.0198662	0.0402328	0.634731
Year[2021]	-0.0002597	0.0402328	0.995007
Severity*Year[2019]	-0.0040187	0.0006932	0.000406
Severity*Year[2020]	-0.0053648	0.0006932	<0.001***
Severity*Year[2021]	-0.0049425	0.0006932	<0.001***

Residual SE: 0.03088 on 8 df. Adjusted R^2 : 0.9726. F-statistic: 77.15. p-value: <0.001***

Table S2.7b: Estimated marginal means for comparisons of R_s resistance as a function of disturbance severity across four years.

Year	Estimated Marginal Means	SE	df	Lower 95% CI	Upper 95% CI
2018	-0.00441	0.0154	8	-0.040	0.0312
2019	-0.22003	0.0154	8	-0.256	-0.1844
2020	-0.28581	0.0154	8	-0.321	-0.2502
2021	-0.24562	0.0154	8	-0.281	-0.2100

Table S2.7c: Tukey's Honest Significant Difference test for R_s resistance as a function of disturbance severity across four years.

Contrasts	Estimate	SE	df	t-ratio	p-value
2018-2019	0.2156	0.0218	8	9.875	<0.001***
2018-2020	0.2814	0.0218	8	12.888	<0.001***
2018-2021	0.2412	0.0218	8	11.047	<0.001***
2019-2020	0.0658	0.0218	8	3.013	0.0653•
2019-2021	0.0256	0.0218	8	1.172	0.6593
2020-2021	-0.0402	0.0218	8	-1.841	0.3230

Table S2.7d: output for R_s resistance post disturbance only

Coefficients	Estimate	SE	t-value	p-value
(Intercept)	0.0022745	0.0229323	0.099	0.923
Severity	-0.0051848	0.0003951	-13.122	<0.001***

Residual SE: 0.04311 on 10 df. Adjusted R²: 0.9396. F-statistic: 172.2, p-value <0.001***

Table S2.8a: Output for regression analysis of R_h resistance as a function of year (2019, 2020, 2021) and disturbance severity (0,45,65,85%). Significance codes: 0.001 = ***, 0.01 = **, 0.05 = *, 0.1 = •.

Predictors	Estimates	SE	p-value
(Intercept)	-0.0124643	0.0966043	0.902
Severity	-0.0006608	0.0016644	0.705
Year[2020]	-0.0224119	0.1366191	0.875
Year[2021]	0.0104790	0.1366191	0.941
Severity*Year[2020]	-0.0012006	0.0023538	0.628
Severity*Year[2021]	-0.0004326	0.0023538	0.860

Residual SE: 0.1049 on 6 df. Adjusted R²: -0.1895. F-statistic: 0.6496. p-value: 0.6737.

Table S2.8b: Estimated marginal means for comparisons of R_h resistance as a function of disturbance severity across three years.

Year	Estimated Marginal Means	SE	df	Lower 95% CI	Upper 95% CI
2019	-0.0447	0.0524	6	-0.173	0.08361
2020	-0.1256	0.0524	6	-0.254	0.00267
2021	-0.0553	0.0524	6	-0.184	0.07300

Table S2.8c: Tukey's Honest Significant Difference test for R_h resistance as a function of disturbance severity across three years.

Contrasts	Estimate	SE	df	t-ratio	p-value
2019-2020	0.0809	0.0741	6	1.092	0.5529
2019-2021	0.0106	0.0741	6	0.143	0.9888
2020-2021	0.0703	0.0741	6	-0.949	0.6324

Table S2.8a: Summary of ANOVA output for vegetation area index (VAI) response to experimental disturbance. Split-split plot design with Severity as whole-plot, Type as split-plot, Year as split-split plot and Replicate as blocking factor. Alpha = 0.05. Significance codes: 0.001 = ***, 0.01 = **, 0.05 = *, 0.1 = •.

Source of Variation	Degrees of Freedom	Sum of Squares	Mean Square	F	p-value
Severity	3	10.565	2.522	14.34	0.002**
Whole Plot Error (Replicate *Severity)	7	1.719	0.246		
Type	1	1.377	1.3774	1.32	0.277
Severity*Type	3	0.428	0.143	0.137	0.936
Split-Plot Error (Replicate*Severity*Type)	10	10.435	1.043		

Year	3	19.34	6.448	20.33	<0.001***
Severity*Year	9	5.837	0.649	2.045	0.047*
Type*Year	3	1.309	0.436	1.376	0.2575
Severity*Type*Year	9	1.768	0.196	0.62	0.776
Split-split Plot Error (Replicate*Severity*Type*Year)	69	21.88	0.317		

Table S2.8b: Summary of Least Significant Difference (LSD) for significant main effects and interactions (Table S7a) with 95% lower and upper confidence levels. Alpha = 0.05. Levels with the same group letter are not significantly different.

Factor	Mean Square Error	DF Error	Critical Value
Severity	1.121	9	2.262

Level	VAI	Lower CL	Upper CL	Min	Max	Groups
0	6.579	6.1553	7.002	4.893	7.895	a
45	6.125	5.688	6.562	4.107	7.507	ab
65	5.898	5.4678	6.328	2.570	7.541	b
85	5.886	5.463	6.309	3.828	7.528	b

Factor	Mean Square Error	DF Error	Critical Value
year	0.317	69	1.995

Level	VAI	Lower CL	Upper CL	Min	Max	Groups
2018	6.699	6.493	6.904	4.437	7.895	a
2019	5.974	5.773	6.176	3.828	7.016	b
2020	6.182	5.983	6.380	3.122	7.549	b
2021	5.671	5.472	5.869	2.570	7.572	c

Factor	Mean Square Error	DF Error	Critical Value
Severity*Year	0.317	69	1.995

Level	VAI	Lower CL	Upper CL	Min	Max	Groups
85:2018	6.854	6.457	7.251	5.982	7.528	a
0:2018	6.792	6.395	7.189	6.020	7.895	ab
0:2020	6.643	6.246	7.041	4.893	7.549	abc
0:2021	6.611	6.214	7.008	5.912	7.572	abc
45:2018	6.595	6.136	7.054	5.873	7.281	abc
65:2018	6.527	6.131	6.925	4.438	7.510	abc
45:2020	6.359	5.961	6.756	5.389	7.507	abcd
0:2019	6.269	5.872	6.666	5.579	6.875	bcde
65:2019	6.138	5.713	6.562	5.304	7.016	cdef

85:2020	5.917	5.520	6.314	3.936	7.009	def
45:2019	5.915	5.517	6.312	4.750	6.947	def
65:2020	5.808	5.411	6.205	3.122	7.541	def
45:2021	5.749	5.352	6.146	4.107	7.208	ef
85:2019	5.597	5.199	5.994	3.829	7.009	fg
85:2021	5.175	4.778	5.573	4.021	6.345	g
65:2021	5.148	4.751	5.545	2.570	6.546	g

Chapter 3: Sustained net ecosystem production across a disturbance severity gradient

Author: Kayla C. Mathes

Contributors: Jeff W. Atkins¹, Cameron Clay², Maxim S. Grigri², Lisa T. Haber², Ariel Johnson², Kerstin M. Niedermaier², Ben-Bond Lamberty³ and Christopher M. Gough¹

Contributor Affiliations:

^{1,2}United States Department of Agriculture Forest Service, Southern Research Station, P.O. Box
700 New Ellenton, SC, 29809

²Department of Biology, Virginia Commonwealth University, Box 842012, 1000 West Cary St.,
Richmond, VA 23284

³Joint Global Change Research Institute, Pacific Northwest National Laboratory, 5825
University Research Ct, College Park, MD 20740

Abstract

The increasing extent of biotic disturbances that produce varying degrees of mortality creates uncertainty for future estimates of temperate forest C balance, or net ecosystem production (NEP). Disturbance severity and fine-scale forest structural properties that vary across a temperate forest landscape are among the factors that could affect NEP following biotic disturbance. We present a three year biometric assessment of NEP and component C fluxes from the Forest Resilience Threshold Experiment (FoRTE), a large-scale experimental disturbance that simulates phloem-disrupting insects. FoRTE contains four levels (0, 45, 65 and 85% gross defoliation) of disturbance severity and was replicated across landscape ecosystems ranging in pre-disturbance structural characteristics. We found stable NEP with increasing disturbance severity for the first three years following phloem-disruption. Stable NEP, even at the highest level of severity, was the result of sustained C uptake—from enhanced subcanopy and sustained canopy production—in tandem with sustained C loss—from slow rates of mortality and lags in disturbance-induced decomposition. Despite the stability of mean landscape-scale NEP, we found a significant interaction with pre-disturbance stand structure and disturbance severity. These results point to the importance of smaller spatial scale structural characteristic that promote material legacies for sustaining C balance at high severities. We conclude that sustained NEP across disturbance severities may support predictions of a stable temperate forest C sink, but longer-term observations are necessary to capture full disturbance response cycles of component C fluxes.

Keywords: carbon balance, forest disturbance, heterotrophic respiration, net ecosystem production, net primary production

1. Introduction

Temperate forests currently account for 34% of global terrestrial C sequestration (Pan et al. 2011), but changing disturbance regimes are threatening the future of this large C sink (Sommerfeld et al. 2018, Edgar and Westfall 2022). Current projections in the US show temperate forests will, on average, remain a strong C sink (Wu et al. 2023), emphasizing the importance of these ecosystems for climate mitigation efforts seeking to preserve and enhance C storage (Fargione et al. 2018). However, rising temperatures and extreme weather events increase the threat of biotic disturbances, and add uncertainty to forecasts of the temperate forest C sink strength (Pugh et al. 2019; Seidl et al. 2017, Flower and Gonzalez-Meler 2015, Albrich et al. 2022). The C cycling consequences of these partial disturbances, which produce gradients of tree mortality (i.e. disturbance severity) on forest landscapes, cannot be predicted from conventional theory (Odum 1969, Harmon et al. 1990; Gough et al. 2013), and most observational studies, which emphasize stand-replacing disturbance (Amiro et al. 2010, Zhao et al. 2021; Campbell et al. 2004; Robinson et al. 2022). Therefore, reducing uncertainties around the future of the temperate forest C sink requires integrative assessments of net C uptake and loss, i.e. net ecosystem production (NEP), following historically understudied, but emerging disturbance sources that produce gradients of severity (Goetz et al. 2012).

Several knowledge gaps persist in our understanding of how, why, and to what extent gradients of disturbance severity affect NEP. For example, while a subset of component fluxes of NEP have been studied across multiple disturbance severities (Levy-Varon et al. 2014, Fu et al. 2017, Grigri et al. 2020, Gough et al. 2021a), studies of total net C balance, or NEP, are typically limited to a single level of severity. Furthermore, the response of NEP to partial disturbance is

variable with some forests exhibiting sustained NEP because of rapid compensatory vegetation growth (Gough et al. 2013) and other displaying immediate declines as decomposition of disturbance-driven detritus increases (Clark et al. 2010; Zhao et al. 2021). NEP assessments across disturbance severity gradients that consider all C uptake and loss fluxes through biomass pools are particularly rare because they are onerous and are made with high uncertainty (Bond-Lamberty et al. 2004, Harmon et al. 2011, Clay et al. 2022). Despite these challenges, biometric approaches to estimating NEP are valuable because they provide a more comprehensive accounting of how all component fluxes respond to disturbance, and in aggregate, affect C balance.

Within forested landscapes, disturbance severity and biotic factors such as forest structure may influence smaller-scale variation in NEP. For example, structural characteristics, such as quantity and arrangement of biomass (i.e. structural complexity, Hardiman et al. 2011) are well established drivers of forest functions, including C cycling (Tang et al. 2017; Gough et al. 2019). Disturbances can alter structure through deteriorating canopy cover and shifting biomass into the coarse woody debris pools, with consequences for C uptake and loss (Ivanov et al. 2022; Curtis and Gough 2018). Furthermore, ecological theory (Johnstone et al. 2016) and empirical studies (Niedermaier et al. 2022; Brown et al. 2010; Taylor et al. 2017) suggests *pre*-disturbance forest structures that promote material legacies (i.e. surviving biomass) from large seed banks or subcanopy vegetation can also drive functional disturbance response. While ecologists have long-studied how stand structure before and after disturbance informs C cycling response (Turner et al. 2016; Atkins et al. 2020; Gough et al. 2022), less is known about how variation in *pre*-disturbance stand structure interacts with disturbance severity to determine landscape level C

cycling and C balance (Gough et al. 2021a). Because temperate forest landscapes are often a composite of fine-scale variation in stand structure (Ehbrecht et al. 2019; Nave et al. 2019), assessing NEP across disturbance severities *and* pre-disturbance stand structures is important for modeling and predicting which systems will show higher stability to future disturbance regimes.

We used a replicated, large-scale manipulation, the Forest Resilience Threshold Experiment (FoRTE), to evaluate how NEP and its component fluxes respond to a gradient of disturbance severity. Established in 2018, FoRTE uses stem-girdling to achieve gross defoliation disturbance severity levels of 0, 45, 65 and 85%, which are replicated across representative temperate forest landscape ecosystem types in the Upper Great Lakes region. We use stem-girdling to mimic disturbances from phloem-disruption insects, such as emerald ash borer (Davis et al. 2019) and mountain pine beetle (Meyer et al. 2018), which are increasing in North American temperate forests (Edgar and Westfall 2022). Our specific objectives are to: 1) quantify 3-year annual NEP across a gradient of disturbance severity, 2) determine which component C fluxes drive NEP's response, and 3) assess whether stand structure prior to disturbance impacts NEP's response to disturbance. We hypothesize that: 1) NEP will not decline in response to rising disturbance severity during the first three years. 2) Relative stability in NEP will be driven by the opposing responses in NPP and R_h . Specifically, increases in subcanopy contributions that fully compensate for losses in canopy NPP_w (Niedermaier et al. 2022; Grigri et al. 2020) and stable R_{sh} (Mathes et al. *in review*) across the severity gradient will be primary drivers of NEP stability in the first three years following disturbance. 3) Pre-disturbance biomass will explain significant variation in NEP response to disturbance.

2. Methods

2.1 Study site and experimental design

Our study site is located at the University of Michigan Biological Station (UMBS) in Pellston, MI, USA (45.56 N, 84.67 W). The mean air temperature is 5.5 °C and mean precipitation is 817 mm (Gough et al. 2021b). The ecosystem is a Northern temperate mixed deciduous-pine forest in transition from early to mid-successional stages. Landscape variation in productivity, microclimate, community composition, diversity and soil types are due to underlying glacial landforms, creating distinct landscape ecosystem types (Pearsall et al. 1995). Our disturbance treatment replicates are located on ecosystems formed from high-elevation outwash plains and interlobate moraines and are representative of the range of forest ecosystems type in the region (Nave et al. 2019). The outwash sites are in successional transition from *Populus gradidentata* dominated canopy to *Acer rubrum*, *Quercus rubra* and *Pinus strobus* dominated canopy and subcanopy. The outwash soils are characterized by excessively well drained sandy spodosols. The moraine sites are in successional transition from *P. gradidentata* dominated canopy to *Acer saccharum*, *Fagus grandifolia*, *Q. rubra* and *Acer pennsylvanicum* dominated canopy and subcanopy. The moraine soils are characterized by well-drained sandy-loam spodosols. (Mathes et al. *in review* ; Pearsall et al. 1995).

The Forest Resilience Threshold Experiment (FoRTE) was established to study structural and functional mechanisms driving C cycling responses across a range of disturbance severities. While previous analyses have focused on early responses in aboveground woody net primary production (Grigri et al. 2020, Niedermaier et al. 2022), leaf-level physiology (Haber et al. *in*

review) and soil respiration (Mathes et al. *in review*), here we synthesize C fluxes to estimate NEP in the first 3 years following disturbance. In June and July 2018 (pre-disturbance) a full canopy stem survey (>8cm diameter at breast height, DBH) was conducted to quantify pre-disturbance biomass, vegetation structure and species composition (Table 3.1). Then, in May 2019, we stem girdled ~ 3600 canopy trees (> 8cm DBH). The experiment was replicated across four distinct landscape-ecosystem types that represent significant variation in community composition, productivity, structural complexity and soil types of the region (Table 3.1, Mathes et al. *in review*).

The four replicates contained four 0.5 ha circular whole plots (n = 16) randomly assigned to targeted levels of gross defoliation from leaf area index measurements of 0% (control), 45%, 65% and 85%, which represent the gradient of disturbance severity (Figure 3.1a). Each whole plot was then split into two 0.25 ha split-plots (n = 32) that were randomly assigned either “top-down” or “bottom-up” disturbance treatments. The “top-down” treatment was achieved by starting with the largest canopy trees by DBH and girdling consecutively smaller trees until the targeted severity level was reached. In contrast, in the “bottom-up” treatment, we started with the smallest trees by DBH and girdled larger trees until the severity level was reached. Finally, within each split-split plot, we established one 0.1 ha subplot (n = 32) where a suite of C fluxes were measured (Figure 3.1b,c, Atkins et al. 2021). Because our research objectives focus on NEP response to the disturbance severity treatments and previously C fluxes have, so far, been minimally impacted by the FoRTE disturbance types (Mathes et al. *in review*, Niedermaier et al. 2022), we excluded assessments of this treatment in this analysis.

2.2. Net Primary Production (NPP)

2.2.1. Above and belowground wood net primary production ($ANPP_w$, $BNPP_w$)

Aboveground woody net primary production ($ANPP_w$) of canopy (>8 cm DBH) and subcanopy (<8 cm DBH) trees were calculated using site-specific protocols (Grigri et al. 2020 and Niedermaier et al. 2022). Briefly, we censused all canopy and subcanopy trees in 2018 and dendrometer bands were installed on 25% of all canopy trees, both girdled and ungirdled ($n = 666$). Dendrometer band readings were recorded at least once during spring and autumn to capture annual stem increment. The DBH increment of unbanded canopy trees was estimated using subplot and species-specific relative growth rates calculated from banded trees of the same species (Grigri et al. 2020). Aboveground biomass (M_a) was estimated from site-level allometric equations (Gough et al. 2007) and annual increments of wood biomass were then scaled to the subplot to calculate canopy $ANPP_w$ ($Mg\ C\ ha^{-1}\ yr^{-1}$). A site-specific C fraction of 0.49 was applied to convert from wood mass to C mass (Gough et al. 2007). Subcanopy $ANPP_w$ was measured from annual DBH measurements of 8 subcanopy trees per subplot. Four vegetation plots were established in each 0.1 ha subplot and 2 subcanopy trees from each vegetation plot were randomly selected (Figure 3.1b). Subcanopy biomass was then calculated with species and site-specific allometric equations and scaled to $ANPP_w$ ($Mg\ C\ ha^{-1}\ yr^{-1}$) based on survey stem densities.

The net primary production ($BNPP_w$) of coarse roots (> 2mm) was estimated from the global relationship between aboveground and belowground woody biomass densities (Cairns et al. 1997). Belowground biomass (M_b) was estimated from subplot-level canopy M_a values using

Equation 1 (Cairns et al. 1997). Annual estimates of production ($\text{Mg C ha}^{-1} \text{ yr}^{-1}$) were derived from annual plot-scale M_b increments, applying a site-specific C fraction of 0.47 to convert from woody to C mass (Gough et al. 2007).

$$\text{Equation 1: } M_b = e^{-1.0850 + 0.9256 * \ln(Ma)}$$

2.2.2 *Fine-root net primary production (NPP_{fr})*

Annual net primary production of fine roots ($< 2\text{mm}$, NPP_{fr}) was calculated using root in-growth cores. We installed 4 hard plastic 2 mm mesh cores to 30 cm depth in each subplot at the beginning of each growing season (Figure 3.1b). In-growth cores were filled with sieved soil taken from nearby sites with similar compositional and soil properties as those from the FoRTE ecosystem types (Pearsall et al. 1995). Cores were harvested each year in mid-November to capture the majority of annual fine-root production. Harvested cores were kept at 4°C until processed to prevent decomposition. Cores were then aggregated by subplot and carefully sieved, washed with DI water and dried for 48 hours at 60°C before weighing. To account for mineral content, three subsamples from each replicate ($n = 12$) were randomly selected and burned in a muffle furnace for 12 hours at 500°C and mineral-free mass adjustments were applied to dry mass root values. Fine-root mass estimates were inferred to a soil depth of 1 m using a site-specific fine-root biomass attenuation curve (Gough et al. 2007). Finally, our control NPP_{fr} estimates were, on average, 60% lower than previously published estimates at our site using multiple methods (Gough et al. 2008), which is consistent with studies showing a frequent underestimation of annual fine-root production from direct in-growth core methods (Fahey and Hughes 1994). To account for this underestimation we normalized our values to published estimates of NPP_{fr} using independent minirhizotron-based methods. To do so, we first adjusted

control values to average published estimates on the same landscape-ecosystem type (Gough et al. 2008). Then, we proportionally adjusted values across the treatments so that relative differences across all values were conserved. In-growth core estimates of root production were then scaled to $\text{Mg C ha}^{-1} \text{ yr}^{-1}$ and a site-specific C fraction of 0.49 was applied (Gough et al. 2007).

2.2.3. Leaf litter (NPP_{ll}) and fine debris production (NPP_{fwd})

We estimated annual leaf (NPP_{ll}) and fine debris (NPP_{fwd}) production from litter traps. Four 0.26 m^2 rectangle fine mesh litter traps positioned ~ 0.5 m above the forest floors were installed in each subplot in 2018 (Figure 3.1b). Litter traps were spatially paired with soil respiration, moisture, and temperature measurements as well as fine-root in-growth cores. Leaf litter and fine debris were collected from all traps every year following leaf fall in November and stored at 4°C to prevent decomposition. Litter was then sorted into leaf and fine debris, dried for 48 hours at 60°C and weighed to determine dry mass. Subplot NPP_{ll} and NPP_{fwd} were determined from scaled values of annual production ($\text{Mg C ha}^{-1} \text{ yr}^{-1}$) and a site-specific C fraction of 0.48 was applied to estimate C mass from dry mass (Gough et al. 2007).

2.3. Heterotrophic respiration (R_h)

2.3.1 Coarse woody debris respiration (R_{cwd})

To estimate the CO_2 efflux associated with coarse woody debris decomposition (R_{cwd} , $\text{MgC ha}^{-1} \text{ yr}^{-1}$), we employed three independent methods because of the high uncertainty associated with this flux (Schmid et al. 2016). For each of these methods we used a coarse woody debris (CWD) survey conducted in summer of 2019 before extensive tree mortality occurred as a pre-

disturbance reference. In this study, CWD is defined as any dead standing or downed woody material > 8 cm DBH. During the survey, we recorded the length and diameters of all CWD material at three points, sorting each sample into one of five decay classes (Marra and Edmonds 1994). The volume of each CWD sample was calculated from diameter and height measurements using the Newton equation described in Harmon and Sexton, 1996. CWD carbon mass (M_{cwd} , Mg C ha⁻¹) was calculated by applying a site- and decay class-specific C fraction to CWD volumes (Gough et al. 2007). The subsequent annual growth of the CWD pool was estimated from annual banded-tree mortality surveys, reassigning newly dead trees to CWD decay class 1 and estimating their volume using Harmon and Sexton (1996). Since individual tree heights were not measured, we derived CWD volumes from estimates of subplot median canopy height via portable canopy lidar (Atkins et al. 2021). Because data from our site suggest the residence time of CWD in a decay class is > 2 years (Schmid et al. 2016), we assumed CWD did not advance to later decay stages during our study (Schmid et al. 2016); thus, annual changes in CWD pool size and, consequently, R_{cwd} , are primarily driven by new tree mortality associated with the experimental disturbance.

We then estimated the flux of CO₂ from CWD (R_{cwd}) using two approaches determining C mass loss from two independently derived decay rates and one approach modeling instantaneous R_{cwd} flux from temperature and moisture values. Our first method ($R_{cwd,1}$) used site- and climate-specific decay constants to estimate mass loss from the total pool of woody debris (Dai et al. 2021, Equation 2):

$$\text{Equation 2: } \ln(M_t) = \ln(M_0) + k_5 * \ln(t+1) - k_4 * t$$

where M_t is the remaining M_{cwd} at time t (years), M_0 is initial M_{cwd} and k_4 and k_5 are climate-specific decay constants ($k_4 = 0.12$, $k_5 = 0.099$). Rather than site-specific and generalized across species, our second approach ($R_{cwd,2}$) used species-specific CWD decay constants (Kahl et al. 2017, Table S3.1). To estimate $R_{cwd,2}$, we first calculated community weighted species-specific decay constants for each subplot based on the biomass proportion of canopy constituents. M_{cwd} loss was then calculated as the product of the community weighted mean decay constant and M_{cwd} . For methods 1 and 2, annual M_{cwd} was always calculated as the sum of remaining M_{cwd} from the previous year and annual M_{cwd} additions from mortality surveys. Subplot estimates of M_{cwd} loss were scaled to annual estimates of $R_{cwd,1}$ and $R_{cwd,2}$ ($Mg\ C\ ha^{-1}\ yr^{-1}$). We assumed the total annual loss of M_{cwd} was equal to the CO_2 flux emitted because of negligible C leaching and exports from the CWD pool (Schmid et al. 2016; Laiho and Prescott, 1999). Our final method ($R_{cwd,3}$) used a site-specific model relating CWD temperature (T_s) and gravimetric water content (θ) to instantaneous R_{cwd} ($\mu mol\ C\ kg^{-2}\ s^{-1}$) (Schmid et al. 2016; Equation 3).

$$\text{Equation 3: } R_{cwd} = -1.2773 * e^{-0.0339 * T + 0.2493(\theta)}$$

Because T_s was not measured continuously, we first developed models relating point measurements within each subplot to continuously recorded T_s from a nearby site. We estimated continuous 6-hour soil temperatures (T_s) for each subplot from regression equations relating continuous T_s measurements from an onsite Ameriflux meteorological tower (US-UMB, Gough et al. 2016) to T_s point measurements (Figures S3.1). For estimates of gravimetric water content (θ), we used site-specific estimates generated for each decay class (Gough et al. 2008). Continuous $R_{cwd,3}$ was then scaled to annual estimates of coarse woody debris C flux ($Mg\ C\ ha^{-1}\ yr^{-1}$).

2.3.2 Soil heterotrophic respiration (R_{sh})

To estimate annual soil heterotrophic respiration (R_{sh}), we employed a multi-step process that yielded four partially independent estimates of R_{sh} for each subplot. For all estimates, we first calculated the annual total soil respiration (R_s) for each subplot from models developed using instantaneous soil respiration measurements. We then estimated the fraction of annual R_s originating from heterotrophs, annual R_{sh} , for each of the control subplots using two global relationships relating R_{sh} to R_s developed from meta-analyses of undisturbed forests. To account for the effects of disturbance severity, we then calculated separate R_{sh} values for the 45%, 65%, and 85% gross defoliation treatments based on relative differences in control and disturbance treatment R_{sh} , determined from jar incubations of root-free soils and an Ecosystem Demography model (ED 2.2 Dorheim et al. 2022). The application of two global models for the derivation of control R_{sh} and two methods for adjusting for disturbance severity generated four R_{sh} estimates per subplot for each year.

Specifically, we measured instantaneous *in-situ* R_s and soil temperature to 7 cm depth (T_s) from 160 soil collars with a LI-COR 6400 3-7 times during the growing season and once in the dormant season between 2019-2021 (Mathes et al. *in review*). Continuous R_s for each year and subplot was estimated using a 2-parameter exponential temperature-response function (Equation 4), and then scaled to annual R_s ($\text{g C m}^{-2} \text{ yr}^{-1}$).

$$\text{Equation 4: } R_s = a * e^{(b * \text{soil } T)}$$

Subplot 6-hourly T_s was calculated from regression models relating concurrent measurements of *in-situ* subplot T_s and continuous flux tower T_s (US-UMB, Gough et al. 2016, Figure S3.1).

Then, to partition R_s and estimate annual R_{sh} ($\text{Mg C ha}^{-1} \text{ yr}^{-1}$) in the control plots, we used two global $R_{sh}:R_s$ relationships (Equation 5 & 6, Bond-Lamberty et al. 2004; Subke et al. 2006).

$$\text{Equation 5: } \ln(R_{sh}) = 1.22 + 0.73 * \ln(R_s)$$

$$\text{Equation 6: } R_{sh}/R_s = -0.138 \ln(R_s) + 1.482$$

We did not use these global relationships to estimate annual R_{sh} in the disturbance treatments because studies at our site (Mathes et al. *in review*) and elsewhere (Hogberg et al. 2001) show that phloem-disruption disturbances can change the relationship between R_{sh} and R_s . Therefore, we used two different approaches to estimate relative response in R_{sh} to the experimental disturbance gradient. Our first method uses measurements of the heterotrophic respiration flux of surface soils using a root-free soil incubation protocol described in Mathes et al. *in review*. Briefly, we collected soil to 10 cm depth from four 1 m² sampling squares located on the north and south ends of each subplot (Figure 3.1c, n = 128) once a year in July or August between 2019-2021. Following field collection, soils were sieved to remove roots and placed in glass jars with a 1 mm ventilation hole. Jars were then incubated for 2 weeks at the average soil temperature on day of collection. Following incubation, unadjusted CO₂ efflux ($\mu\text{mol CO}_2 \text{ m}^{-2} \text{ s}^{-1}$) was measured with a LI-6400 portable gas analyzer (LI-COR Inc, Lincoln, NE, USA) and custom cuvette system fitted to soil filled glass jars. R_{sh} ($\mu\text{mol CO}_2 \text{ g}^{-1} \text{ s}^{-1}$) was estimated by converting fixed area based efflux measurements ($\mu\text{mol CO}_2 \text{ m}^{-2} \text{ s}^{-1}$) to soil sample-specific dry mass R_{sh} . For our second method, we used Ecosystem Demography 2.2. (ED 2.2) projections of C fluxes subjected to the FoRTE experimental design (Dorheim et al. 2022) to determine relative differences in R_{sh} across the disturbance severities. ED 2.2. uses a cohort-based approach to

solve systems of differential equations that describe energy and carbon movement through a terrestrial ecosystem following a simulation of disturbance (Dorheim et al. 2022).

Finally, we estimated annual R_{sh} ($Mg\ C\ ha^{-1}\ yr^{-1}$) for all disturbance severities and years by adjusting control R_{sh} , measured from two global $R_{sh}:R_h$ relationships, to the relative change across disturbance severities measured from jar incubations ($R_{sh,1}$ & $R_{sh,2}$) and modeled using ED ($R_{sh,3}$ & $R_{sh,4}$). Specifically, annual R_{sh} in each disturbance severity was calculated as the product of annual control R_{sh} ($Mg\ C\ ha^{-1}\ yr^{-1}$) and jar R_{sh} (control): jar R_{sh} (disturbance severity), and separately from the product of annual control R_{sh} and ED modeled R_{sh} (control) : ED modeled R_{sh} (disturbance severity).

2.4 Net ecosystem production (NEP)

To estimate annual net ecosystem production (NEP), we used a biometric approach that summarizes the component NPP (i.e. C sinks) and R_h (i.e. C source) fluxes (Clay et al. 2022; Gough et al. 2007; Gough et al. 2008). Because estimates of heterotrophic respiration, in particular, are highly uncertain, we present twelve separate estimates of NEP derived from the combination of independent estimates of R_{cwd} and R_{sh} . We show the standard error for each NEP estimate as the quadratic sum of component flux errors (Gough et al. 2007). Sources of error include spatial variation across experimental replicates and, for modeled estimates of R_{cwd} and R_{sh} , compounding error associated with modeled continuous T_s . Net ecosystem production (NEP) was estimated as:

$$NEP = (ANPP_w + BNPP_w + NPP_{ll} + NPP_{fwd} + NPP_{fr}) - (R_{sh} + R_{cwd})$$

2.5 Statistical analysis

To analyze the effect of disturbance severity on NEP (O1) and all above and belowground C fluxes (O2), we ran repeated measures split-plot fully replicated ANOVA models with alpha values set to 0.05 (Gough et al. 2021a; Mathes et al *in review*). We used replicates as the blocking factor, severity as the whole-plot factor and year as the split-plot factor. All models met assumptions of equality of variance and normality without transformation except for subcanopy ANPP_w, which required a log transformation. The error in all statistical analyses was an expression of spatial variation in measured fluxes. Our statistical analyses compared average rather than method-specific R_{sh}, R_{cwd} and NEP values. Post-hoc pairwise analyses (alpha = 0.05) were performed using Fisher's Least Significant Difference (LSD) tests (See Table S3.2 – S3.11 for full ANOVA models and post-hoc output).

To assess how pre-disturbance stand structure impacts NEP disturbance response (O3), we ran a multivariate regression analysis testing NEP as a function of pre-disturbance biomass, severity and year. The analysis met all assumptions of normality, equality of variance and influential values without transformation (See Table S3.12 for full regression model output). All analyses were performed in R (R Core Team 2022), the split-plot ANOVA was made in the package “stats” (R Core Team 2022), the LSD test was conducted using the package “agricolae” (de Mendiburu 2021) and all figures were made in the package “ggplot2” (Wickham 2016).

3. Results

3.1. Net primary production fluxes and disturbance severity

We observed stable total NPP across the disturbance severity gradient in the first three years following phloem-disruption (Figure 3.2a, $F = 1.147$; $p\text{-value} = 0.36$), with total NPP averaging $6.15 \text{ Mg C ha}^{-1} \text{ yr}^{-1}$ between 2019-2021. The overall stability of total NPP was driven by offsetting changes in component fluxes, which exhibited opposing responses to increasing disturbance severity in the first three years (Figure 3.3). Across disturbance severities and for the first three years post disturbance, we found stable canopy ANPP_w , averaging $2.39 \text{ Mg C ha}^{-1} \text{ yr}^{-1}$ (Figure 3.3a, $F = 0.622$, $p\text{-value} = 0.71$), BNPP_w , averaging $0.62 \text{ Mg C ha}^{-1} \text{ yr}^{-1}$ (Figure 3.3c, $F = 0.62$, $p\text{-value} = 0.71$), and NPP_{fwd} , averaging $0.43 \text{ Mg C ha}^{-1} \text{ yr}^{-1}$ (Figure 3.3e, $F = 0.770$, $p\text{-value} = 0.60$) (Table 3.2). In contrast, subcanopy ANPP_w increased with increasing disturbance severity beginning in the second year after phloem-disrupting disturbance (Figure 3.3b, $F = 7.04$, $p\text{-value} = <0.001$). Two years following disturbance in 2021, subcanopy ANPP_w was 221, 336, 450% higher than the control at 45, 65, 85% severities, respectively. Rather than increasing, NPP_{fl} was lower than the control in the 65 and 85% severities during the third year following disturbance (Figure 3.3d, $F = 2.39$, $p\text{-value} = 0.05$) and NPP_{fr} declined across the severity gradient starting in the first year following disturbance (Figure 3.3f, $p\text{-value} = 0.05$). In 2021, NPP_{fl} of the 65 and 85% severity levels was 17.8 and 24.4% lower than that of the control, respectively, and NPP_{fr} in the 85% disturbance severity treatment was, on average, 47.5% lower than that of control. Canopy NPP_w contributed the most to total NPP, comprising 38.9% of total NPP, on average.

3.2. Heterotrophic respiration fluxes and disturbance severity

Regardless of the method, total heterotrophic respiration and its component fluxes did not differ among disturbance severity treatments in the first 3 years (Figure 3.2b, $F = 0.332$, $p\text{-value} =$

0.91). Both R_{cwd} (Figure 3.4a, $F = 1.4$, $p\text{-value} = 0.26$) and R_{sh} (Figure 3.4b, $F = 0.35$, $p\text{-value} = 0.9$) were stable with increasing disturbance severity for the first three years. The three methods used to estimate R_{cwd} produced comparable values, averaging 0.74, 0.76 and 0.89 $\text{Mg C ha}^{-1} \text{ yr}^{-1}$ for methods 1, 2, and 3, respectively (Table 3.3). Similarly, R_{sh} derived using four independent approaches resulted in similar values of 6.42 and 6.44 $\text{Mg C ha}^{-1} \text{ yr}^{-1}$ for empirical incubation based methods ($R_{\text{sh},1}$, $R_{\text{sh},2}$) and 6.72 and 6.74 $\text{Mg C ha}^{-1} \text{ yr}^{-1}$ when estimated from the ED model ($R_{\text{sh},3}$, $R_{\text{sh},4}$, Table 3.3). R_{cwd} and R_{h} had grand means of 6.58 $\text{Mg C ha}^{-1} \text{ yr}^{-1}$ and 0.80 $\text{Mg C ha}^{-1} \text{ yr}^{-1}$, respectively, with mean R_{h} totaling 7.37 $\text{Mg C ha}^{-1} \text{ yr}^{-1}$.

3.3. Net ecosystem production and disturbance severity

Net ecosystem production did not decline with increasing disturbance severity in the first three years following phloem-disruption (Figure 3.5, $F = 0.614$, $p\text{-value} = 0.71$) because of the relative stability of NPP and R_{h} . The grand mean of NEP across the 12 estimates was -1.23 $\text{Mg C ha}^{-1} \text{ yr}^{-1}$ (Table 3.4) because estimates of C loss via R_{sh} were consistently higher than C uptake via NPP.

3.4. Net ecosystem production and pre-disturbance stand structure

While average NEP and component C fluxes were generally stable across the disturbance severity gradient, pre-disturbance stand structure, which varied across the experimental landscape ecosystem types (Table 1, Figure S3.2), was an important predictor of NEP response. Translating landscape ecosystem types from distinct categorical groups to a continuous range of pre-disturbance stand structure, we found the relationship between NEP and pre-disturbance biomass was dependent on disturbance severity. Specifically, NEP increased with increasing pre-

disturbance biomass in the 65 and 85% disturbance severities across the first three years post-disturbance (Figure 3.6, $R^2 = 0.38$, $F = 5.2$, $p\text{-value} = <0.001$).

4. Discussion

Supporting our hypothesis, we observed stable net ecosystem production with increasing disturbance severity for the first three years following phloem-disruption as a result of stable C uptake and loss. Notably, our findings extend to the highest level of disturbance severity, 85% gross defoliation. Similarly, stable or minimal declines in NEP have been observed following a separate phloem-disrupting experiment at our site (Gough et al. 2013) and after insect defoliation (Clark et al. 2022; Hicke et al. 2012). However, our findings contrast with studies showing large declines in NEP following fire (Zhao et al. 2021), insects (Clark et al. 2010) and harvest (Law et al. 2004). Our results add to growing evidence that some temperate forests can functionally withstand the increasing threat of partial disturbance events (Stuart-Haëntjens et al. 2015; Gough et al. 2013).

With respect to C uptake, the compensatory growth of healthy vegetation offset declines from stem-girdled trees, stabilizing total NPP as disturbance severity increased. Canopy tree NPP_w , the largest contributor to total NPP, was sustained because canopy trees continued to grow during the first year following stem girdling (Grigri et al. 2020) and, in subsequent years, the contributions of subcanopy NPP_w proportionally increased over time and with greater disturbance severity (Niedermaier et al. 2022). This release of subcanopy vegetation is consistent with studies showing increased light availability (Brown et al. 2010; Kumar et al. 2018; De Pauw et al. 2022) and reallocation of limiting nutrients (Nave et al. 2011) promotes compensatory

response from surviving vegetation. In contrast, NPP_{II} temporarily declined at higher levels of disturbance severity, suggesting that surviving vegetation may have produced fewer but more resource-use efficient leaves (Stuart-Haëntjens et al. 2015; Kunert et al. 2019). Additionally, we observed declines in NPP_{fr} , which is consistent with our findings of sustained declines in the autotrophic soil respiration (Mathes et al. *in review*). However, these declines in NPP_{II} and NPP_{fr} were not sufficient to significantly reduce total NPP, even at the highest disturbance severity.

On the C loss side of the equation, we did not find changes in heterotrophic fluxes from soils or coarse woody debris across the disturbance severity gradient for the first three years. Stable R_h , despite a large influx of coarse woody debris, suggests that the decomposition of stem-girdled trees was minimal in the first 3 years, which is consistent theory suggesting increasing responses in R_h lag behind onset of biotic disturbances (Harmon et al. 2011). However, our R_{sh} results contrast with those showing large influxes of detritus (Ekberg et al. 2007) and changes in soil microclimate (Mayer et al. 2017) increased R_{sh} in the first year following fire (Hu et al. 2021), clear-felling (Makiranta et al. 2010) and windthrow disturbances (Mayer et al. 2017).

Additionally, the lack of response from R_{cwd} contrasts studies showing substantial increases R_{cwd} in the second year following insect defoliation (Renninger et al. 2014). A lag between the large influx of CWD and increased R_h fluxes at our site may be caused by relatively low decomposition rates in early decay classes (Schmid et al. 2016), and lags in disturbance-driven canopy structural changes and associated drivers of decomposition. For example, at our site, we found minimal changes in soil microclimate (i.e. soil temperature and moisture) across disturbance severities (Atkins et al. *in review*) that was most likely the result of temporal lags in canopy deterioration and vegetation area index (VAI) response (Mathes et al. *in review*),

suggesting that sun exposure did not increase on the forest floor. The maintenance of soil temperature and moisture, which are main abiotic drivers of decomposition, may have contributed to minimal changes in both R_{sh} and R_{cwd} , for the first three years. Finally, we found that phloem-disruption, which severs the flow of carbohydrates belowground (Hogberg et al. 2001), caused significant and sustained declines in autotrophic activity (Mathes et al. *in review*). This suppression of labile C to the rhizosphere (i.e. root-microbe interface, Huo et al. 2017) may have diminished exudation rates that support microbial decomposition, further preventing increases in R_{sh} .

Despite the stability of mean landscape-scale NEP over time, pre-disturbance stand structure influenced smaller spatial scale (i.e., plot-level) variation in NEP at higher disturbance severities, signaling the importance of material legacies. We observed a significant interaction between pre-disturbance biomass and disturbance severity, with more biomass-rich plots sustaining higher levels of NEP when disturbance severities were 65% and 85% gross defoliation. Our results are consistent with prior observations from our site (Gough et al. 2021a; Niedermaier et al. 2022), and ecological theory (Johnstone et al. 2016) that suggests material legacies, which are constrained by the amount of starting biomass, are primary drivers of disturbance response and can support sustained C uptake (Campbell et al. 2004; Brown et al. 2010). Specifically, our findings suggest that material legacies in the form of surviving subcanopy and canopy trees became increasingly important for stabilizing NEP with increasing disturbance severity. This pattern is consistent with studies across disturbance types from fire (Pausas and Fernandez-Munoz 2012), wind, (Seidl et al. 2011) and insects (Hicke & Jenkins 2008), showing that pre-disturbance land management strategies that alter forest structure drove the sensitivity of

functional response to future disturbance events (Seidl et al. 2016). Finally, the variability in NEP attributed to plot-level biomass in tandem with stable landscape-level NEP across severities suggests that small-spatial scale differences in stand structure may be as—if not more—important as severity for predicting NEP response to disturbance.

Notably, our estimates of mean NEP were consistently negative, regardless of our methodology, suggesting that either the forests were C sources or systematic bias arising from uncertainty yielded unrealistically low values. Despite the use of multiple independent methods to estimate R_{sh} and R_{cwd} , C losses were consistently higher than C uptake (i.e., total NPP), resulting in negative NEP values. Our negative values are consistent with recent (2021) biometric estimates from a nearby site (Clay et al. 2022) and from a global analysis of R_h (Bond-Lamberty et al. 2018) showing temperature extremes are increasing annual soil respiration. However, our NEP values are substantially lower than concurrently measured fluxes from a nearby meteorological tower which show that NEP is positive and increasing, but becoming more variable over time (Gough et al. 2021b). The incongruencies with flux tower estimates, as well as the high uncertainty associated with estimates of R_h fluxes, suggest our biometric methods may have produced artificially high R_h values. This is consistent with a global synthesis of NEP showing biometric estimates are generally lower than tower estimates (Xu et al. 2014). Although our NEP values are low, we have no reason to believe that relative differences across experimental disturbance treatments suffer from bias.

Our findings underscore the large degree of variation in disturbance response among forest ecosystems and disturbance sources and severities, while strongly suggesting that the pace of tree

physiological decline and mortality is an important consideration. Contextualizing our results to the growing body of work on NEP following disturbance, we highlight two factors that are important drivers of C balance response. First, stand structural properties that promote material legacies can strengthen compensatory responses from surviving vegetation, particularly at high disturbance severities (Brown et al. 2010; Campbell et al. 2004). Therefore, forests with greater pre-disturbance biomass, or with higher structural complexity that supports growth from multiple forest strata (Gough et al. 2016b), are more likely to show sustained, or even enhanced C uptake, despite substantial losses from disturbed trees (Niedermaier et al. 2022). Additionally, results from our site show enhanced subcanopy physiology occurred in advance of increased light availability (Haber et al. *in review*). These results highlight the importance of not only the *amount* of pre-disturbance biomass, but the capacity and rate at which that surviving biomass can reallocate limited nutrients to sustain C uptake. Second, the rate of mortality will determine when disturbance-driven decomposition begins, and this is largely driven by disturbance source (Atkins et al. 2020). At our site, canopy structure remained mostly intact for the first couple years (Mathes et al. *in review*), resulting in a stable soil microclimate and a lagged pulse of detritus and response in heterotrophic respiration. These results are consistent with other phloem-disrupting or defoliating insect disturbances that produce slower rates of mortality and physiological decline (Schmid et al. 2016; Clark et al. 2018). In contrast, fast rates of mortality from fire or windthrow that cause immediate deterioration of canopy structure will promote rapid changes in soil microclimate and a large pulse of detritus to fuel heterotrophic respiration (Mayer et al. 2017; Hu et al. 2021; Ekberg et al. 2007). Further resolving how these processes drive NEP response to disturbance is crucial to better forecasting the strength of the temperate forest C sink with the increasing threat of disturbances across severities and sources.

5. Conclusions

Our results yielded support for all of our hypotheses, demonstrating that the net C balance of a forested landscape was sustained in the first three years following phloem-disrupting disturbance, even at the highest levels of severity. First, we found NEP was sustained across the disturbance severity gradient for the first three years, which supports predictions of sustained C balance in temperate forest ecosystems (Wu et al. 2023). Second, stable NEP was the result of sustained C uptake—from enhanced subcanopy and sustained canopy production—in tandem with sustained C loss—from slow rates of mortality and lags in disturbance-induced decomposition. Third, our results point to the importance of pre-disturbance stand-structural properties that promote material legacies for sustaining C balance at high severities. Substantial variability in patterns of C balance across the literature warrants further investigation into the mechanisms that support C balance stability following changing disturbance regimes. Finally, while our results show stable NEP across multiple years, continued monitoring of C fluxes as disturbance-driven structural changes continue to unfold will be necessary to understand long-term consequences to C balance.

Literature Cited

- Amiro, B. D., A. G. Barr, J. G. Barr, T. A. Black, R. Bracho, M. Brown, J. Chen, K. L. Clark, K. J. Davis, A. R. Desai, and others. 2010. Ecosystem carbon dioxide fluxes after disturbance in forests of North America. *Journal of Geophysical Research: Biogeosciences* 115.
- Atkins, J. W., E. Agee, A. Barry, K. M. Dahlin, K. Dorheim, M. S. Grigri, L. T. Haber, L. J. Hickey, A. G. Kamoske, K. Mathes, and others. 2021. The fortedata R package:

- Open-science datasets from a manipulative experiment testing forest resilience. *Earth System Science Data* 13:943–952.
- Atkins, J. W., B. Bond-Lamberty, R. T. Fahey, L. T. Haber, E. Stuart-Haëntjens, B. S. Hardiman, E. LaRue, B. E. McNeil, D. A. Orwig, A. E. L. Stovall, and others. 2020. Application of multidimensional structural characterization to detect and describe moderate forest disturbance. *Ecosphere* 11.
- Atkins J.W., Shiklomanov, A., Mathes K.C., Bond-Lamberty B., Gough C.M. Effects of forest structural and compositional change on forest microclimates. *In review*.
- Bond-Lamberty, B., V. L. Bailey, M. Chen, C. M. Gough, and R. Vargas. 2018. Globally rising soil heterotrophic respiration over recent decades. *Nature* 560:80–83.
- Bond-Lamberty, B., C. Wang, and S. T. Gower. 2004. A global relationship between the heterotrophic and autotrophic components of soil respiration? *Global Change Biology* 10:1756–1766.
- Brown, M., T. A. Black, Z. Nestic, V. N. Foord, D. L. Spittlehouse, A. L. Fredeen, N. J. Grant, P. J. Burton, and J. A. Trofymow. 2010. Impact of mountain pine beetle on the net ecosystem production of lodgepole pine stands in British Columbia. *Agricultural and Forest Meteorology* 150:254–264.
- Cairns, M. A. 1997. Root biomass allocation in the world's upland forests. *Oecologia* 111:1–11.
- Campbell, J. L., O. J. Sun, and B. E. Law. 2004. Disturbance and net ecosystem production across three climatically distinct forest landscapes. *Global Biogeochemical Cycles* 18:1–11.
- Clark, K. L., C. Aoki, M. Ayres, J. Kabrick, and M. R. Gallagher. 2022. Insect infestations and the persistence and functioning of oak-pine mixedwood forests in the mid-Atlantic

- region, USA. PLoS ONE 17.
- Clark, K. L., H. J. Renninger, N. Skowronski, M. Gallagher, and K. V. R. Schäfer. 2018. Decadal-scale reduction in forest net ecosystem production following insect defoliation contrasts with short-term impacts of prescribed fires. *Forests* 9.
- Clark, K. L., N. Skowronski, and J. Hom. 2010. Invasive insects impact forest carbon dynamics. *Global Change Biology* 16:88–101.
- Clay, C., L. Nave, K. Nadelhoffer, C. Vogel, B. Propson, J. Den Uyl, L. J. Hickey, A. Barry, and C. M. Gough. 2022. Fire after clear-cut harvesting minimally affects the recovery of ecosystem carbon pools and fluxes in a Great Lakes forest. *Forest Ecology and Management* 519.
- Curtis, P. S., and C. M. Gough. 2018. Forest aging, disturbance and the carbon cycle. *New Phytologist* 219(4): 118-1193.
- Dai, Z., C. C. Trettin, A. J. Burton, M. F. Jurgensen, D. S. Page-Dumroese, B. T. Forschler, J. S. Schilling, and D. L. Lindner. 2021. Coarse woody debris decomposition assessment tool: Model development and sensitivity analysis. PLoS ONE 16.
- Dorheim, K., C. M. Gough, L. T. Haber, K. C. Mathes, A. N. Shiklomanov, and B. Bond-Lamberty. 2022. Climate Drives Modeled Forest Carbon Cycling Resistance and Resilience in the Upper Great Lakes Region, USA. *Journal of Geophysical Research: Biogeosciences* 127:1–15.
- Edgar, C. B., and J. A. Westfall. 2022. Timing and extent of forest disturbance in the Laurentian Mixed Forest. *Frontiers in Forests and Global Change* 5:1–15.
- Ehbrecht, M., P. Schall, C. Ammer, M. Fischer, and D. Seidel. 2019. Effects of structural heterogeneity on the diurnal temperature range in temperate forest ecosystems. *Forest*

- Ecology and Management 432:860–867.
- Ekberg, A., N. Buchmann, and G. Gleixner. 2007. Rhizospheric influence on soil respiration and decomposition in a temperate Norway spruce stand. *Soil Biology and Biochemistry* 39:2103–2110.
- Fargione, J. E., S. Bassett, T. Boucher, S. D. Bridgham, R. T. Conant, S. C. Cook-Patton, P. W. Ellis, A. Falcucci, J. W. Fourqurean, T. Gopalakrishna, H. Gu, B. Henderson, M. D. Hurteau, K. D. Kroeger, T. Kroeger, T. J. Lark, S. M. Leavitt, G. Lomax, R. I. McDonald, J. P. Megonigal, D. A. Miteva, C. J. Richardson, J. Sanderman, D. Shoch, S. A. Spawn, J. W. Veldman, C. A. Williams, P. B. Woodbury, C. Zganjar, M. Baranski, P. Elias, R. A. Houghton, E. Landis, E. Mcglynn, W. H. Schlesinger, J. V Siikamaki, A. E. Sutton-Grier, and B. W. Griscom. 2018. Natural climate solutions for the United States. *Page Sci. Adv.* 4 eaat1869.
- Flower, C. E., and M. A. Gonzalez-Meler. 2015. Responses of temperate forest productivity to insect and pathogen disturbances. *Annual Review of Plant Biology* 66:547–569.
- Fu, Z., D. Li, O. Hararuk, C. Schwalm, Y. Luo, L. Yan, and S. Niu. 2017. Recovery time and state change of terrestrial carbon cycle after disturbance. *Environmental Research Letters* 12.
- Goetz, S. J., B. Bond-Lamberty, B. E. Law, J. A. Hicke, C. Huang, R. A. Houghton, S. McNulty, T. O'Halloran, M. Harmon, A. J. H. Meddens, E. M. Pfeifer, D. Mildrexler, and E. S. Kasichke. 2012. Observations and assessment of forest carbon dynamics following disturbance in North America. *Journal of Geophysical Research: Biogeosciences* 117.
- Gough, C. M., J. W. Atkins, B. Bond-Lamberty, E. A. Agee, K. R. Dorheim, R. T. Fahey, M. S. Grigri, L. T. Haber, K. C. Mathes, S. C. Pennington, A. N. Shiklomanov, and J. M.

- Tallant. 2021a. Forest Structural Complexity and Biomass Predict First-Year Carbon Cycling Responses to Disturbance. *Ecosystems* 24:699–712.
- Gough, C. M., J. W. Atkins, R. T. Fahey, P. S. Curtis, G. Bohrer, B. S. Hardiman, L. J. Hickey, L. E. Nave, K. M. Niedermaier, C. Clay, J. M. Tallant, and B. Bond-Lamberty. 2022. Disturbance has variable effects on the structural complexity of a temperate forest landscape. *Ecological Indicators* 140.
- Gough, C. M., J. W. Atkins, R. T. Fahey, and B. S. Hardiman. 2019. High rates of primary production in structurally complex forests. *Ecology* 100.
- Gough, C. M., G. Bohrer, and P. S. Curtis. 2016a. AmeriFlux US-UMd UMBS Disturbance, Dataset. <https://ameriflux.lbl.gov/>.
- Gough, C. M., G. Bohrer, B. S. Hardiman, L. E. Nave, C. S. Vogel, J. W. Atkins, B. Bond-Lamberty, R. T. Fahey, A. T. Fotis, M. S. Grigri, and and others. 2021b. Disturbance-accelerated succession increases the production of a temperate forest. *Ecological Applications* 31:1–17.
- Gough, C. M., P. S. Curtis, B. S. Hardiman, C. M. Scheuermann, and B. Bond-Lamberty. 2016b. Disturbance, complexity, and succession of net ecosystem production in North America's temperate deciduous forests. *Ecosphere* 7:1–15.
- Gough, C. M., B. S. Hardiman, L. E. Nave, G. Bohrer, K. D. Maurer, C. S. Vogel, K. J. Nadelhoffer, and P. S. Curtis. 2013. Sustained carbon uptake and storage following moderate disturbance in a Great Lakes forest. *Ecological Applications* 23:1202–1215.
- Gough, C. M., C. S. Vogel, K. H. Harrold, K. George, and P. S. Curtis. 2007. The legacy of harvest and fire on ecosystem carbon storage in a north temperate forest. *Global Change Biology* 13:1935–1949.

- Gough, C. M., C. S. Vogel, H. P. Schmid, H. B. Su, and P. S. Curtis. 2008. Multi-year convergence of biometric and meteorological estimates of forest carbon storage. *Agricultural and Forest Meteorology* 148:158–170.
- Grigri, M. S., J. W. Atkins, C. Vogel, B. Bond-Lamberty, and C. M. Gough. 2020. Aboveground wood production is sustained in the first growing season after phloem-disrupting disturbance. *Forests* 11:1–19.
- Haber, L.T., Atkins, J.W., Bond-Lamberty B., Gough, C.M., Dynamic subcanopy leaf traits drive resistance of net primary production across a disturbance severity gradient. *Frontier in forests and Global Change*, *in review*.
- Hardiman, B. S., G. Bohrer, C. M. Gough, C. S. Vogel, and P. S. Curtis. 2011. The role of canopy structural complexity in wood net primary production of a maturing northern deciduous forest. *Ecology*. 92(9): 1818-1827.
- Harmon, M. E., Ferrell, W. K. Franklin, and Jerry F. 1990. Effects on Carbon Storage of Conversion of Old-Growth Forests to Young Forests. *Science* 247(4943): 699.
- Harmon, M. E., B. Bond-Lamberty, J. Tang, and R. Vargas. 2011. Heterotrophic respiration in disturbed forests: A review with examples from North America. *Journal of Geophysical Research*. 116. G00k04.
- Harmon, M. E., and J. Sexton. 1996. Guidelines for Measurements of Woody Detritus in Forest Ecosystems. U.S. LTER Network Office. 20.
- Hicke, J. A., C. D. Allen, A. R. Desai, M. C. Dietze, R. J. Hall, E. H. T. Hogg, D. M. Kashian, D. Moore, K. F. Raffa, R. N. Sturrock, and J. Vogelmann. 2012, January. Effects of biotic disturbances on forest carbon cycling in the United States and Canada. *Global Change Biology* 18:7-34.

- Hicke, J. A., and J. C. Jenkins. 2008. Mapping lodgepole pine stand structure susceptibility to mountain pine beetle attack across the western United States. *Forest Ecology and Management* 255:1536–1547.
- Högberg, P., A. Nordgren, N. Buchmann, A. F. S. Taylor, A. Ekblad, M. N. Högberg, G. Nyberg, M. Ottosson-Löfvenius, and D. J. Read. 2001. Large-scale forest girdling shows that current photosynthesis drives soil respiration. *Nature* 411:789–792.
- Hu, T., B. Zhao, F. Li, X. Dou, H. Hu, and L. Sun. 2021. Effects of fire on soil respiration and its components in a Dahurian larch (*Larix gmelinii*) forest in northeast China: Implications for forest ecosystem carbon cycling. *Geoderma* 402.
- Huo, C., Y. Luo, and W. Cheng. 2017. Rhizosphere priming effect: A meta-analysis. *Soil Biology and Biochemistry* 111:78–84.
- Ivanov, A. V., M. A. Salo, V. Y. Tolstikova, S. V. Bryanin, and D. G. Zamolodchikov. 2022. Effects of Windfall on Soil Surface Carbon Emission and Fine Root Stocks in the Central Sikhote-Alin. *Eurasian Soil Science* 55:1405–1413.
- Johnstone, J. F., C. D. Allen, J. F. Franklin, L. E. Frelich, B. J. Harvey, P. E. Higuera, M. C. Mack, R. K. Meentemeyer, M. R. Metz, G. L. W. Perry, T. Schoennagel, and M. G. Turner. 2016. Changing disturbance regimes, ecological memory, and forest resilience. *Frontiers in Ecology and the Environment* 14:369–378.
- Kahl, T., T. Arnstadt, K. Baber, C. Bäessler, J. Bauhus, W. Borken, F. Buscot, A. Floren, C. Heibl, D. Hessenmöller, M. Hofrichter, B. Hoppe, H. Kellner, D. Krüger, K. E. Linsenmair, E. Matzner, P. Otto, W. Purahong, C. Seilwinder, E. D. Schulze, B. Wende, W. W. Weisser, and M. M. Gossner. 2017. Wood decay rates of 13 temperate tree species

- in relation to wood properties, enzyme activities and organismic diversities. *Forest Ecology and Management* 391:86–95.
- Law, B. E., D. Turner, J. Campbell, O. J. Sun, S. Van Tuyl, W. D. Ritts, and W. B. Cohen. 2004. Disturbance and climate effects on carbon stocks and fluxes across Western Oregon USA. *Global Change Biology* 10:1429–1444.
- Levy-Varon, J. H., W. S. F. Schuster, and K. L. Griffin. 2014. Rapid rebound of soil respiration following partial stand disturbance by tree girdling in a temperate deciduous forest. *Oecologia* 174:1415–1424.
- Mäkiranta, P., T. Riutta, T. Penttilä, and K. Minkkinen. 2010. Dynamics of net ecosystem CO₂ exchange and heterotrophic soil respiration following clearfelling in a drained peatland forest. *Agricultural and Forest Meteorology* 150:1585–1596.
- Mathes K.C, Pennington, S. Rodriguez, C., Bond-Lamberty B., Atkins J.W., Vogel C.S., Gough, C.M. Sustained three-year declines in forest soil respiration are proportional to disturbance severity. *Ecosystems*, *in review*.
- Mayer, M., H. Sandén, B. Rewald, D. L. Godbold, and K. Katzensteiner. 2017. Increase in heterotrophic soil respiration by temperature drives decline in soil organic carbon stocks after forest windthrow in a mountainous ecosystem. *Functional Ecology* 31:1163–1172.
- de Mendiburu, F. 2021. *_agricolae: Statistical Procedures for Agricultural Research_*. R package
- Nave, L. E., J. M. Le Moine, C. M. Gough, and K. J. Nadelhoffer. 2019. Multidecadal trajectories of soil chemistry and nutrient availability following cutting vs. Burning disturbances in upper great lakes forests. *Canadian Journal of Forest Research* 49:731–742.
- Niedermaier, K. M., J. W. Atkins, M. S. Grigri, B. Bond-lamberty, and C. M. Gough. 2022.

- Structural complexity and primary production resistance are coupled in a temperate forest. *Frontiers in Forests and Global Change*.
- Odum, E. P. 1969. The strategy of ecosystem development. *Science* 164:262–270.
- Pan, Y., R. A. Birdsey, Fang J., Houghton R., Kauppi P. E., Kurz W. A., Phillips O. L., and Shvidenko A. 2011. A Large and Persistent Carbon Sink in the World's Forests. *Science* 333:988–933.
- Pausas, J. G., and S. Fernández-Muñoz. 2012. Fire regime changes in the Western Mediterranean Basin: From fuel-limited to drought-driven fire regime. *Climatic Change* 110:215–226.
- Pearsall, D. R., B. V Barnes, G. R. Zogg, M. Lapin, R. R. Ring, and D. Ring. 1995. Landscape ecosystems of the University of Michigan Biological Station. *School of Natural Resources & Environment* 66.
- Pugh, T. A. M., A. Arneeth, M. Kautz, B. Poulter, and B. Smith. 2019. Important role of forest disturbances in the global biomass turnover and carbon sinks. *Nature Geoscience* 12:730–735.
- R Core Team. 2022. R: A language and environment for statistical computing. R Foundation for Statistical Computing, Vienna, Austria.
- Renninger, H. J., N. Carlo, K. L. Clark, and K. V. R. Schäfer. 2014. Modeling respiration from snags and coarse woody debris before and after an invasive gypsy moth disturbance. *Journal of Geophysical Research: Biogeosciences* 119:630–644.
- Robinson, A. J., C. E. Defrenne, W. J. Roach, C. C. Dymond, B. J. Pickles, and S. W. Simard. 2022. Harvesting Intensity and Aridity Are More Important Than Climate Change in Affecting Future Carbon Stocks of Douglas-Fir Forests. *Frontiers in Forests and Global Change* 5.

- Schmid, A. V., C. S. Vogel, E. Liebman, P. S. Curtis, and C. M. Gough. 2016. Coarse woody debris and the carbon balance of a moderately disturbed forest. *Forest Ecology and Management* 361:38–45.
- Seidl, R., M. J. Schelhaas, and M. J. Lexer. 2011. Unraveling the drivers of intensifying forest disturbance regimes in Europe. *Global Change Biology* 17:2842–2852.
- Seidl, R., T. A. Spies, D. L. Peterson, S. L. Stephens, and J. A. Hicke. 2016. Searching for resilience: Addressing the impacts of changing disturbance regimes on forest ecosystem services. *Journal of Applied Ecology* 53:120–129.
- Seidl, R., D. Thom, M. Kautz, D. Martin-Benito, M. Peltoniemi, G. Vacchiano, J. Wild, D. Ascoli, M. Petr, J. Honkaniemi, and and others. 2017. Forest disturbances under climate change. *Nature Climate Change* 7:395–402.
- Sommerfeld, A., C. Senf, B. Buma, A. W. D'Amato, T. Després, I. Díaz-Hormazábal, S. Fraver, L. E. Frelich, Á. G. Gutiérrez, S. J. Hart, and and others. 2018. Patterns and drivers of recent disturbances across the temperate forest biome. *Nature Communications* 9:4355.
- Stuart-Haëntjens, E. J., P. S. Curtis, R. T. Fahey, C. S. Vogel, and C. M. Gough. 2015. Net primary production of a temperate deciduous forest exhibits a threshold response to increasing disturbance severity. *Ecology* 96:2478–2487.
- Taylor, B. N., A. E. Patterson, M. Ajayi, R. Arkebauer, K. Bao, N. Bray, R. M. Elliott, P. P. G. Gauthier, J. Gersony, R. Gibson, M. Guerin, S. Lavenhar, C. Leland, L. Lemordant, W. Liao, J. Melillo, R. Oliver, C. M. Prager, W. Schuster, N. B. Schwartz, C. Shen, K. P. Terlizzi, and K. L. Griffin. 2017. Growth and physiology of a dominant understory shrub, *Hamamelis virginiana*, following canopy disturbance in a temperate hardwood forest. *Canadian Journal of Forest Research* 47:193–202.

- Turner, M. G., T. G. Whitby, D. B. Tinker, and W. H. Romme. 2016. Twenty-four years after the Yellowstone Fires: Are postfire lodgepole pine stands converging in structure and function? *Ecology* 97:1260–1273.
- Wickham, H. 2016. *ggplot2: Elegant Graphics for Data Analysis*.
- Wu, C., S. R. Coffield, M. L. Goulden, J. T. Randerson, A. T. Trugman, and W. R. L. Anderegg. 2023. Uncertainty in US forest carbon storage potential due to climate risks. *Nature Geoscience*.
- Xu, B., Y. Yang, P. Li, H. Shen, and J. Fang. 2014. Global patterns of ecosystem carbon flux in forests: A biometric data-based synthesis. *Global Biogeochemical Cycles* 28:962–973.
- Zhao, B., Q. Zhuang, N. Shurpali, K. Köster, F. Berninger, and J. Pumpanen. 2021. North American boreal forests are a large carbon source due to wildfires from 1986 to 2016. *Scientific Reports* 11.
- Zhao, S., K. Chen, C. Wu, and Y. Mao. 2018. Effects of simulated warming on soil respiration to XiaoPo lake. Page IOP Conference Series: Earth and Environmental Science. Institute of Physics Publishing.113(1).

Tables

Table 3.1: The vegetation characteristics, landforms and soil textures of treatment replicates in the Forest Resilience Threshold Experiment (FoRTE) before disturbance severity treatments were implemented. Species abbreviations are as follows: POGR (*Populus grandidentata*), ACSA (*Acer rubrum*), FAGR (*Fagus grandifolia*), QURU (*Quercus rubra*), PIST (*Pinus strbous*).

	A	B	C	D
Canopy Tree (> 8 cm DBH) composition	POGR (61%) ACSA (17%) ACRU (10%) FAGR (10%)	POGR (58%) ACRU (24%) QURU (9%) FAGR (4%)	QURU (43%) POGR (39%) PIST (6%) ACRU (6%)	QURU (72%) POGR (19%) PIST (4%) FAGR (1%)
Stem Density (Stems ha ⁻¹ , > 8 cm)	865 (32)	888 (46)	910 (55)	796 (81)
Shannon's index of species diversity	1.05 (0.09)	1.05 (0.05)	1.04 (0.11)	0.92 (0.10)
Leaf area index (dimensionless)	4.1 (0.15)	3.6 (0.08)	3.5 (0.10)	2.9 (0.18)
Biomass (kg C ha ⁻¹)	264,6000 (15,800)	229,900 (24,700)	197,000 (13,900)	155,900 (19,000)
Canopy rugosity (m)	28.8 (3.6)	22.3 (2.3)	14.2 (1.7)	8.9 (1.1)
Landform	Moraine	High-elevation outwash over moraine	High-elevation outwash plain	High-elevation outwash plain
Soil Texture	Sandy loam, calcareous	Medium sand, non-calcareous	Sand, calcareous	Sand, calcareous
Drainage	Well drained	Well drained	Excessively drained	Excessively drained

Table 3.2: Mean (\pm SE) NPP fluxes ($\text{Mg C ha}^{-1} \text{ yr}^{-1}$) across disturbances severities and years. SE represents variation across experimental replicates. Canopy and subcanopy ANPP_w = Aboveground woody net primary production, BNPP_w = Belowground woody net primary production, NPP_{ll} = leaf litter primary production, NPP_{fwd} = fine woody debris primary production, NPP_{fr} = fine-root primary production.

Severity (%)	canopy ANPP_w	subcanopy ANPP_w	BNPP_w	NPP_{ll}	NPP_{fwd}	NPP_{fr}
2019						
0	2.01 (0.09)	0.12 (0.04)	0.51 (0.02)	0.64 (0.12)	0.39 (0.09)	2.10 (0.43)
45	2.30 (0.32)	0.14 (0.04)	0.58 (0.08)	0.72 (0.08)	0.41 (0.22)	1.90 (0.49)
65	2.49 (0.42)	0.12 (0.04)	0.64 (0.1)	0.73 (0.13)	0.25 (0.07)	1.29 (0.26)
85	2.47 (0.43)	0.13 (0.05)	0.62 (0.11)	0.69 (0.14)	0.32 (0.14)	1.24 (0.46)
2020						
0	2.31 (0.27)	0.09 (0.04)	0.58 (0.06)	0.89 (0.11)	0.44 (0.18)	2.34 (0.45)
45	2.60 (0.53)	0.30 (0.16)	0.66 (0.13)	0.95 (0.06)	0.43 (0.11)	1.30 (0.33)
65	2.79 (0.59)	0.28 (0.13)	0.71 (0.15)	1.06 (0.23)	0.36 (0.09)	1.07 (0.17)
85	2.93 (0.85)	0.40 (0.1)	0.73 (0.21)	1.00 (0.18)	0.92 (0.49)	1.30 (0.37)
2021						
0	2.26 (0.44)	0.14 (0.1)	0.57 (0.1)	1.11 (0.11)	0.50 (0.12)	2.07 (0.67)
45	2.32 (0.4)	0.46 (0.25)	0.58 (0.1)	1.02 (0.1)	0.35 (0.03)	1.81 (0.44)
65	2.02 (0.52)	0.61 (0.3)	0.51 (0.13)	0.91 (0.19)	0.23 (0.04)	1.31 (0.28)
85	2.15 (0.25)	0.78 (0.19)	0.54 (0.06)	0.85 (0.13)	0.52 (0.16)	0.88 (0.21)

Table 3.3: Mean (\pm SE) R_h fluxes ($\text{Mg C ha}^{-1} \text{ yr}^{-1}$) across disturbances severities and years from 3 and 4 independent estimates of R_{cwd} and R_h , respectively. SE represents quadratic sum of compounding error from spatial variation (replicates) and uncertainty around modeled soil temperature estimates. R_{cwd} = coarse woody debris respiration and R_{sh} = soil heterotrophic respiration.

Severity (%)	$R_{\text{cwd},1}$	$R_{\text{cwd},2}$	$R_{\text{cwd},3}$	$R_{\text{sh},1}$	$R_{\text{sh},2}$	$R_{\text{sh},3}$	$R_{\text{sh},4}$
2019							
0	0.72 (0.31)	0.71 (0.37)	1.03 (0.83)	6.22 (1.11)	6.26 (1.1)	6.22 (1.11)	6.26 (1.1)
45	0.89 (0.46)	0.88 (0.55)	0.97 (0.89)	6.40 (1.43)	6.44 (1.42)	6.26 (1.11)	6.30 (1.1)
65	0.49 (0.14)	0.51 (0.17)	0.72 (0.61)	6.31 (1.39)	6.35 (1.38)	6.29 (1.11)	6.33 (1.1)
85	0.75 (0.21)	0.66 (0.26)	0.82 (0.62)	6.30 (1.37)	6.34 (1.37)	6.32 (1.11)	6.36 (1.11)
2020							
0	0.68 (0.29)	0.67 (0.35)	1.05 (0.94)	6.30 (1.45)	6.34 (1.41)	6.30 (1.45)	6.34 (1.41)
45	0.84 (0.44)	0.84 (0.52)	1.04 (1.03)	5.64 (1.42)	5.68 (1.38)	6.32 (1.45)	6.36 (1.41)
65	0.48 (0.14)	0.49 (0.16)	0.70 (0.65)	5.06 (1.53)	5.10 (1.5)	6.34 (1.45)	6.38 (1.41)
85	0.83 (0.19)	0.74 (0.26)	0.88 (0.78)	6.04 (1.49)	6.08 (1.46)	6.36 (1.45)	6.40 (1.41)
2021							
0	0.70 (0.32)	0.69 (0.38)	0.97 (0.97)	7.57 (2.95)	7.57 (2.09)	7.57 (2.95)	7.57 (2.09)
45	1.06 (0.35)	1.02 (0.44)	1.04 (1.07)	7.61 (2.85)	7.61 (2.01)	7.55 (2.95)	7.54 (2.09)
65	0.72 (0.16)	0.75 (0.18)	0.68 (0.74)	6.07 (2.67)	6.08 (1.89)	7.54 (2.95)	7.54 (2.09)
85	0.96 (0.3)	0.88 (0.37)	0.85 (0.82)	7.49 (3.08)	7.49 (2.15)	7.53 (2.94)	7.53 (2.09)

Table 3.4: Mean (\pm SE) net ecosystem production (NEP, Mg C ha⁻¹ yr⁻¹) across disturbances severities and years. 12 independent estimates are the result of all combinations of R_{cwd} and R_h methods. SE represents quadratic sum of compounding error across component fluxes.

Severity (%)	NEP ₁	NEP ₂	NEP ₃	NEP ₄	NEP ₅	NEP ₆	NEP ₇	NEP ₈	NEP ₉	NEP ₁₀	NEP ₁₁	NEP ₁₂
2019												
0	-1.19 (1.45)	-1.19 (1.45)	-1.17 (1.45)	-1.17 (1.45)	-1.49 (1.46)	-1.49 (1.46)	-1.22 (1.46)	-1.22 (1.46)	-1.21 (1.62)	-1.21 (1.62)	-1.53 (1.62)	-1.53 (1.62)
45	-1.07 (1.67)	-1.20 (1.67)	-1.06 (1.59)	-1.20 (1.59)	-1.16 (1.68)	-1.29 (1.68)	-1.11 (1.61)	-1.24 (1.61)	-1.10 (1.81)	-1.24 (1.81)	-1.19 (1.74)	-1.33 (1.74)
65	-1.26 (1.52)	-1.28 (1.52)	-1.28 (1.42)	-1.30 (1.42)	-1.48 (1.53)	-1.50 (1.53)	-1.30 (1.42)	-1.32 (1.42)	-1.31 (1.67)	-1.34 (1.67)	-1.52 (1.57)	-1.55 (1.57)
85	-1.61 (1.58)	-1.59 (1.57)	-1.53 (1.52)	-1.50 (1.52)	-1.68 (1.58)	-1.66 (1.58)	-1.65 (1.53)	-1.63 (1.53)	-1.57 (1.71)	-1.54 (1.71)	-1.72 (1.66)	-1.70 (1.66)
2020												
0	-0.28 (1.62)	-0.28 (1.61)	-0.27 (1.62)	-0.27 (1.61)	-0.64 (1.64)	-0.64 (1.62)	-0.32 (1.64)	-0.32 (1.62)	-0.31 (1.81)	-0.31 (1.8)	-0.68 (1.81)	-0.68 (1.8)
45	-0.92 (1.66)	-0.24 (1.65)	-0.91 (1.66)	-0.23 (1.65)	-1.11 (1.68)	-0.43 (1.67)	-0.96 (1.67)	-0.28 (1.66)	-0.95 (1.85)	-0.27 (1.84)	-1.15 (1.84)	-0.47 (1.83)
65	-0.54 (1.64)	0.73 (1.64)	-0.56 (1.64)	0.72 (1.63)	-0.77 (1.65)	0.51 (1.64)	-0.58 (1.64)	0.70 (1.63)	-0.60 (1.79)	0.68 (1.78)	-0.81 (1.78)	0.47 (1.77)
85	0.11 (1.84)	0.43 (1.83)	0.20 (1.84)	0.52 (1.83)	0.06 (1.85)	0.38 (1.84)	0.07 (1.85)	0.39 (1.84)	0.16 (1.99)	0.48 (1.98)	0.02 (1.99)	0.34 (1.98)
2021												
0	-1.62 (2.09)	-1.62 (1.87)	-1.61 (2.09)	-1.61 (1.87)	-1.89 (2.09)	-1.89 (1.87)	-1.62 (2.09)	-1.62 (1.87)	-1.61 (2.24)	-1.61 (2.04)	-1.89 (2.24)	-1.89 (2.04)
45	-2.07 (2.08)	-2.14 (1.87)	-2.03 (2.08)	-2.10 (1.86)	-2.05 (2.09)	-2.12 (1.88)	-2.07 (2.09)	-2.13 (1.88)	-2.03 (2.24)	-2.10 (2.05)	-2.05 (2.25)	-2.12 (2.05)
65	-2.65 (2.03)	-1.19 (1.82)	-2.68 (2.09)	-1.22 (1.87)	-2.61 (2.03)	-1.15 (1.83)	-2.65 (2.1)	-1.19 (1.88)	-2.68 (2.15)	-1.22 (1.96)	-2.61 (2.22)	-1.15 (2.01)
85	-2.78 (2.07)	-2.74 (1.83)	-2.70 (2.05)	-2.66 (1.82)	-2.67 (2.08)	-2.63 (1.84)	-2.77 (2.06)	-2.74 (1.83)	-2.70 (2.19)	-2.66 (1.96)	-2.67 (2.17)	-2.63 (1.96)

Figures

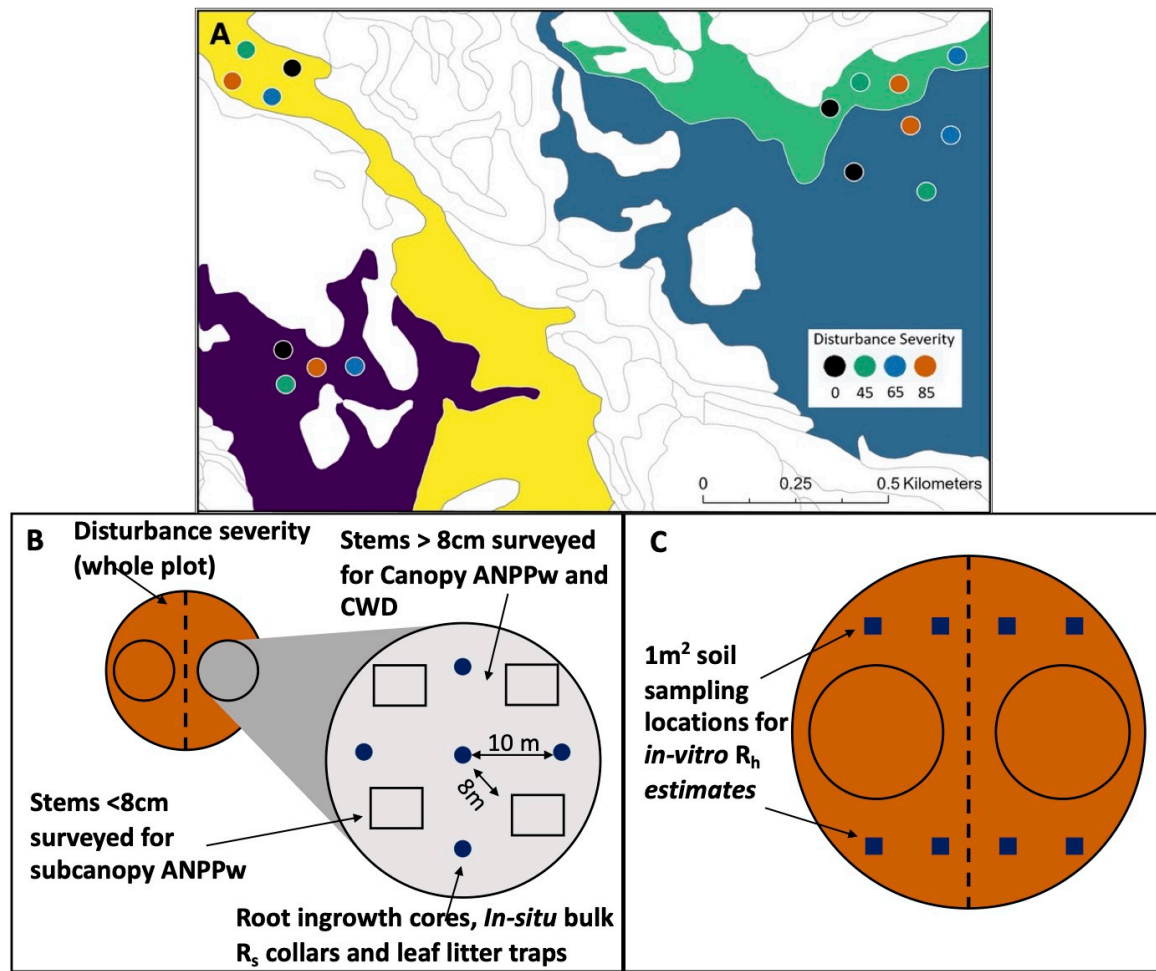


Figure 3.1: Forest Resilience Threshold Experiment (FoRTE) **A)** plot distribution map, **B)** experimental design and layout of all component NPP flux measurements **C)** layout of soil sampling locations for *in-vitro* heterotrophic soil respiration (R_{sh}) estimates.

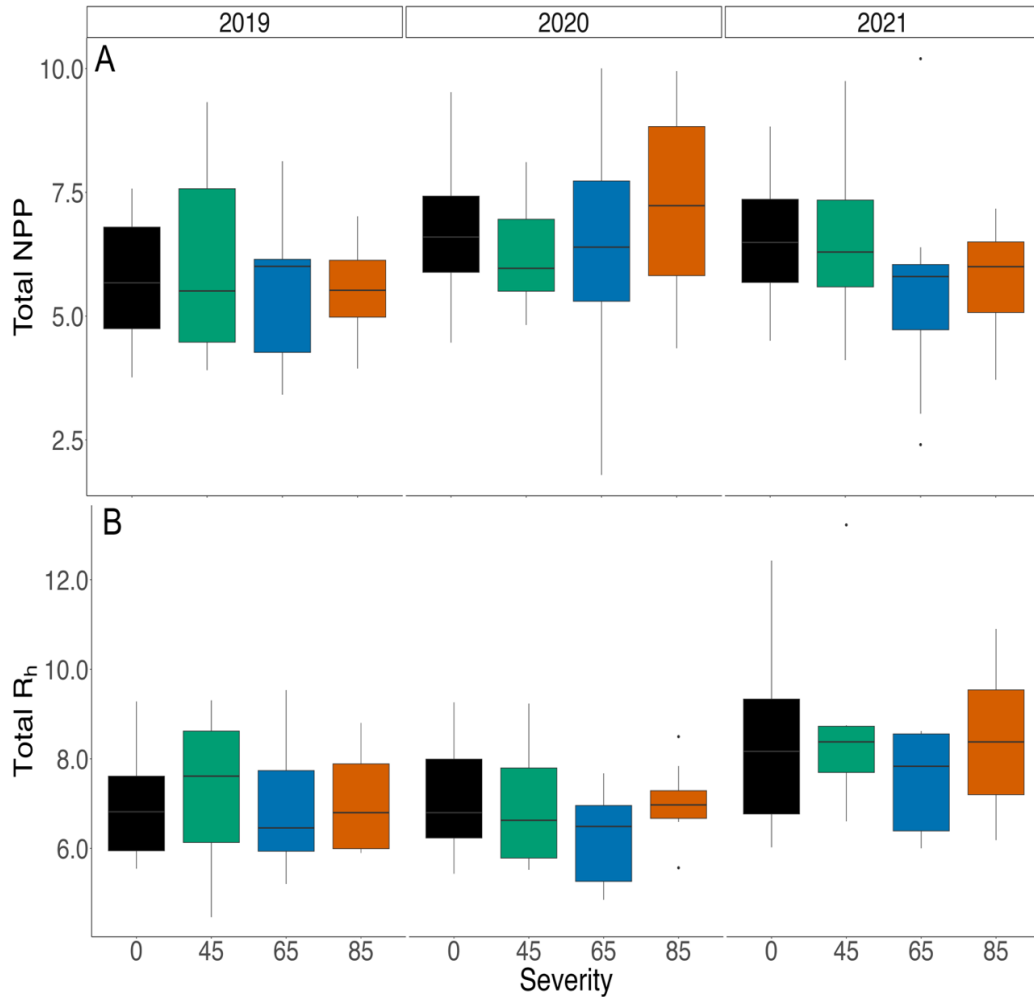


Figure 3.2: Boxplots displaying median, interquartile range (middle 50% of range) and minimum and maximum **A)** Total NPP (sum of all NPP component fluxes) ($F = 1.147$; $p\text{-value} = 0.36$), and **B)** total R_h (sum of R_{sh} and R_{cwd} averaged across methods) ($F = 0.332$, $p\text{-value} = 0.91$) across disturbance severities (2019-2021). Fluxes are presented as $\text{Mg C ha}^{-1} \text{ yr}^{-1}$.

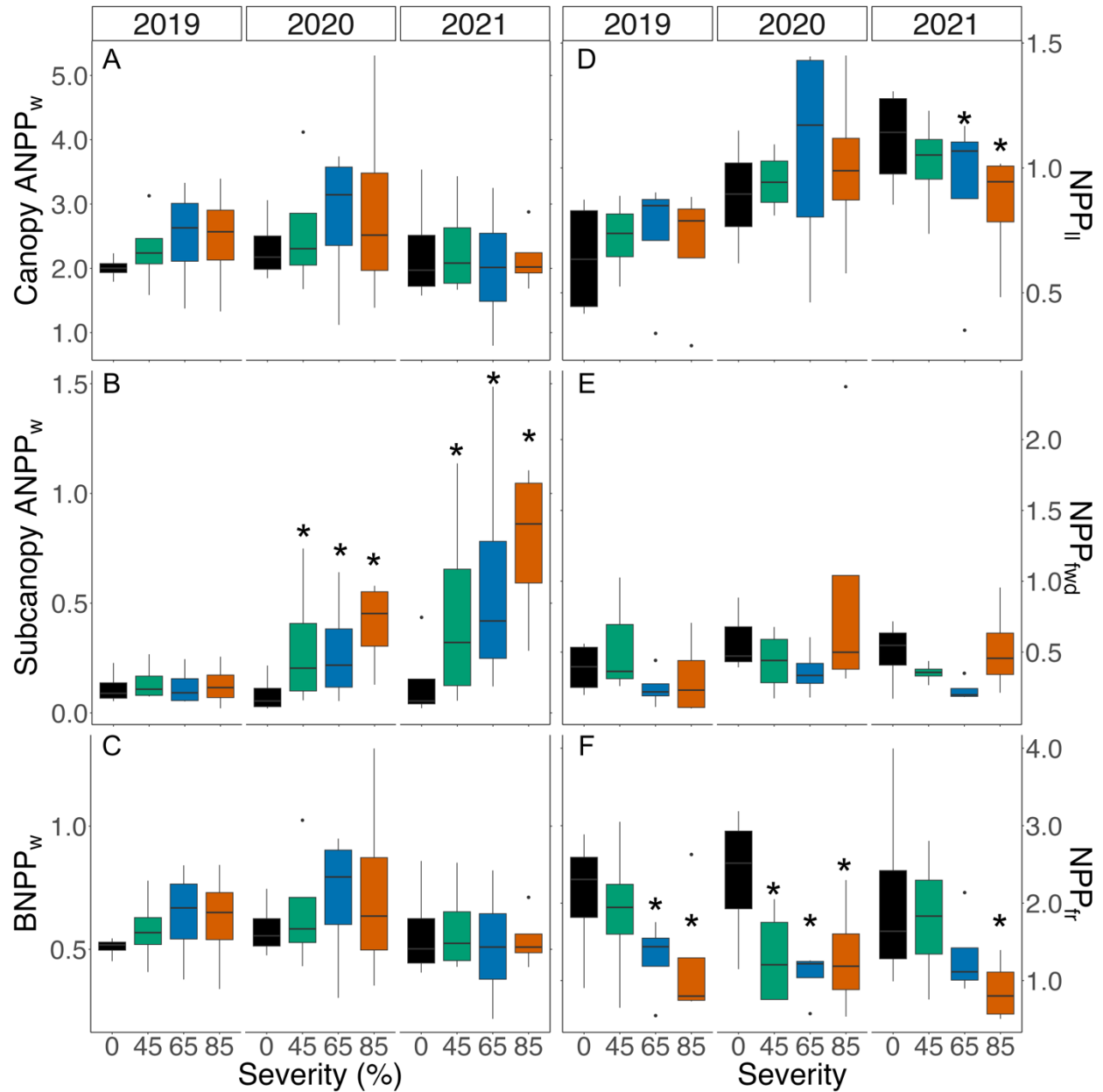


Figure 3.3: Boxplots displaying median, interquartile range (middle 50% of range) and minimum and maximum **A)** Canopy ANPP_w ($F = 0.622$, $p = 0.71$), **B)** Subcanopy ANPP_w ($F = 7.04$, $p < 0.001$), **C)** BNPP_w ($F = 0.62$, $p = 0.71$), **D)** NPP_{II} ($s F = 2.39$, $p = 0.05$), **E)** NPP_{fwd} ($F = 0.77$, $p = 0.60$), and **F)** NPP_{fr} (p -value = 0.05) across disturbance severities (2019-2021). Asterisks (*) indicates pair-wise significant differences from the control. All fluxes are presented as $\text{Mg C ha}^{-1} \text{ yr}^{-1}$.

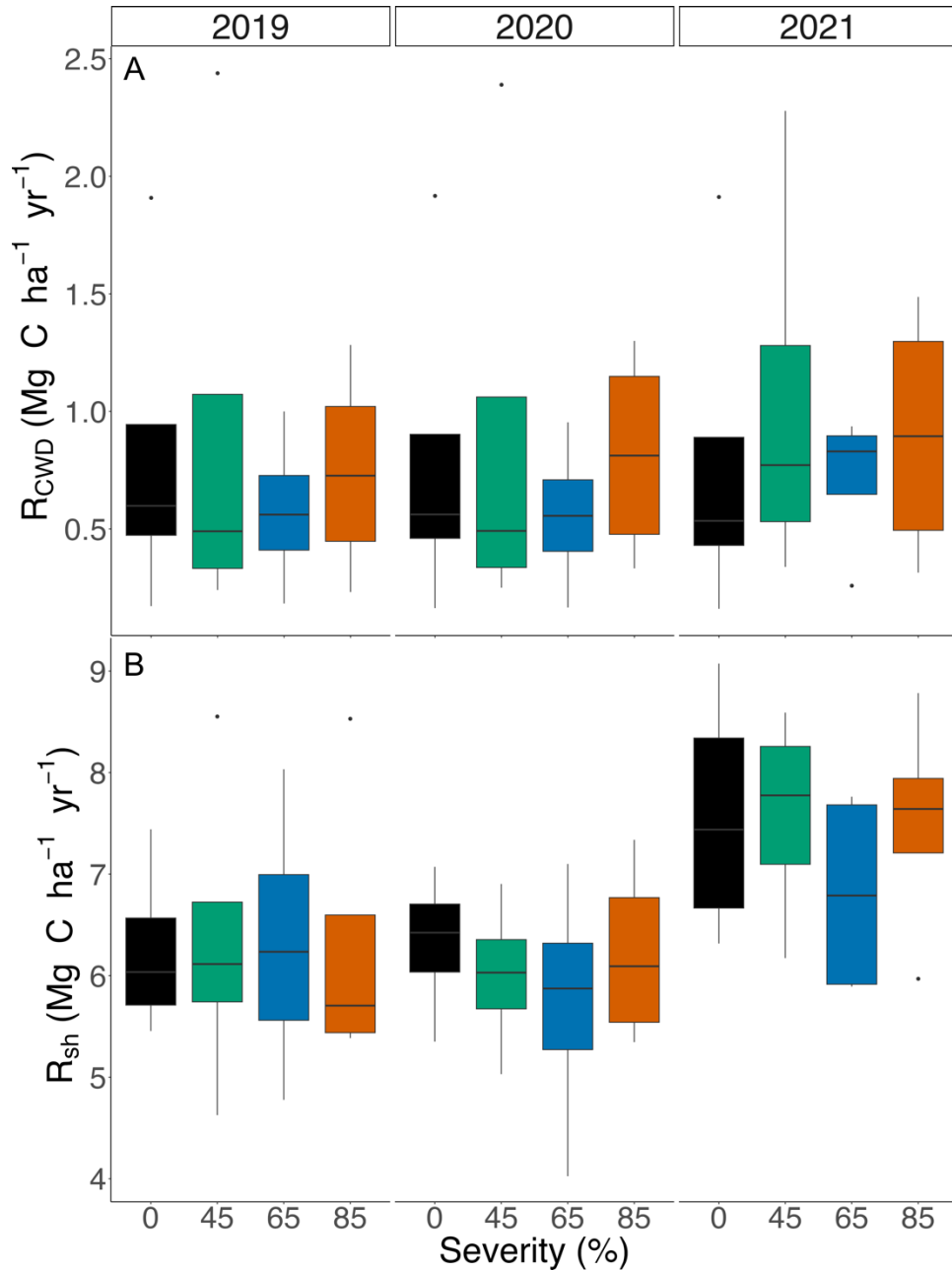


Figure 3.4: Boxplots displaying median, interquartile range (middle 50% of range) and minimum and maximum **A)** R_{cwd} , averaged across 3 methods ($F = 1.4$, $p\text{-value} = 0.26$), and **B)** R_{sh} ($F = 0.35$, $p\text{-value} = 0.9$) averaged across 4 methods and across disturbance severities (2019-2021). Fluxes are presented as Mg C ha⁻¹ yr⁻¹.

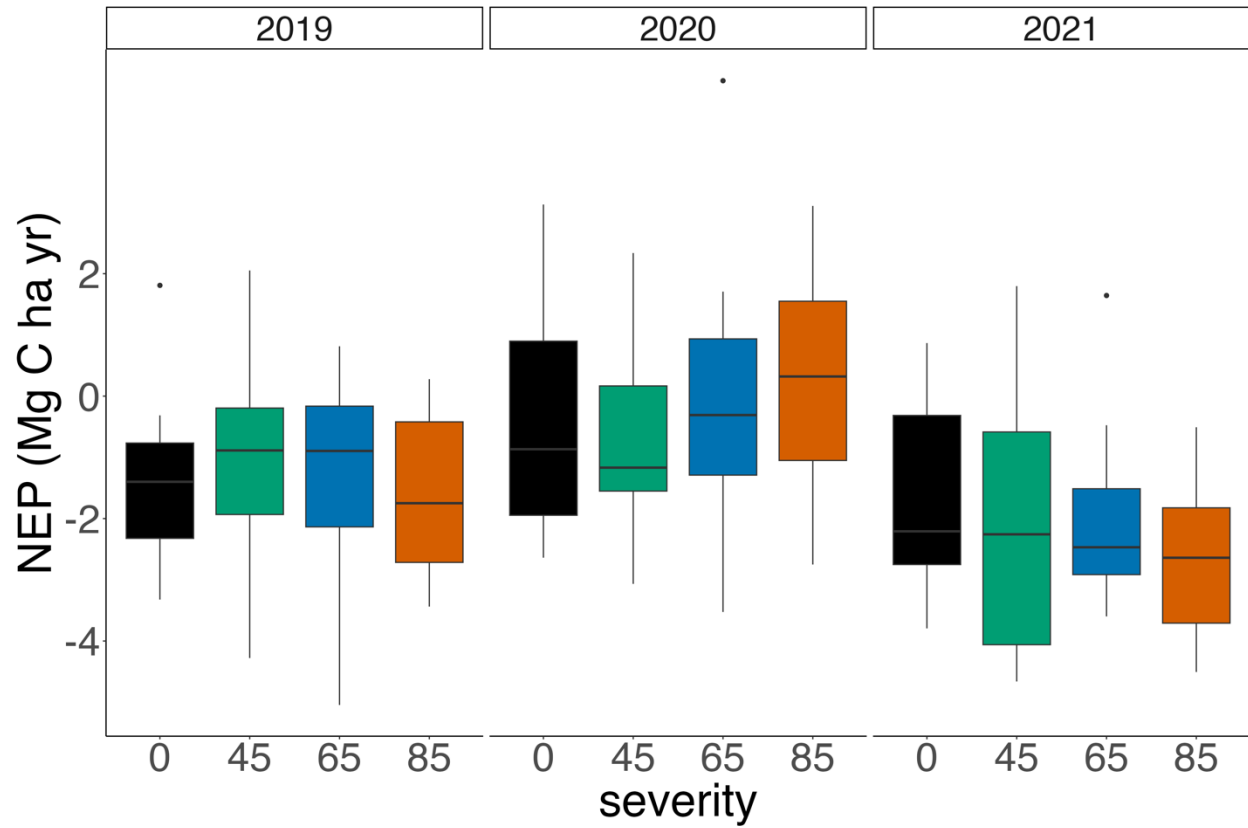


Figure 3.5: Boxplots displaying median, interquartile range (middle 50% of range) and minimum and maximum NEP across disturbance severities (2019-2021) and averaged across methods.

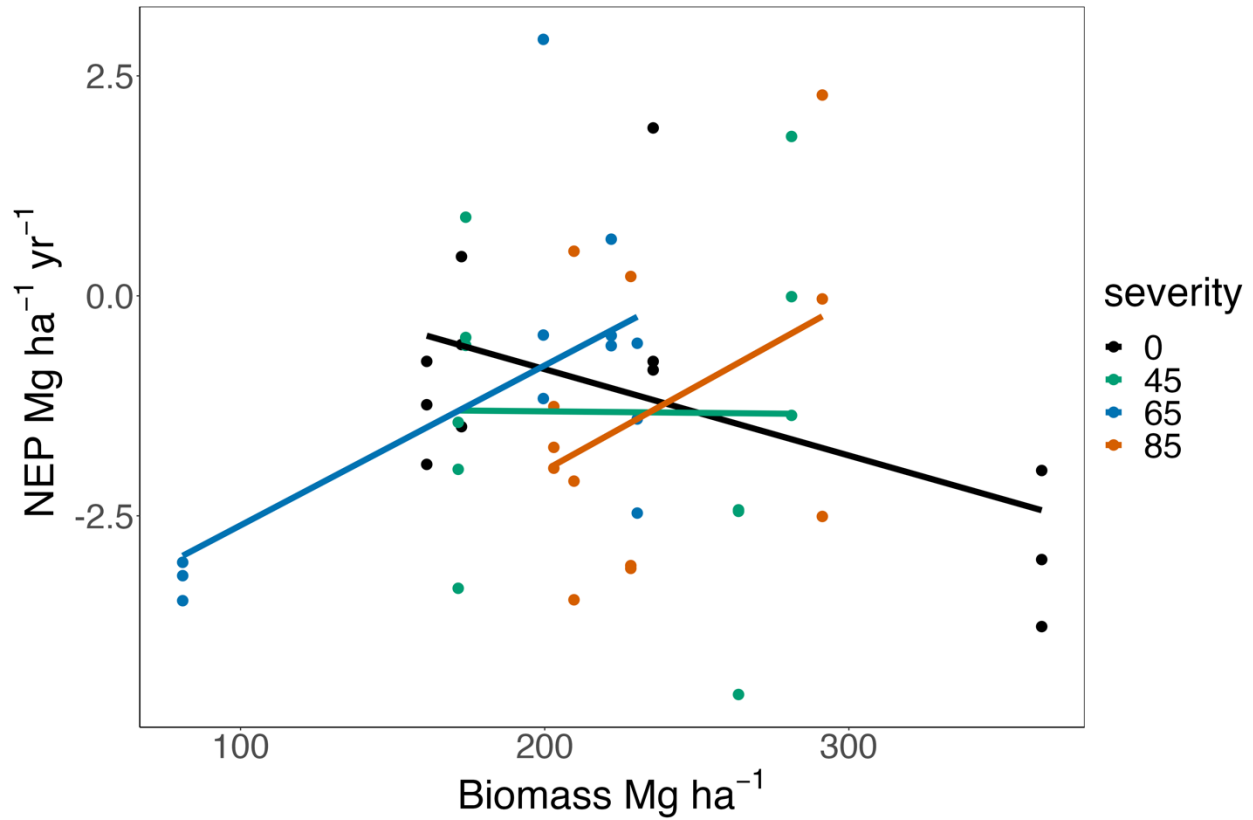
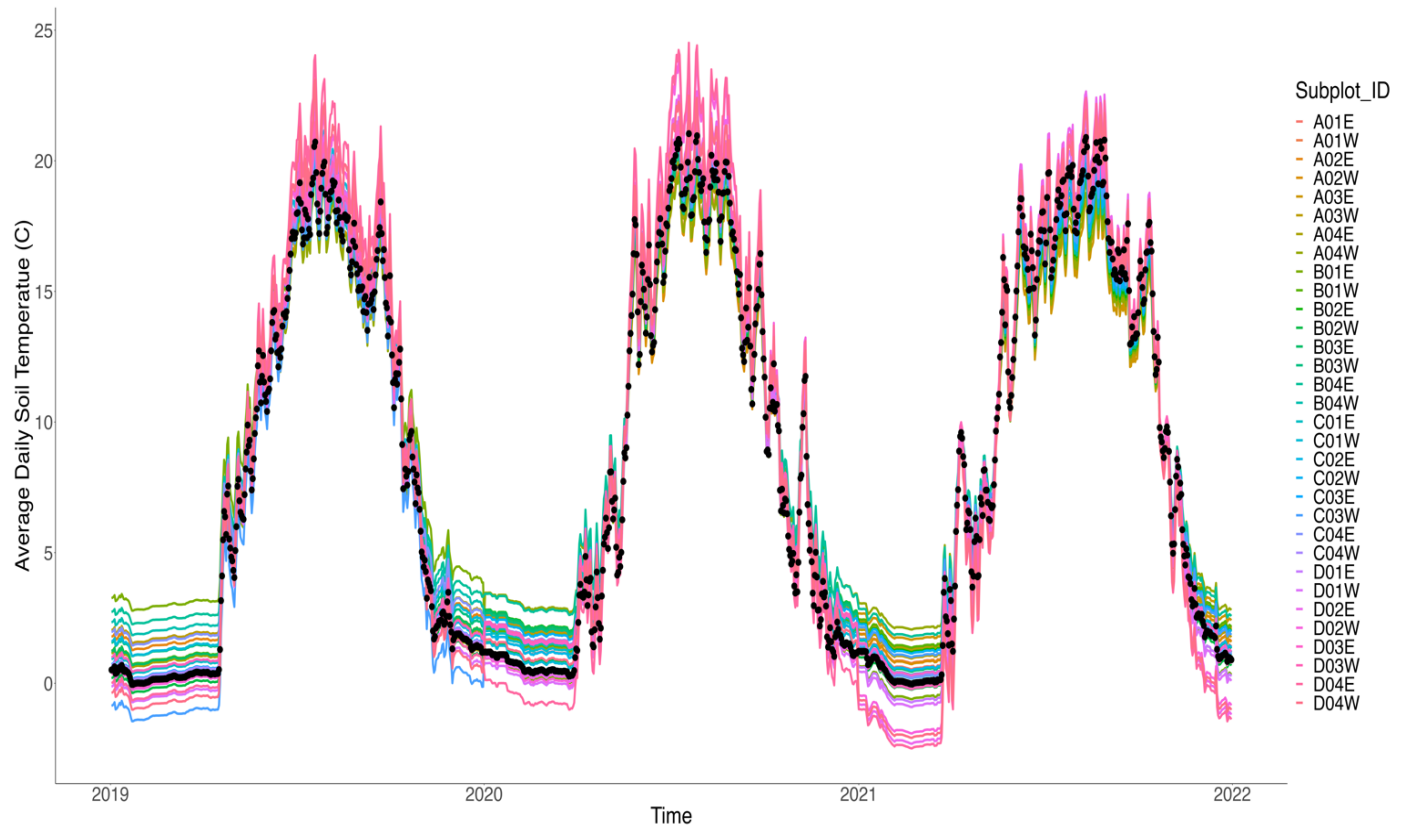


Figure 3.6: NEP averaged across methods as a function of pre-disturbance biomass, 2019-2021. Colored lines represent significant interaction between pre-disturbance biomass and disturbances severity (Adjusted $R^2 = 0.35$, $F = 4.8$, p -value = 0.002).

Chapter 3 Appendix:



Figures S3.1: Modeled average daily soil temperature (T_s , °C) to 7cm depth across all subplots.

Black dots represent flux tower measurements of T_s (US-UMB, Gough et al. 2016).

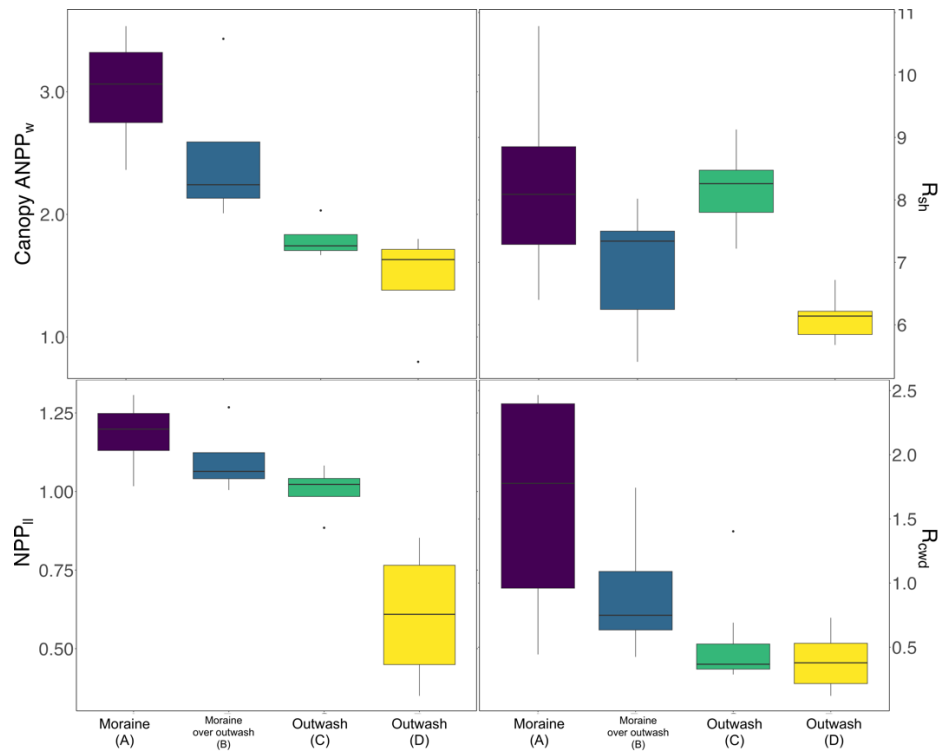


Figure S3.2: Boxplots displaying median, interquartile range (middle 50% of range) and minimum and maximum component C fluxes across experimental replicates (2019-2021) and averaged across disturbance severity.

Table S3.1: Genus-specific decay constants from Kahl et al. 2017 used to calculate coarse woody debris flux (Method 2).

Genus	Decay Rate (y^{-1})
<i>Acer</i>	0.05
<i>Betula</i>	0.042
<i>Fagus</i>	0.069
<i>Pinus</i>	0.015
<i>Populus</i>	0.055
<i>Quercus</i>	0.021
<i>Abies</i>	0.035
<i>Tsuga</i>	0.002

Table S3.2a: Summary of ANOVA output for canopy NPP_w response to experimental disturbance. Split plot design with Severity as whole-plot, Year as split plot and Replicate as blocking factor. Alpha = 0.05. Significance codes: 0.001 = ***, 0.01 = **, 0.05 = *, 0.1 = •.

Source of Variation	Degrees of Freedom	Sum of Squares	Mean Square	F	p-value
Severity	3	1.35	0.45	0.19	0.90
Replicate	3	28.3	9.43	4.04	0.05*
Whole Plot Error (Replicate *Severity)	9	21.01	2.336		
Year	2	3.80	1.9	3.60	0.04*
Severity*Year	6	1.97	0.33	0.62	0.71
Split-split Plot Error (Replicate*Severity *Year)	24	12.67	0.53		

Table S3.3a: Summary of ANOVA output for subcanopy NPP_w response to experimental disturbance. Split plot design with Severity as whole-plot, Year as split plot and Replicate as blocking factor. Alpha = 0.05. Significance codes: 0.001 = ***, 0.01 = **, 0.05 = *, 0.1 = •.

Source of Variation	Degrees of Freedom	Sum of Squares	Mean Square	F	p-value
Severity	3	11.53	3.85	2.18	0.16
Replicate	3	14.07	4.69	2.66	0.11
Whole Plot Error (Replicate *Severity)	9	15.85	1.76		
Year	2	7.65	3.83	24.01	<0.001***
Severity*Year	6	6.73	1.12	7.04	<0.001***
Split-split Plot Error (Replicate*Severity *Year)	24	3.82	0.16		

Table S3.3b: Summary of Least Significant Difference (LSD) for significant Severity*Year interaction (Table S3.3a) with 95% lower and upper confidence levels. Alpha = 0.05. Levels with the same group letter are not significantly different.

Factor	Mean Square Error	DF Error	Critical Value	LSD
Severity*Year	0.16	24	2.06	0.58

Level	Log Subcanopy NPP _w	Groups
85:2021	-0.37	a
65:2021	-0.88	ab
85:2020	-1.05	bc
45:2021	-1.34	bcd
45:2020	-1.63	cde
65:2020	-1.64	de
45:2019	-2.10	ef
0:2019	-2.32	fg
65:2019	-2.32	fg
85:2019	-2.40	fg
0:2021	-2.62	fg
0:2020	-2.86	g

Table S3.4: Summary of ANOVA output for BNPP_w response to experimental disturbance. Split plot design with Severity as whole-plot, Year as split plot and Replicate as blocking factor. Alpha = 0.05. Significance codes: 0.001 = ***, 0.01 = **, 0.05 = *, 0.1 = •.

Source of Variation	Degrees of Freedom	Sum of Squares	Mean Square	F	p-value
Severity	3	0.04	0.01	0.21	0.89
Replicate	3	0.79	0.26	3.80	0.05*
Whole Plot Error (Replicate *Severity)	9	0.62	0.07		
Year	2	0.12	0.06	3.67	0.04*
Severity*Year	6	0.06	0.01	0.62	0.71
Split-split Plot Error (Replicate*Severity *Year)	24	0.39	0.02		

Table S3.5a: Summary of ANOVA output for NPP_{II} response to experimental disturbance. Split plot design with Severity as whole-plot, Year as split plot and Replicate as blocking factor. Alpha = 0.05. Significance codes: 0.001 = ***, 0.01 = **, 0.05 = *, 0.1 = •.

Source of Variation	Degrees of Freedom	Sum of Squares	Mean Square	F	p-value
Severity	3	0.02	0.00	0.12	0.94
Replicate	3	1.82	0.51	8.92	0.005**
Whole Plot Error (Replicate *Severity)	9	0.61	0.07		
Year	2	0.82	0.41	26.19	<0.001***
Severity*Year	6	0.23	0.04	2.39	0.05*
Split-split Plot Error (Replicate*Severity *Year)	24	0.38	0.02		

Table S3.5b: Summary of Least Significant Difference (LSD) for significant Severity*Year interaction (Table S3.5a) with 95% lower and upper confidence levels. Alpha = 0.05. Levels with the same group letter are not significantly different.

Factor	Mean Square Error	DF Error	Critical Value	LSD
Severity*Year	0.02	24	2.06	0.18

Level	NPP _{II}	Groups
0:2021	1.11	a
65:2020	1.06	ab
45:2021	1.01	abc
85:2020	1.00	abc
45:2020	0.95	abc
65:2021	0.91	bcd
0:2020	0.89	bcde
85:2021	0.85	cdef
65:2019	0.73	defg
45:2019	0.72	efg
85:2019	0.69	fg
0:2019	0.64	g

Table S3.6: Summary of ANOVA output for NPP_{fwd} response to experimental disturbance. Split plot design with Severity as whole-plot, Year as split plot and Replicate as blocking factor. Alpha = 0.05. Significance codes: 0.001 = ***, 0.01 = **, 0.05 = *, 0.1 = •.

Source of Variation	Degrees of Freedom	Sum of Squares	Mean Square	F	p-value
Severity	3	2.04	0.68	1.58	0.28
year	2	0.59	0.29	0.68	0.54
Replicate	3	3.38	1.12	2.63	0.13
Whole Plot Error (Replicate *Severity)	7	3.00	0.43		
Year	2	1.66	0.83	3.02	0.07•
Severity*Year	6	1.27	0.21	0.77	0.60
Split-split Plot Error (Replicate*Severity *Year)	22	6.05	0.28		

Table S3.7a: Summary of ANOVA output for NPP_{fr} response to experimental disturbance. Split plot design with Severity as whole-plot, Year as split plot and Replicate as blocking factor. Alpha = 0.05. Significance codes: 0.001 = ***, 0.01 = **, 0.05 = *, 0.1 = •.

Source of Variation	Degrees of Freedom	Sum of Squares	Mean Square	F	p-value
Severity	3	8.07	2.69	2.66	0.11
Replicate	3	7.20	2.40	2.40	0.14
Whole Plot Error (Replicate *Severity)	9	9.11	1.01		
Year	2	0.16	0.08	0.28	0.76
Severity*Year	6	1.41	0.23	0.80	0.58
Split-split Plot Error (Replicate*Severity *Year)	24	7.01	0.29		

Table S3.7b: Summary of Least Significant Difference (LSD) for significant Severity*Year interaction (Table S3.7a) with 95% lower and upper confidence levels. Alpha = 0.05. Levels with the same group letter are not significantly different.

Factor	Mean Square Error	DF Error	Critical Value	LSD
Severity*Year	0.29	24	2.06	0.79

Level	NPP_{fr}	Groups
0:2020	1.11	a
0:2019	1.06	ab
0:2021	1.01	abc
45:2019	1.00	abcd
45:2021	0.95	abcde
65:2021	0.91	bcdef
45:2020	0.89	cdef
85:2020	0.85	cdef
65:2019	0.73	cdef
85:2019	0.72	def
65:2020	0.69	ef

Table S3.8: Summary of ANOVA output for $R_{\text{c wd}}$ response to experimental disturbance. Split plot design with Severity as whole-plot, Year as split plot and Replicate as blocking factor. Alpha = 0.05. Significance codes: 0.001 = ***, 0.01 = **, 0.05 = *, 0.1 = •.

Source of Variation	Degrees of Freedom	Sum of Squares	Mean Square	F	p-value
Severity	3	1.17	0.39	0.24	0.86
Replicate	3	34.3	11.4	7.15	0.01**
Whole Plot Error (Replicate *Severity)	9	14.4	1.6		
Year	2	0.43	0.21	3.91	0.03*
Severity*Year	6	0.43	0.07	1.32	0.28
Split-split Plot Error (Replicate*Severity *Year)	24	1.31	0.05		

Table S3.9: Summary of ANOVA output for R_{sh} response to experimental disturbance. Split plot design with Severity as whole-plot, Year as split plot and Replicate as blocking factor. Alpha = 0.05. Significance codes: 0.001 = ***, 0.01 = **, 0.05 = *, 0.1 = •.

Source of Variation	Degrees of Freedom	Sum of Squares	Mean Square	F	p-value
Severity	3	1.145	0.48	0.75	0.55
Replicate	3	30.1	10.0	15.6	0.0001***
Whole Plot Error (Replicate *Severity)	9	5.79	0.64		
Year	2	15.3	7.66	14.45	<0.0001***
Severity*Year	6	1.09	0.18	0.35	0.91
Split-split Plot Error (Replicate*Severity *Year)	24	12.7	0.53		

Table S3.10: Summary of ANOVA output for total NPP response to experimental disturbance. Split plot design with Severity as whole-plot, Year as split plot and Replicate as blocking factor. Alpha = 0.05. Significance codes: 0.001 = ***, 0.01 = **, 0.05 = *, 0.1 = •.

Source of Variation	Degrees of Freedom	Sum of Squares	Mean Square	F	p-value
Severity	3	4.50	1.50	0.36	0.78
Replicate	3	53.5	17.8	4.25	0.04*
Whole Plot Error (Replicate *Severity)	9	37.7	4.20		
Year	2	13.65	6.82	4.60	0.02*
Severity*Year	6	10.2	1.70	1.15	0.36
Split-split Plot Error (Replicate*Severity *Year)	24	35.63	1.48		

Table S3.11: Summary of ANOVA output for total R_h response to experimental disturbance. Split plot design with Severity as whole-plot, Year as split plot and Replicate as blocking factor. Alpha = 0.05. Significance codes: 0.001 = ***, 0.01 = **, 0.05 = *, 0.1 = •.

Source of Variation	Degrees of Freedom	Sum of Squares	Mean Square	F	p-value
Severity	3	7.47	2.49	0.82	0.51
Replicate	3	80.5	26.83	8.85	0.005**
Whole Plot Error (Replicate *Severity)	9	27.26	3.03		
Year	2	35.4	17.7	16.5	<0.001***
Severity*Year	6	2.15	0.36	0.33	0.91
Split-split Plot Error (Replicate*Severity *Year)	24	25.8	1.08		

Table S3.11: Summary of ANOVA output for mean NEP response to experimental disturbance. Split plot design with Severity as whole-plot, Year as split plot and Replicate as blocking factor. Alpha = 0.05. Significance codes: 0.001 = ***, 0.01 = **, 0.05 = *, 0.1 = •.

Source of Variation	Degrees of Freedom	Sum of Squares	Mean Square	F	p-value
Severity	3	1.10	0.37	0.03	0.99
Replicate	3	32.8	10.9	0.92	0.47
Whole Plot Error (Replicate *Severity)	9	107	11.8		
Year	2	58.6	29.3	13.5	<0.001***
Severity*Year	6	8.11	1.35	0.63	0.71
Split-split Plot Error (Replicate*Severity *Year)	24	52.0	2.17		

Table S3.12: Output for regression analysis of NEP as a function of pre-disturbance biomass, disturbance severity and year (2019, 2020, 2021). Significance codes: 0.001 = ***, 0.01 = **, 0.05 = *, 0.1 = •.

Predictors	Estimates	Standard Error	p-value
(Intercept)	1.20	1.21	0.33
Severity	-0.08	0.02	0.003**
Biomass	-0.01	0.004	0.03*
Year[2020]	1.16	0.49	0.02*
Year[2021]	-0.73	0.49	0.14
Severity*Biomass	0.00	0.000	0.002**

Residual SE: 1.38 on 42 df. R^2 : 0.38. F-statistic: 5.2. p-value: **<0.001*****

**Chapter 4: Dynamic rhizosphere processes drive immediate soil respiration response to
phloem-disruption**

Author: Kayla C. Mathes

Contributors: Tatum Delany¹, Lisa Nalliah², Christopher M. Gough³

Contributor Affiliations:

Department of Biology, Virginia Commonwealth University, Box 842012, 1000 West Cary
St., Richmond, VA 23284.

¹ Institute of Environment and Sustainability, University of California Los Angeles, 619 Charles
E. Young Drive East, Box 951496, Los Angeles, CA 90095.

² Goshen College, 1700 S Main St, Goshen, IN 46526.

³ Department of Biology, Virginia Commonwealth University, Box 842012, 1000 West Cary
St., Richmond, VA 23284.

Abstract

Global change is causing an increase in phloem-disrupting forest disturbances with uncertain consequences for soil respiration (R_s), the largest outward flux from terrestrial ecosystems.

Substantial variability in immediate R_s response to phloem-disruption illustrates the need to better understand how fine-scale rhizosphere processes that regulate R_s unfold within days-to-weeks following disturbance. Given the patchy mortality that results from phloem-disrupting disturbances, addressing dynamic changes in resource allocation and root physiology from both disturbed and surviving trees may help resolve variability in stand-level R_s responses.

We initiated the Short-term Rhizosphere Response to Experimental Disturbance (ShRRED), a controlled disturbance manipulation, to examine the fine-scale soil biochemical and fine-root traits that could regulate immediate R_s response to phloem-disruption. ShRRED is situated in a Northern temperate forest and consists of paired control and girdled plots containing a single surviving canopy tree at plot-center. We found sustained stand-level R_s within the first 100 days following disturbance, maintenance of root non-structural carbohydrates in girdled trees, and greater stand-level soil nitrogen that may have facilitated changes in fine-root structure and C storage in surviving trees. We conclude that early responses from surviving tree roots in advance of full functional decline in girdled trees may have supported sustained stand-level R_s in the first year.

Key words: forest disturbance, non-structural carbohydrates, phloem-disruption, fine-roots, rhizosphere, soil nitrogen, soil respiration

1. Introduction

Phloem-disrupting disturbances from insects are increasing in North American temperate forests (Dietze and Matthes 2014, Sommerfeld et al. 2018, Edgar and Westfall 2022), with uncertain consequences for soil respiration (R_s), the largest efflux of carbon from terrestrial ecosystems (Binkley et al. 2006, Lei et al. 2021). Phloem-disrupting disturbances are often caused by host-specific wood boring insects such as mountain pine beetles and emerald ash borers (Davis et al. 2019, Quirion et al. 2021) that eliminate the transport of carbohydrates from the canopy to roots. While many studies have examined R_s following phloem-disrupting disturbances (Högberg et al. 2001, Bhupinderpal-Singh et al. 2003, Frey et al. 2006, Ekberg et al. 2007), there is substantial variation in the timing, direction, and magnitude of response. While some studies found R_s exhibited immediate, multi-year declines after phloem-disruption (Mathes et al. *in review*), others report only temporary reductions (Levy-Varon et al. 2012, 2014) or found no changes in R_s following phloem-disruption (Aubrey and Teskey 2018, Fraterrigo et al. 2018, Nottingham et al. 2022). Because these disturbances result in heterogeneously distributed tree mortality (Flower et al. 2015, Atkins et al. 2020), interpreting stand-scale changes in R_s requires understanding of rhizosphere (i.e. soil-root interface) changes and interactions among girdled and surviving trees.

Identifying the near-term rhizosphere responses to phloem-disrupting disturbance is crucial to understanding why observed responses in stand-scale R_s are variable. R_s is driven by several interacting factors in the rhizosphere, including the storage of nonstructural carbohydrates (NSCs) available to fuel root metabolism and functioning (Nakane et al. 1996, Brüggemann et al. 2011, Epron et al. 2012). If root functioning is compromised, phloem-disruption may, in turn,

increase stand-scale soil nitrogen (N) availability (Zeller et al. 2008, Nave et al. 2011), stimulating changes in the root traits of surviving trees that are relevant to R_s . Specifically, soil N enrichment promotes the production of smaller diameter, higher surface area absorptive fine-roots that facilitate more efficient nutrient uptake (Kochsiek et al. 2013, Fort and Freschet 2020, Cabugao et al. 2021). Absorptive fine-roots are also more metabolically active, with high exudation and respiration rates (McCormack et al. 2015). While these rhizosphere responses to phloem-disruption are well-characterized individually, integrative understanding of root-soil interactions at multiple spatial scales is required to improve ecosystem models' representation of disturbance (Berkelhammer et al. 2022), determine why ecosystems exhibit different responses to the same disturbance (Dietze and Matthes 2014), and forecast changes in ecosystem C balance.

We initiated a girdling experiment to characterize the interacting rhizosphere processes that regulate the response of stand-scale R_s to phloem-disruption. Specifically, we examined how R_s responds to phloem-disruption in the first 100 days and how this ecosystem-wide flux relates to changes in soil available N, root NSCs, fine-root exudation rates, and root structural traits associated with nutrient acquisition and R_s . We hypothesized immediate declines in stand-level R_s following phloem-disruption will parallel: 1) An increase in stand soil N availability, 2) declines in root NSC concentrations in girdled trees, 3) a proliferation of smaller absorptive fine-roots with higher surface area:volume and exudation rates from surviving trees 4) and an increase in root NSC concentration in surviving trees in response to the N enriched environment (Figure 4.1).

2. Methods

2.1. Study Site and Experimental Design

Our study took place at the University of Michigan Biological Station (UMBS) near Pellston, MI. (45.56 N, 84.67 W). The mean annual air temperature and precipitation are 5.5°C and 817 mm, respectively (Gough et al. 2021). Our site is a ~ 110 year old mixed temperate hardwood and pine dominated forest undergoing succession from big-toothed aspen (*Populus grandidentata*) dominated canopy to Eastern white pine (*Pinus strobus*), Northern red oak (*Quercus rubra*) and red maple (*Acer rubrum*) dominated canopy and sub-canopy. Soils are excessively well-drained sandy spodosols derived from unconsolidated material formed by high-elevation glacial outwash plains (Pearsall et al. 1995).

We initiated the Short-term Rhizosphere Response to Experimental Disturbance (ShRRED), a small-scale controlled disturbance manipulation to examine the soil biochemical and fine-root properties that could regulate ecosystem-scale R_s response to phloem-disruption. In May of 2022, we established eight 100 m² plots arranged in a rectangular pattern with a 10-15 m buffer between plots (Figure 4.2a). All plots were located on the same landscape ecosystem type (Pearsall et al. 1995) and were uniform in species composition, aboveground biomass, stem density and soil composition (Table 4.1). Plots were centered around one ungirdled canopy *Q. rubra* tree, hereafter referred to as the “surviving focal tree” in the disturbance treatment or “control focal tree” in the control plots (>20 cm DBH, Figure 4.2b). Considering that natural phloem-disrupting disturbances create patchy mortality, leaving a mix of surviving and girdled trees in the landscape (Flower et al. 2015), our goal was to recreate the immediate surroundings of a surviving tree on a disturbed landscape. Then, capture changes in soil biochemical responses

at the plot-level and immediate rhizosphere responses from individual surviving and girdled trees. Given that our small plots were surrounded by undisturbed forest, we only chose one focal surviving tree per plot to create a completely disturbed environment surrounding the focal tree. *Q. rubra* was chosen as the focal species given its high dominance and density in the canopy within the study ecosystem type (Table 4.1) and unlike *P. grandidentata*, does not have a clonal root structure that would create additional uncertainty. The first focal *Q. rubra* tree was randomly selected within the approved manipulation boundary and the subsequent focal trees were assigned by locating the nearest *Q. rubra* (> 20 cm DBH) outside of the plot and buffer boundary. Plots were randomly assigned either disturbance (n = 4) or control (n = 4) and following pre-treatment data collection in mid-May 2022, we stem-girdled 38 canopy (> 8cm DBH) and 132 subcanopy (>1.4 meters tall) trees in the 4 disturbance plots on May 30 and 31, 2022. All canopy and subcanopy trees in the disturbance plots were girdled except for the focal surviving *Q. rubra*. (See Figure 4.2a,b for plot design.)

2.2. Soil respiration (R_s)

We measured bulk soil respiration (R_s , $\mu\text{molCO}_2 \text{ m}^{-2} \text{ s}^{-1}$) one time before and 6 times following girdling disturbance between May 26 and September 9, 2022 (- 4 - 101 days after girdling). We established 4 locations to measure *in-situ* R_s arranged in a square half-way between the “focal” tree and the plot corner (Figure 4.2b). We measured R_s with a LI-6400 portable gas analyzer with a 10 cm diameter cuvette (LI-COR Inc, Lincoln, NE, USA) and used a removable collar technique with a 10 cm diameter PVC collar with a foam seal. At each measurement location, two R_s values were recorded and averaged for analysis. The settings during measurements were as follows: 400-420 ppm target CO_2 concentration with measurement range from 390-410 ppm

to 410-430 ppm ($\Delta = 10$), 10 second gap between drawdown and measurements (Dead Time), 20 second minimum measurement time, 120 second maximum measurement time, 80 cm² soil surface area within chamber and 500 ($\mu\text{mol s}^{-1}$) drawdown flow rate. To minimize the confounding of treatment and time-of-day, plot sampling order was randomized for each measurement campaign. R_s was not taken within 24 hours of any rain event nor within 48 hours of heavy rainfall. R_s was measured concurrently with soil temperature (T_s , °C) to 7 cm depth using a digital thermometer (Hanna Instruments, Inc, Smithfield RI) and 20 cm integrated soil volumetric water content (VWC, %) using a CS620 soil moisture probe (Campbell Scientific, Inc, Logan, UT, USA).

2.3. Coarse root non-structural carbohydrates (NSC): Girdled and surviving trees

To measure coarse root non-structural carbohydrates (NSC) following disturbance we extracted phloem tissue from surviving focal trees and girdled trees in the disturbance plots and the focal trees in the control plots. We then ran colorimetric assays three times between July 13 and 25 (44-56 days after girdling). We used an increment borer to extract phloem from the four focal surviving trees and four girdled *Q. rubra* trees in the disturbance plots and the four focal trees in the control plots (Figure 4.2b). Phloem was extracted from a coarse root located from the base of the tree. All extractions were standardized for position on the tree (cardinal direction) and all repeat extractions were taken from the same location on the coarse roots. Samples were placed on ice in the field and taken back to the lab for analysis. Phloem tissue samples were lyophilized, pulverized using a ball mill and extracted with 80% and 45% HEPES buffered ethanol. Colorimetric assays were run in a spectrophotometer set to 490 nm using 80% redistilled phenol as the reagent and reading absorbance levels every 30 seconds for 5 minutes. Percent non-

structural carbohydrate concentrations were calculated from the proportion of NSC concentration to sample dry mass.

2.4. Total soil Nitrogen (NH_4^+ and NO_3^-)

To assess total available inorganic soil nitrogen (N) following phloem-disruption we extracted soil cores and determined NH_4^+ and NO_3^- concentrations 4 times between June 28 and July 25 (28 - 56 days after girdling). We established 4 soil sampling locations spatially paired with R_s measurements, located halfway between the edge of the plot and the focal *Q. rubra* tree (Figure 4.2b). We collected O and A horizon soil to 10 cm depth and concurrently recorded soil temperature (T_s , °C) to 7 cm depth. Soil was transported to the lab on ice and stored at 4°C for 24 hours. Soil was separated from roots, coarse fragments, and debris with 2 mm sieve and the 4 soil samples from each plot were homogenized before extraction ($n = 8$). ~5 g of each sample was weighed and dried at 60°C for 24 hours to determine gravimetric water content. An additional 5 g of wet soil was taken from each sample, extracted with 25 ml KCl, shaken and left to settle at 1°C for 24 hours. The KCl supernatant was then diluted with 50% HCl and extracts were analyzed for NH_4^+ and NO_3^- concentrations (ug/L) in an autoanalyzer (Seal Analytical AA3 Autoanalyzer, info). Inorganic soil N concentrations were then converted to mg NH_4^+ and NO_3^- / kg dry soil.

2.5 Focal surviving tree fine-root structure: Field sampling and root analysis

To assess whether there was a shift to higher proportions of absorptive fine-roots in surviving focal trees within the disturbance plots, we measured two structural traits that distinguish absorptive from transport roots: fine-root surface area (cm^2):volume (cm^3) (SAV) and average

fine-root diameter (mm) (McCormack et al. 2015). We used a modified protocol described in Weemstra et al. 2020. Three times during the growing season, we extracted three 10 cm depth soil cores of the O and A horizons 0.5 m away from the surviving focal tree in all 8 plots (Figure 4.2b). Root attenuation data across multiple temperate tree species suggests a stem-center rooting distribution with declines in root mass moving away from the stem within the first 10 m (Rewald and Leuschner 2009). Therefore, while core samples taken from 0.5 m may have captured fine-roots from neighboring trees, we assumed that the majority of fine-roots within core samples were from the focal trees. Soil cores were stored in a 4 °C fridge for 24 hours and then carefully sieved and washed with deionized water. Roots were separated into fine (<2 mm diameter) and coarse (>2 mm diameter) roots and scanned with a winRhizo root scanner (Regent Instruments) to determine total fine-root surface area, mean diameter and mean root volume. Fine-roots were then oven-dried at 60°C for 48 hours to determine dry mass. Finally, to determine ash-free mass, subsamples were burned in a muffle furnace at 500 °C for 12 hours.

2.6. Surviving tree fine-root exudation: Field procedure and extraction

To assess whether a proliferation in absorptive fine-roots in surviving focal trees resulted in increased exudation rates, we measured total non-particulate organic carbon in fine-roots surrounding the surviving focal and control focal trees. We used a modified *in-situ* fine-root extraction method adapted from Phillips et al. 2008 and Abramoff and Finzi 2016. Surrounding the base of all surviving focal *Q. rubra* trees in the disturbance plots and focal trees in the control plots (n = 8) (Figure 4.2b), we uncovered three separate intact fine-roots (15-20 cm). Roots were thoroughly washed with deionized water to remove all soil and debris. Washed and intact roots were then inserted into a 30 mL sterile plastic cuvette filled with sterile pure sand (Fisher

Scientific, Inc.) and 10 mL of a C-free nutrient solution (0.5 mM NH_4NO_3 , 0.1 mM KH_2PO_4 , 0.2 mM K_2SO_4 , 0.2 mM MgSO_4 , 0.3 mM CaCl_2). Tops of cuvettes were covered with parafilm and the entire cuvette was covered with tin foil to prevent desiccation. Roots were then left for 24 hours to recover from excavation. After the recovery period, the nutrient solution was pulled from each cuvette and discarded using a three-stop cock and syringe. 15 mL of additional nutrient solution was added, cuvettes were rewrapped in tin foil and left for 24 hours. After the incubation period, extract was pulled from cuvettes and an additional 10 mL was inserted and immediately removed from the cuvette to make sure all root extract was captured. The 25 mL of extract was immediately placed on ice in the field and then stored in a 0 °C freezer. Finally, fine-roots were cut, wrapped in a moist towel and placed in a 4 °C fridge. Following field procedures, we performed a Whatman filtration to remove particulate matter and the three pseudo samples from each tree were homogenized before analysis. Samples were analyzed for total non-particulate organic carbon (NOC, mg/L) using a TOC analyzer (Shimadzu Scientific Instruments). Exudation rate ($\text{g C g root}^{-1} \text{ day}^{-1}$) was scaled to $\text{g C m}^{-2} \text{ d}^{-1}$ using fine root biomass (g root m^{-2}) from soil cores.

2.7 Statistical analysis

All statistical analyses and comparisons were chosen *a priori* from the hypothesized progression of rhizosphere changes following phloem-disruption (Figure 4.1). First, to assess changes in stand-level R_s and soil N availability (NH_4^+ and NO_3^-) (O1), we ran repeated measures ANOVAs with alpha values set to 0.1 to assess changes over time and statistical differences between disturbance and control plots. The experimental unit was the plot average over the 4 paired measurement locations within each plot (Figure 4.1b, $n = 8$). R_s , NH_4^+ and NO_3^- all required log

transformations in order meet ANOVA model assumptions of equality of variance and normality. Given the large variation in R_s across the growing season, we also calculated R_s “resistance” to isolate patterns in R_s relative to the control. Resistance is a log effect-size ratio describing the magnitude of initial response to disturbance normalized to a control (Hillebrand et al. 2018, Mathes et al. 2021).

$$\text{Equation 1: } \textit{resistance} = \ln\left(\frac{\textit{Disturbance } R_s}{\textit{Control } R_s}\right)$$

To assess how phloem-disruption impacts non-structural carbohydrate (NSC) concentration of girdled trees (O2) we ran similar repeated measures ANOVAs described above and compared girdled trees within the disturbance plots to trees within the control plots. NSC concentration required a log transformation to meet model assumptions. To assess how fine-roots near the surviving focal tree within the disturbance plots were responding to phloem-disruption (O3), we first ran similar repeated-measure ANOVAs described above looking at differences between average fine-root surface area: volume (SAV), average fine-root diameter and fine-root exudation rates. The experimental unit was the average of four sampling locations surrounding each focal tree for each plot ($n = 8$). None of the three fine-root metrics required transformation to meet model assumptions. Additionally, we ran an asymptotic test to compare the heterogeneity across plots in fine-root structural and functional traits from surviving focal and control trees. Specifically, we used an asymptotic test developed by Feltz and Miller 1996 to statistically compare the coefficient of variation across multiple populations. Lastly, to synthesize how roots from surviving trees within the disturbance plots were responding to changes in N availability (O3), we ran separate multivariate linear regression analyses to test how soil available N impacts fine-root SAV, average root diameter, fine-root exudation and

coarse root NSCs between the control and surviving focal trees in the disturbance plots. With a logarithmic transformation of NSCs and SAV, all models met the assumptions of normality, equality of variance, autocorrelation, linearity and influential outliers. (For all ANOVA models and linear regression output see Tables S4.1-7).

3. Results

3.1. Soil respiration (R_s)

We observed no differences in R_s between the control and disturbance stands from four days before to 99 days after the phloem-disruption (Figure 4.3a, F-value = 0.032, p-value = 0.86). However, R_s varied significantly over time (F-value = 12.94, p-value <0.001), reaching a low of $3.2 \mu\text{mol CO}_2 \text{ m}^{-2} \text{ s}^{-1}$ in May to $13.0 \mu\text{mol CO}_2 \text{ m}^{-2} \text{ s}^{-1}$ in mid-July (Figure 4.3a). R_s resistance values, normalized for temporal changes, were not significantly different from zero (Figure 4.3b), indicating phloem-disruption had no initial effect on stand-level R_s .

3.2. Non-structural carbohydrate concentrations (NSC)

Phloem-disruption did not reduce NSC concentrations in the coarse roots of girdled trees. We found no significant difference in the coarse root NSC concentrations of girdled trees and control trees between 44 and 56 days after disturbance (F-value = 0.01, p-value = 0.92). NSC concentrations in the control trees averaged 15.6% and NSC concentration in the girdled trees averaged 16.2%. (Figure 4.4).

3.3. Soil available nitrogen (NH_4^+ and NO_3^-)

Phloem-disruption enriched soil available nitrogen by increasing stand-level NH_4^+ concentrations. We observed significantly greater concentrations of soil NH_4^+ in the disturbance plots than in the control plot between 28 and 56 days after stem-girdling (Figure 4.5a, F-value = 3.23, p-value = 0.08). In contrast, we found no significant difference in NO_3^- concentrations between the disturbance and control plots (Figure 4.5b, F-value = 0.57, p-value = 0.81). Soil available NH_4^+ averaged 2884 (mg NH_4^+ /kg soil) in the control and 5561 (mg NH_4^+ /kg soil) in the disturbance plots. Soil available nitrate averaged 101.6 (mg NO_3^- /kg soil) in the control and 91.5 (mg NO_3^- /kg soil) in the disturbance plots.

3.4. *Surviving tree rhizosphere structure and function*

To investigate whether the fine-roots of surviving trees structurally or functionally responded to an influx of nutrients, we assessed fine-root traits associated with nutrient acquisition from surviving trees in the disturbance plots. While there was no significant difference in mean fine-root structural traits and exudation rates between surviving focal trees in the disturbance and control focal trees, disturbance increased the heterogeneity of fine-root structure in surviving trees. Specifically, we found no significant difference between fine-root surface area (cm^2): volume (cm^3) (SAV), which averaged 76.4 in the disturbance and 76.5 in the control (Figure 4.6A, F-value = 0.137, p-value = 0.7), average fine-root diameter (mm), which averaged 0.54 mm in the disturbance and 0.53 mm in the control (Figure 4.6B, F-value = 0.12, p-value = 0.73) or fine-root exudation rates, which averaged 0.036 (mg non-particulate organic carbon/g soil) in the disturbance and 0.042 (mg non-particulate organic carbon/ g soil) in the control (Figure 4.6C, F-value = 0.17, p-value = 0.68). However, the fine-root SAV and diameters of surviving trees in the disturbance stands exhibited statistically greater variability than those in the control plots.

The average coefficient of variation (C_v) of SAV from fine-roots near surviving focal trees and control focal trees was 13.15 and 5.87, respectively (Figure 4.6D, $D'AD = 4.65$, p - value = 0.03) and the C_v of average fine-root diameter near surviving trees in the disturbance and control trees was 12.45 and 6.26, respectively (Figure 4.6E, $D'AD = 3.66$, p -value = 0.05).

3.5. Soil available nitrogen and surviving tree rhizosphere structure and function

The degree of soil nitrogen enrichment in disturbed stands correlated with root NSC concentrations, suggesting a linkage between the two and R_s . We observed a positive relationship between soil available NH_4^+ and the root NSC concentrations of surviving focal trees in the disturbance plots (Figure 4.7, $R^2 = 0.51$, p -value = 0.017, Disturbance: NH_4^+ interaction: F -value = 2.44, p -value = 0.025). This positive relationship was not observed in the control plots, nor was there a significant relationship between soil available NH_4^+ and NSCs in girdled trees ($R^2 = 0.23$, p -value = 0.40). This relationship suggests that an increase in stand-level soil NH_4^+ in the disturbance plots may have stimulated C storage belowground from surviving focal trees. However, this positive relationship between soil available NH_4^+ and surviving tree NSC was not mediated by a positive relationship between fine-root structural or functional metrics as hypothesized. There was no significant relationship between soil available NH_4^+ and SAV ($R^2 = 0.07$, p -value = 0.67) , average fine-root diameter ($R^2 = 0.08$, p -value = 0.66) nor fine-root exudation ($R^2 = 0.46$, p -value = 0.43).

4. Discussion

Contrary to our hypothesis and some prior observations from our site, stand R_s did not decline within the first 100 days of phloem-disruption. While we hypothesized immediate declines in R_s

followed by early signs of recovery (Figure 4.1), we found no response in R_s across the first year following phloem-disruption. These results not only add to the growing variability in R_s response to phloem-disruption across systems (Högberg et al. 2001, Levy-Varon et al. 2014, Fraterrigo et al. 2018), but also at our site, with some showing declines in R_s within 2 months (Mathes et al *in review*) and others showing stable R_s for the first two years following phloem-disruption (Clippard et al. 2022). While several questions remain regarding this variability in R_s response, both within and among sites, our cross-scale analysis—from root to ecosystem functions—identifies several rhizosphere changes that occur within days-to-weeks following disturbance that can may help explain stable R_s immediately following phloem-disruption.

The unexpected maintenance of root NSCs in girdled trees may be a primary driver of the sustained R_s that we observed in the first year following phloem-disruption. While studies show that girdling eliminates the phloem-transported labile C to the rhizosphere (Hoberg et al. 2001; Levy-Varon et al. 2012; Nottingham et al. 2022; Anderson et al. 2005), our analysis, along with others (Aubrey and Teskey 2018), suggest maintenance of NSCs in girdled trees can sustain R_s , at least initially. Variability in NSC response to girdling could be caused by pre-disturbance differences in C allocation and storage belowground, which are often higher in more climatically stressful (Mai et al. 2015; Aubrey and Teskey 2018) and nutrient-limited (Gill and Finzi 2016; Miao et al. 2022) environments. Our stands were situated on the low end of productivity and nutrient availability at our site (Pearsall et al. 1995), which could have supported high pre-disturbance C stored belowground and buffered the impacts of phloem-disruption in the rhizosphere C cycle, at least initially. Additionally, variability in NSC storage could be driven from abiotic conditions from the previous growing season (Ni et al. 2022). For example,

interannual variability in precipitation and vapor pressure deficit, which are established drivers of C sequestration (Sulman et al. 2016), may contribute to temporal variability in NSC storage. Therefore, pre-disturbance ecological and climatic conditions may be important drivers of initial R_s response to phloem-disrupting, mediated by rates of NSC storage.

Despite sustained root NSCs in girdled trees, higher soil NH_4^+ in disturbance stands suggests that the N demand of girdled trees may have declined. We observed significantly higher available NH_4^+ in the disturbance plots starting 28 days after girdling, which is consistent with our hypothesis and other studies showing declines in root NH_4^+ uptake following phloem-disruption (Zeller et al. 2008, Chen et al. 2012, Davis et al. 2019). However, increases in NH_4^+ were not paired with declines in root NSC concentration in the girdled trees, which was unexpected because NSCs are an established driver of root function, including N uptake (Nave et al. 2011, Wang and Wang 2021). Instead, our results suggest other mechanisms caused immediate N demand of girdled trees to decline. One hypothesis is mycorrhizal associations with girdled roots – a well-documented mechanism of plant N uptake (Smith and Smith 2011) – declined within the first year following phloem-disruption. Studies across forest types have shown declines in mutualistic mycorrhizal-root associations and a shift towards more saprotrophic fungi communities following phloem-disruption, caused by the severing of photosynthate belowground that supports mycorrhizal growth (Yarwood et al. 2008; Lindahl et al. 2010; Castillo et al. 2018). These shifts have been shown within first year and as soon as one month after girdling (Högberg & Högberg, 2002). While root NSC concentration was not different in girdled trees, the discontinuation of *new* C supply to the rhizosphere from girdling may have weakened these fungal associations (Fellbaum et al. 2011), and therefore suppressed N uptake in girdled trees.

Soil N enrichment may have driven changes in the fine-root structure of surviving focal trees nested within disturbance stands, facilitating the reallocation of this limiting resource. Studies show absorptive roots, which are smaller and have high exudation rates and surface area:volume (SAV), are favored over denser, larger and metabolically less-active transport roots under high soil nutrient conditions (McCormack et al. 2015, Fort and Freschet 2020, Cabugao et al. 2021). However, shifts in these fine-root traits from surviving trees in response to girdling of neighboring trees have been poorly characterized (Flower et al. 2015). While we did not observe a hypothesized increase in fine-root traits associated with nutrient uptake from surviving focal trees, our results provide two lines of evidence that surviving focal trees are responding to girdling of neighboring trees within the first growing season. First, we found high variability in SAV and average fine-root diameter across the surviving trees, which suggests these surviving trees may be responding heterogeneously to the changing resource environment following phloem-disruption as a result of patchy distribution of soil N availability within the soil profile (Rajaniemi 2003, Lak et al. 2020). Second, we found an increase in surviving tree root NSCs with increasing soil N availability, suggesting surviving trees began to reallocate the newly available N, promoting enhanced C assimilation and storage (Ågren et al. 2012, Tang et al. 2018, Zhang et al. 2022) in the first year. These results, paired with sustained root NSC concentrations in girdled trees, suggest that surviving trees can respond to disturbance-induced soil resource changes in advance of complete functional decline of neighboring girdled trees.

Finally, we acknowledge the limitations of our study. First, while our objectives focused on examining immediate rhizosphere processes following-phloem-disruption, by limiting our study to one growing season, we may not have captured the full cascade of responses that occurred within the first year. Second, we assumed soil samples taken at a distance of 0.5 m from the stem were mostly capturing fine-roots from the focal tree. While data from multiple temperate species supports this by showing a stem-centered pattern of root growth that declines with increasing distance from the tree within the first 10 m (Rewald and Leuschner 2009, Farrior 2019), environmental conditions, particularly water stress, can shift patterns of lateral root proliferation (Agee et al. 2021). Therefore, the high variation in fine-root structural traits found in the disturbance plots could be the result of soil cores capturing both fine-roots from surviving and closely neighboring girdled trees. Regardless, high variability in fine-root structure surrounding the focal surviving trees that was not present in the control plots still suggests that fine-root traits are changing in response to phloem-disruption within the first year. Finally, the small sample size of the experimental design limits the strength of our analysis. However, the uniform pre-disturbance ecological characteristics and soil properties across the plots (Table 4.1, Pearsall et al. 1995), which were randomly selected to disturbance or control, minimized confounding variables that could lead to incorrect conclusions about the impact of the disturbance treatment.

Conclusions

Several interacting mechanisms likely sustained R_s following phloem disruption, including maintenance of root NSCs in girdled trees, and greater soil N availability potentially facilitating changes in fine-root structure and belowground C storage in surviving trees. Sustained root NSCs in girdled trees during the first year following phloem-disruption suggests that pre-

disturbance conditions that regulate C allocation belowground, such as stand-productivity and climate, might drive variability in R_s immediately following phloem-disruption. Additionally, surviving trees responded to enriched soil nitrogen *before* complete functional decline of disturbed trees, which may have helped sustain ecosystem-scale functions, including R_s . Finally, the dynamic yet heterogenous responses in fine-root traits surrounding surviving focal trees highlights the need to more fully understand the role surviving trees play in regulating R_s and other important C fluxes following partial disturbances. Continued assessments of the timing and the specific rhizosphere structural and functional processes that support resource reallocation may also help predict longer-term stability of ecosystem functions to future disturbances.

Literature Cited

- Abramoff, R. Z., and A. C. Finzi. 2016. Seasonality and partitioning of Root allocation to rhizosphere soils in a midlatitude forest. *Ecosphere* 7.
- Agee, E., L. He, G. Bisht, V. Couvreur, P. Shahbaz, F. Meunier, C. M. Gough, A. M. Matheny, G. Bohrer, and V. Ivanov. 2021. Root lateral interactions drive water uptake patterns under water limitation. *Advances in Water Resources* 151.
- Ågren, G. I., J. Å. M. Wetterstedt, and M. F. K. Billberger. 2012. Nutrient limitation on terrestrial plant growth - modeling the interaction between nitrogen and phosphorus. *New Phytologist* 194:953–960.
- Amiro, B. D., A. G. Barr, J. G. Barr, T. A. Black, R. Bracho, M. Brown, J. Chen, K. L. Clark, K. J. Davis, A. R. Desai, and others. 2010. Ecosystem carbon dioxide fluxes after disturbance in forests of North America. *Journal of Geophysical Research*:

Biogeosciences 115.

- Atkins, J. W., B. Bond-Lamberty, R. T. Fahey, L. T. Haber, E. Stuart-Haëntjens, B. S. Hardiman, E. LaRue, B. E. McNeil, D. A. Orwig, A. E. L. Stovall, J. M. Tallant, J. A. Walter, and C. M. Gough. 2020. Application of multidimensional structural characterization to detect and describe moderate forest disturbance. *Ecosphere* 11.
- Aubrey, D. P., and R. O. Teskey. 2018. Stored root carbohydrates can maintain root respiration for extended periods. *New Phytologist* 218:142–152.
- Bentz, B. J., J. Rgnire, C. J. Fettig, E. M. Hansen, J. L. Hayes, J. A. Hicke, R. G. Kelsey, J. F. Negron, and S. J. Seybold. 2010. Climate change and bark beetles of the western United States and Canada: Direct and indirect effects. *BioScience* 60:602–613.
- Berkehammer, M., B. Drewniak, B. Ahlswede, and M. A. Gonzalez-Meler. 2022. Root Foraging Alters Global Patterns of Ecosystem Legacy From Climate Perturbations. *Journal of Geophysical Research: Biogeosciences* 127.
- Bhupinderpal-Singh, A. Nordgren, M. O. Löfvenius, M. N. Högberg, P. E. Mellander, and P. Högberg. 2003. Tree root and soil heterotrophic respiration as revealed by girdling of boreal Scots pine forest: Extending observations beyond the first year. *Plant, Cell and Environment* 26:1287–1296.
- Binkley, D., J. L. Stape, E. N. Takahashi, and M. G. Ryan. 2006. Tree-girdling to separate root and heterotrophic respiration in two Eucalyptus stands in Brazil. *Oecologia* 148:447–454.
- Brüggemann, N., A. Gessler, Z. Kayler, S. G. Keel, F. Badeck, M. Barthel, P. Boeckx, N. Buchmann, E. Bruognoli, J. Esperschütz, O. Gavrichkova, J. Ghashghaie, N. Gomez-Casnovas, C. Keitel, A. Knohl, D. Kuptz, S. Palacio, Y. Salmon, Y. Uchida, and M.

- Bahn. 2011. Carbon allocation and carbon isotope fluxes in the plant-soil-atmosphere continuum: A review.
- Busby, P. E., and C. D. Canham. 2011. An exotic insect and pathogen disease complex reduces aboveground tree biomass in temperate forests of eastern North America. *Canadian Journal of Forest Research* 41:401–411.
- Cabugao, K. G., D. Yaffar, N. Stenson, J. Childs, J. Phillips, M. A. Mayes, X. Yang, D. J. Weston, and R. J. Norby. 2021. Bringing function to structure: Root–soil interactions shaping phosphatase activity throughout a soil profile in Puerto Rico. *Ecology and Evolution* 11:1150–1164.
- Chen, D., L. Zhou, J. Wu, J. Hsu, Y. Lin, and S. Fu. 2012. Tree girdling affects the soil microbial community by modifying resource availability in two subtropical plantations. *Applied Soil Ecology* 53:108–115.
- Clark, K. L., H. J. Renninger, N. Skowronski, M. Gallagher, and K. V. R. Schäfer. 2018. Decadal-scale reduction in forest net ecosystem production following insect defoliation contrasts with short-term impacts of prescribed fires. *Forests* 9.
- Clippard, E. A., S. I. Haruna, P. S. Curtis, C. Clay, B. Bond, K. Mathes, C. S. Vogel, and C. M. Gough. 2022. Decadal forest soil respiration following stem girdling. *Trees*.
- Davis, J. C., J. P. Shannon, M. J. Van Grinsven, N. W. Bolton, J. W. Wagenbrenner, R. K. Kolka, and T. G. Pypker. 2019. Nitrogen cycling responses to simulated emerald ash borer infestation in *Fraxinus nigra*-dominated wetlands. *Biogeochemistry* 145:275–294.
- Dietze, M. C., and J. H. Matthes. 2014. A general ecophysiological framework for modelling the impact of pests and pathogens on forest ecosystems. *Ecology Letters* 17:1418–1426.
- Edgar, C. B., and J. A. Westfall. 2022. Timing and extent of forest disturbance in the Laurentian

- Mixed Forest. *Frontiers in Forests and Global Change* 5:1–15.
- Ekberg, A., N. Buchmann, and G. Gleixner. 2007. Rhizospheric influence on soil respiration and decomposition in a temperate Norway spruce stand. *Soil Biology and Biochemistry* 39:2103–2110.
- Epron, D., M. Bahn, D. Derrien, F. A. Lattanzi, J. Pumpanen, A. Gessler, P. Högberg, P. Maillard, M. Dannoura, D. Gérant, and N. Buchmann. 2012, June. Pulse-labelling trees to study carbon allocation dynamics: A review of methods, current knowledge and future prospects.
- Farrior, C. E. 2019. Theory predicts plants grow roots to compete with only their closest neighbours. *Proceedings of the Royal Society B: Biological Sciences* 286.
- Feltz, C. J., and G. E. Miller. 1996. An asymptotic test for the equality of coefficients of variation from k populations. *Statistics in Medicine* 15:647–658.
- Fort, F., and G. T. Freschet. 2020. Plant ecological indicator values as predictors of fine-root trait variations. *Journal of Ecology* 108:1565–1577.
- Fraterrigo, J. M., K. Ream, and J. D. Knoepp. 2018. Tree Mortality From Insect Infestation Enhances Carbon Stabilization in Southern Appalachian Forest Soils. *Journal of Geophysical Research: Biogeosciences* 123:2121–2134.
- Frey, B., F. Hagedorn, and F. Giudici. 2006. Effect of girdling on soil respiration and root composition in a sweet chestnut forest. *Forest Ecology and Management* 225:271–277.
- Gough, C. M., G. Bohrer, B. S. Hardiman, L. E. Nave, C. S. Vogel, J. W. Atkins, B. Bond-Lamberty, R. T. Fahey, A. T. Fotis, M. S. Grigri, and others. 2021. Disturbance-accelerated succession increases the production of a temperate forest. *Ecological Applications* 31:1–17.

- Hillebrand, H., S. Langenheder, K. Lebet, E. Lindström, Ö. Östman, and M. Striebel. 2018. Decomposing multiple dimensions of stability in global change experiments. *Ecology Letters* 21:21–30.
- Högberg, M. N., and P. Högberg. 2002. Extramatrical ectomycorrhizal mycelium contributes one-third of microbial biomass and produces, together with associated roots, half the dissolved organic carbon in a forest soil. *New Phytologist* 154:791–795.
- Högberg, P., A. Nordgren, N. Buchmann, A. F. S. Taylor, A. Ekblad, M. N. Högberg, G. Nyberg, M. Ottosson-Löfvenius, and D. J. Read. 2001. Large-scale forest girdling shows that current photosynthesis drives soil respiration. *Nature* 411:789–792.
- Kochsiek, A., S. Tan, and S. E. Russo. 2013. Fine root dynamics in relation to nutrients in oligotrophic Bornean rain forest soils. *Plant Ecology* 214:869–882.
- Lak, Z. A., H. Sandén, M. Mayer, D. L. Godbold, and B. Rewald. 2020. Plasticity of root traits under competition for a nutrient-rich patch depends on tree species and possesses a large congruency between intra-and interspecific situations. *Forests* 11.
- Lei, J., X. Guo, Y. Zeng, J. Zhou, Q. Gao, and Y. Yang. 2021. Temporal changes in global soil respiration since 1987. *Nature Communications* 12:1–9.
- Levy-Varon, J. H., W. S. F. Schuster, and K. L. Griffin. 2012. The autotrophic contribution to soil respiration in a northern temperate deciduous forest and its response to stand disturbance. *Oecologia* 169:211–220.
- Levy-Varon, J. H., W. S. F. Schuster, and K. L. Griffin. 2014. Rapid rebound of soil respiration following partial stand disturbance by tree girdling in a temperate deciduous forest. *Oecologia* 174:1415–1424.
- Mathes, K. C., Y. Ju, C. Kleinke, C. Oldfield, G. Bohrer, B. Bond-Lamberty, C. S. Vogel, K.

- Dorheim, and C. M. Gough. 2021. A multidimensional stability framework enhances interpretation and comparison of carbon cycling response to disturbance. *Ecosphere* 12.
- Mathes K.C, Pennington, S. Rodriguez, C., Bond-Lamberty B., Atkins J.W., Vogel C.S., Gough, C.M. Sustained three-year declines in forest soil respiration are proportional to disturbance severity. *In review*.
- Mccormack, M. L., I. A. Dickie, D. M. Eissenstat, T. J. Fahey, C. W. Fernandez, D. Guo, A. Erik, C. M. Iversen, and R. B. Jackson. 2015. Tansley review Redefining fine roots improves understanding of below-ground contributions to terrestrial biosphere processes:505–518.
- Meyer, G., Black, T. A., Jassal, R. S., Nestic, Z., Coops, N. C., Christen, A., Fredeen, A. L., Spittlehouse, D. L., Grant, N. J., Foord, V. N., & Bowler, R. (2018). Simulation of net ecosystem productivity of a lodgepole pine forest after mountain pine beetle attack using a modified version of 3-PG. *Forest Ecology and Management*, 412, 41–52.
<https://doi.org/10.1016/j.foreco.2018.01.034>
- Nakane, K., T. Kohno, and T. Horikoshi. 1996. Root respiration rate before and just after clear-felling in a mature, deciduous, broad-leaved forest. *Page Ecological Research*.
- Nave, L. E., C. M. Gough, K. D. Maurer, G. Bohrer, B. S. Hardiman, J. Le Moine, A. B. Munoz, K. J. Nadelhoffer, J. P. Sparks, B. D. Strahm, and and others. 2011. Disturbance and the resilience of coupled carbon and nitrogen cycling in a north temperate forest. *Journal of Geophysical Research: Biogeosciences* 116:1–14.
- Nottingham, A. T., A. W. Cheesman, T. Riutta, C. E. Doughty, E. Telford, W. Huaraca Huasco, M. Svátek, J. Kvasnica, N. Majalap, Y. Malhi, P. Meir, and Y. Arn Teh. 2022. Large contribution of recent photosynthate to soil respiration in tropical dipterocarp forest

- revealed by girdling. *Journal of Ecology* 110:387–403.
- Pearsall, D. R., B. V. Barnes, G. R. Zogg, M. Lapin, R. R. Ring, and D. Ring. 1995. Landscape ecosystems of the University of Michigan Biological Station. *School of Natural Resources & Environment* 66.
- Phillips, R. P., Y. Erlitz, R. Bier, and E. S. Bernhardt. 2008. New approach for capturing soluble root exudates in forest soils. *Functional Ecology* 22:990–999.
- Quirion, B. R., G. M. Domke, B. F. Walters, G. M. Lovett, J. E. Fargione, L. Greenwood, K. Serbesoff-King, J. M. Randall, and S. Fei. 2021. Insect and Disease Disturbances Correlate With Reduced Carbon Sequestration in Forests of the Contiguous United States. *Frontiers in Forests and Global Change* 4.
- Rajaniemi, T. K. 2003. Basic and Applied Ecology Evidence for size asymmetry of belowground competition. *Page Basic Appl. Ecol.*
- Rewald, B., and C. Leuschner. 2009. Belowground competition in a broad-leaved temperate mixed forest: Pattern analysis and experiments in a four-species stand. *European Journal of Forest Research* 128:387–398.
- Sommerfeld, A., C. Senf, B. Buma, A. W. D'Amato, T. Després, I. Díaz-Hormazábal, S. Fraver, L. E. Frelich, Á. G. Gutiérrez, S. J. Hart, and others. 2018. Patterns and drivers of recent disturbances across the temperate forest biome. *Nature Communications* 9:4355.
- Sulman, B. N., Roman, D. T., Yi, K., Wang, L., Phillips, R. P., & Novick, K. A. (2016). High atmospheric demand for water can limit forest carbon uptake and transpiration as severely as dry soil. *Geophysical Research Letters*, 43(18), 9686–9695.
- Tang, Z., W. Xu, G. Zhou, Y. Bai, J. Li, X. Tang, D. Chen, Q. Liu, W. Ma, G. Xiong, H. He, N. He, Y. Guo, Q. Guo, J. Zhu, W. Han, H. Hu, J. Fang, and Z. Xie. 2018. Patterns of plant

- carbon, nitrogen, and phosphorus concentration in relation to productivity in China's terrestrial ecosystems. *Proceedings of the National Academy of Sciences of the United States of America* 115:4033–4038.
- Wang, Z., and C. Wang. 2021. Magnitude and mechanisms of nitrogen-mediated responses of tree biomass production to elevated CO₂: A global synthesis. *Journal of Ecology* 109:4038–4055.
- Weemstra, M., N. Kiorapostolou, J. van Ruijven, L. Mommer, J. de Vries, and F. Sterck. 2020. The role of fine-root mass, specific root length and life span in tree performance: A whole-tree exploration. *Functional Ecology* 34:575–585.
- Zeller, B., J. Liu, N. Buchmann, and A. Richter. 2008. Tree girdling increases soil N mineralisation in two spruce stands. *Soil Biology and Biochemistry* 40:1155–1166.
- Zhang, P., X.-T. Lü, M.-H. Li, T. Wu, and G. Jin. 2022. N limitation increases along a temperate forest succession: evidences from leaf stoichiometry and nutrient resorption. *Journal of Plant Ecology* 15:1021–1035.

Tables

Table 4.1: Physical and ecological site characteristics between the disturbance and control plots.

Landform, soil type and soil drainage information was taken from Pearsall et al. 1995 and vegetation and soil micrometeorology measurements were taken one week prior to disturbance initiation.

	Disturbance	Control
Landform	High elevation outwash plain	High elevation outwash plain
Soil type	Calcareous sand	Calcareous sand
Soil drainage	Excessively well drained	Excessively well drained
Canopy biomass (kg C ha ⁻¹)	102,349 (5197)	101,278 (4471)
Canopy stem density (Stems ha ⁻¹)	950 (132)	950 (119)
Canopy composition	QURU (65.10%) POGR (23.85%) ACRU (7.43%) FAGR (1.93%) PIRE (1.03%)	POGR (66.11%) QURU (16.83%) PIRE (12.35%) ACRU (3.47%) PIST (1.24%)
Soil temperature (T _s , °C)	11.3 (0.03)	11.37 (0.05)
Soil volumetric water content (VWC%)	14.03 (0.38)	11.65 (0.45)

Figures

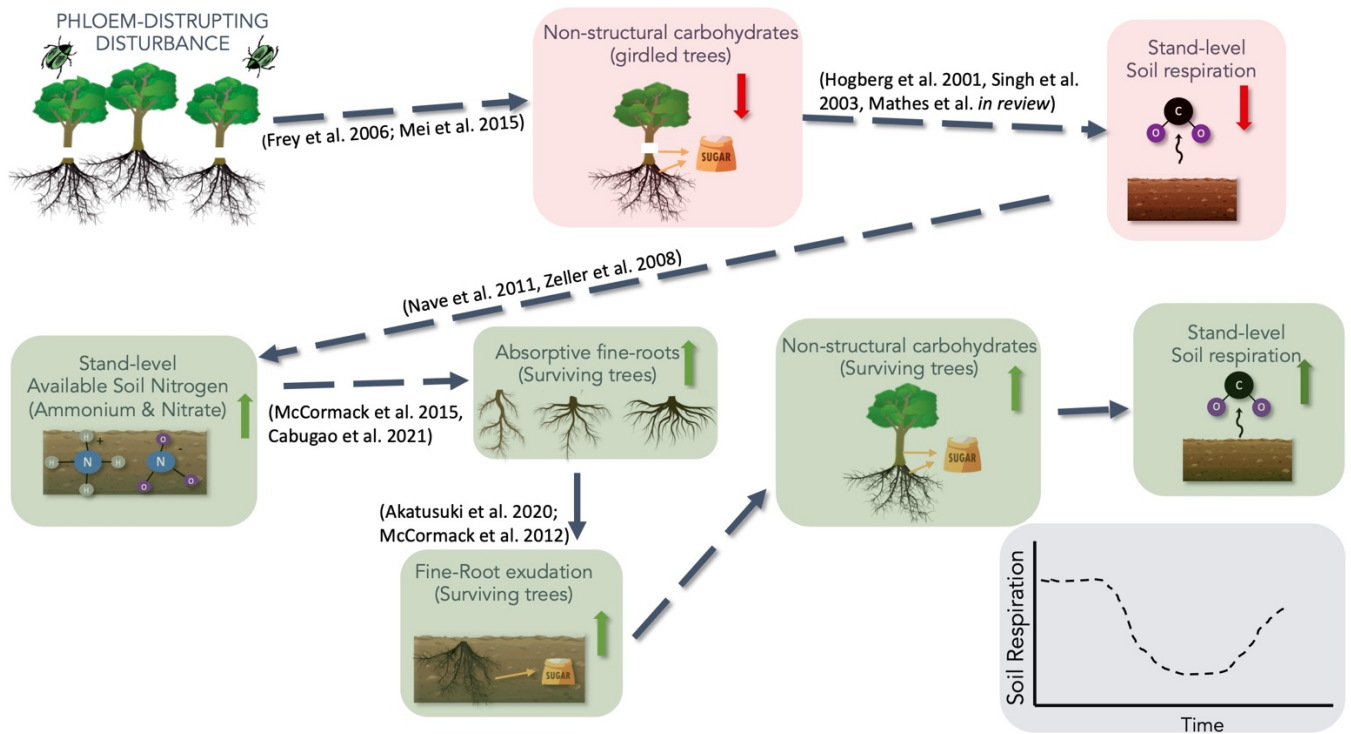


Figure 4.1: Illustration of hypothesized changes in stand and root-level rhizosphere processes following phloem-disruption and the consequences for stand-scale R_s .

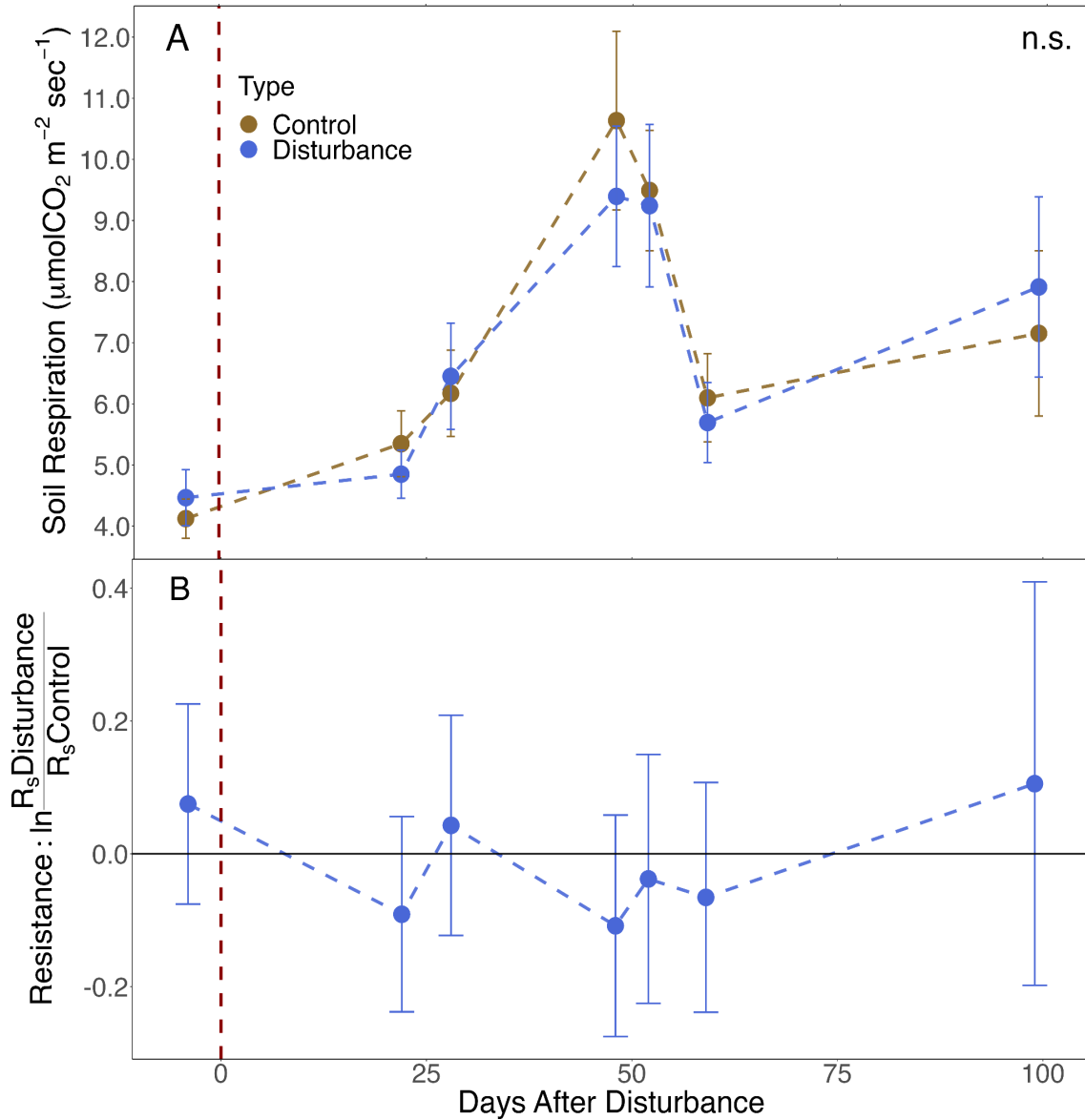


Figure 4.3: A) Time series of mean instantaneous R_s values (\pm S.E.) between the disturbance and control plots (F-value = 0.032, p-value = 0.86), and **B)** log response ratios of R_s in disturbance as compared to control, or “resistance”. Values overlapping with zero indicate complete resistance. Time series shows 4 days before girdling disturbance to 99 days after disturbance. Dashed horizontal red line indicates day of disturbance (May 31, 2022).

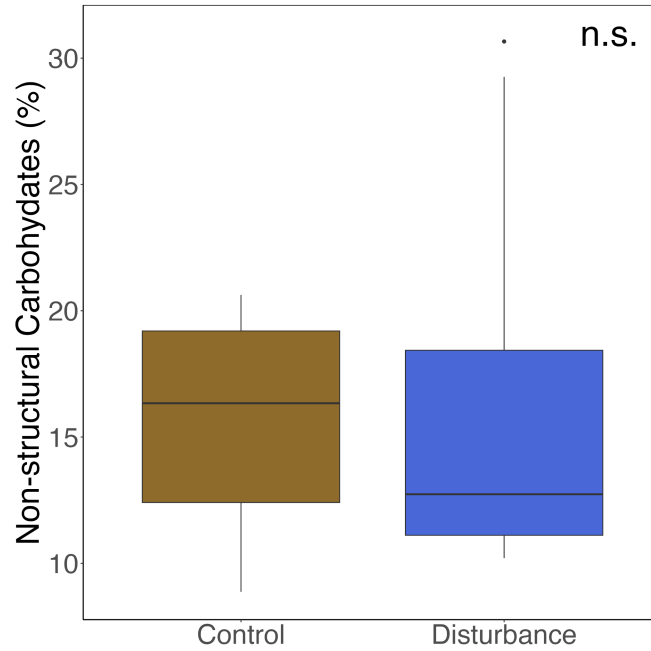


Figure 4.4: Boxplots showing median, interquartile range (middle 50% of range) and minimum and maximum root NSC concentration (%) between control trees and girdled trees in the disturbance plots. (F-value = 0.01, p-value = 0.9). Values were averaged across measurement times (44-58 days after girdling).

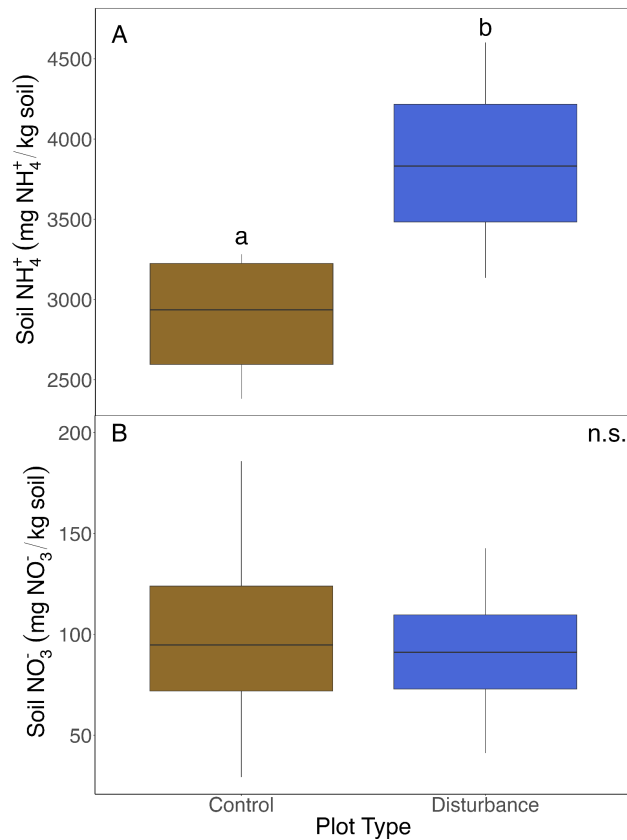


Figure 4.5: Boxplots showing median, interquartile range (middle 50% of range), minimum and maximum **A)** soil available ammonium (NH₄⁺) between control (ungirdled) and disturbance (girdled) plots. ($F = 3.76$, $p = 0.08$) and **B)** soil available nitrate (NO₃⁻) between control (ungirdled) and disturbance (girdled) plots ($F = 0.06$, $p = 0.8$). Values were averaged across measurement times (28-56 days after girdling).

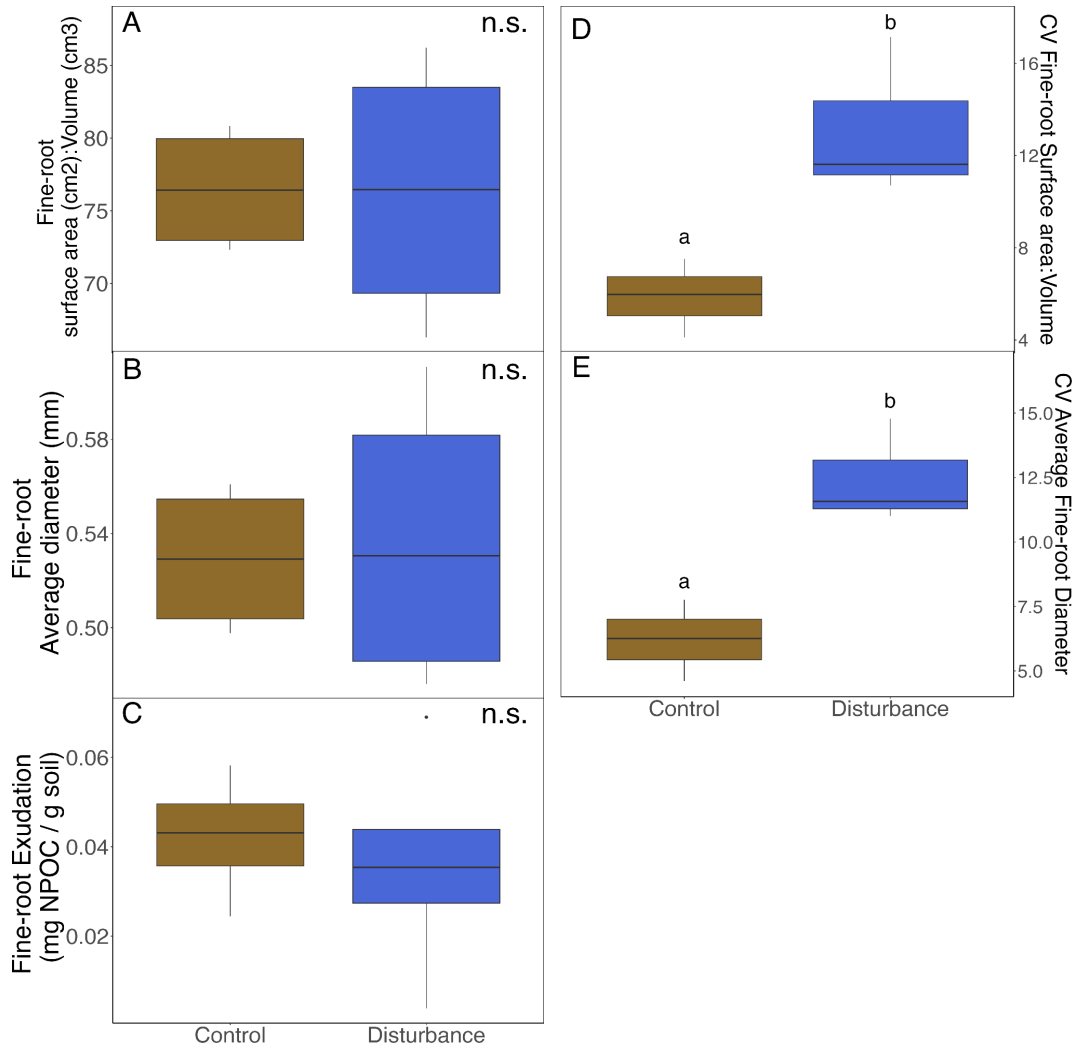


Figure 4.6: Boxplots shows median, interquartile range (middle 50% of range), minimum and maximum fine-root structural and functional traits in control focal trees and surviving focal trees within the disturbance. **A)** Average fine-root surface area (cm²):volume (cm³) ratio (F-value = 0.137, p-value = 0.7), **B)** Average fine-root diameter (mm) (F-value = 0.12, p-value = 0.73), **C)** Average fine-root exudation (F-value = 0.17, p-value = 0.68), **D)** coefficient of variance (C_v) for Fine-root SAV (D'AD = 4.65, p - value = 0.03) and **E)** C_v of average fine-root diameter (mm) (D'AD = 3.66, p-value = 0.05) between the control and the surviving focal trees in the disturbance plots. Values were averaged across measurement times (28-56 days after girdling).

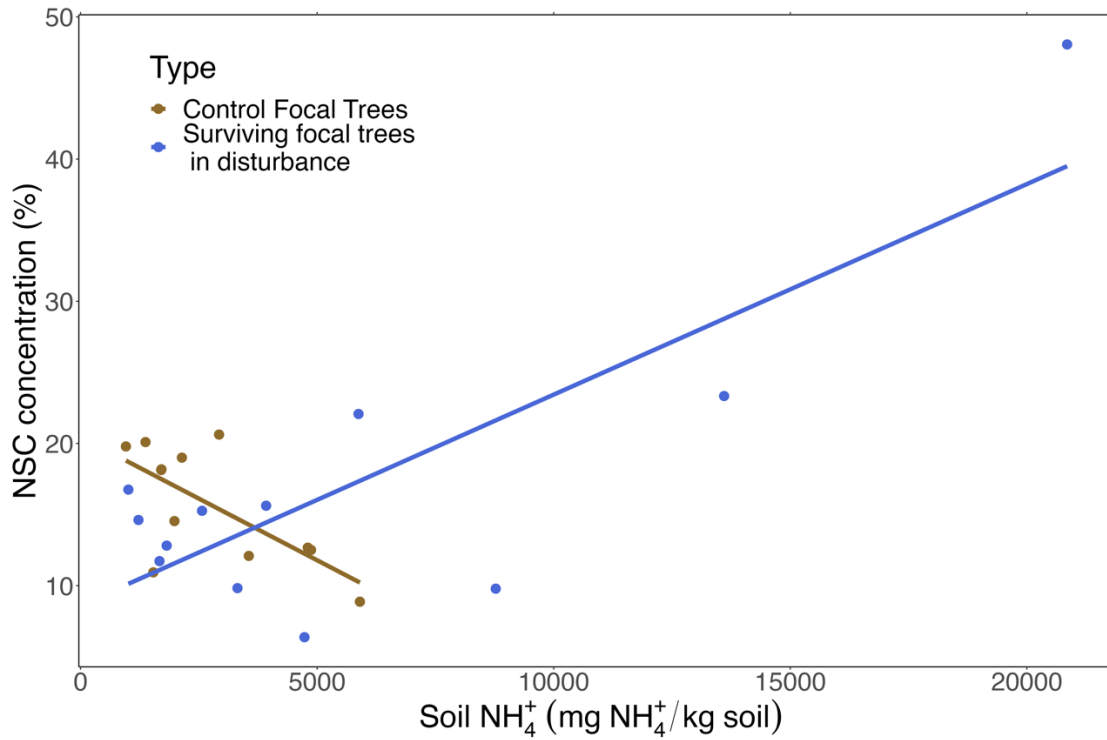


Figure 4.7: Root NSC concentration in control focal trees and surviving focal trees within the disturbance plots as a function of soil available ammonium (NH₄⁺). ($R^2 = 0.51$, $F = 3.79$, p -value = 0.017).

Chapter 4 Appendix:

Table S4.1: ANOVA output for stand-level soil respiration across 7 measurement dates within the 100 days following disturbance. Type represents 2 treatment types (disturbance or control). Alpha = 0.10. Significance codes: 0.001 = ***, 0.01 = **, 0.05 = *, 0.1 = •.

	Factor	Df	SS	MS	F-value	p-value
<i>Error: Plot</i>	Residuals	1	0.43	0.43		
<i>Error: within</i>	Type	1	0.002	0.0018	0.032	0.86
	Date	6	4.43	0.74	12.93	<0.001***
	Type:Date	6	0.087	0.015	0.254	0.96
	Residuals	41	2.34	0.057		

Table S4.2: ANOVA output for root non-structural carbohydrates from girdled trees across 3 measurement dates within the 100 days following disturbance. Type represents 2 treatment types (disturbance or control). Alpha = 0.10. Significance codes: 0.001 = ***, 0.01 = **, 0.05 = *, 0.1 = •.

	Factor	Df	SS	MS	F-value	p-value
<i>Error: Plot</i>	Residuals	1	0.23	0.23		
<i>Error: within</i>	Type	1	0.0014	0.001	0.01	0.92
	Date	2	0.005	0.003	0.02	0.98
	Residuals	19	2.47	0.13		

Table S4.3a: ANOVA output for stand-level soil ammonium across 4 measurement dates within the 100 days following disturbance. Type represents 2 treatment types (disturbance or control). Alpha = 0.10. Significance codes: 0.001 = ***, 0.01 = **, 0.05 = *, 0.1 = •.

	Factor	Df	SS	MS	F-value	p-value
<i>Error:Plot</i>	Residuals	1	0.02	0.02		
<i>Error:within</i>	Type	1	1.72	1.72	3.23	0.08•
	Date	3	1.56	0.52	0.97	0.42
	Residuals	26	13.81	0.53		

Table S4.3b: Summary of Least Significant Difference (LSD) for significant effects (**Table S4.3a**) with 95% lower and upper confidence levels. Alpha = 0.10. Levels with the same group letter are not significantly different.

Factor	Mean Square Error	DF Error	Critical Value
Type	0.53	26	1.71

Level	Log ammonium	Lower CL	Upper CL	Min	Max	Groups
Control	7.82	6.86	8.68	6.86	8.68	a
Disturbance	8.29	5.463	6.309	6.92	9.95	b

Table S4.4: ANOVA output for stand-level soil nitrate across 4 measurement dates within the 100 days following disturbance. Type represents 2 treatment types (disturbance or control). Alpha = 0.10. Significance codes: 0.001 = ***, 0.01 = **, 0.05 = *, 0.1 = •.

	Factor	Df	SS	MS	F-value	p-value
<i>Error:Plot</i>	Residual	1	5107	5107		
<i>Error:within</i>	Type	1	743	743	0.057	0.813
	Date	3	68878	22959	1.759	0.180
	Residuals	26	339301	13050		

Table S4.5: ANOVA output for **A)** fine-root surface area:volume and **B)** average fine-root diameter from focal control trees and focal surviving trees in the disturbance plots across 3 measurement dates within the 100 days following disturbance. Type represents 2 treatment types (disturbance or control). Alpha = 0.10. Significance codes: 0.001 = ***, 0.01 = **, 0.05 = *, 0.1 = •.

A:

	Factor	df	SS	MS	F-value	p-value
<i>Error: Plot</i>	Residuals	3	0.11	0.04		
<i>Error: within</i>	Type	1	0.0	0.0	0.06	0.8
	Date	2	0.02	0.01	2.2	0.15
	Residuals	17	0.08	0.00		

B:

	Factor	df	SS	MS	F-value	p-value
<i>Error: Plot</i>	Residuals	3	0.10	0.04		
<i>Error: within</i>	Type	1	0.0	0.0	0.14	0.72
	Date	2	0.02	0.01	2.8	0.09•
	Residuals	17	0.07	0.00		

Table S4.6: Asymptotic CV test output: test for differences in CV of fine-root surface area:volume, average fine-root diameter and root exudates between focal control trees and focal surviving trees in the disturbance plots. Significance codes: 0.001 = ***, 0.01 = **, 0.05 = *, 0.1 = •.

Estimate	D'AD	p-value
fine-root surface area:volume	4.66	0.03*
average fine-root diameter	3.67	0.05*
root exudates	1.08	0.30

Table S4.7a: Output for regression analysis of root NSC concentration from focal control trees and focal surviving trees in the disturbance as a function of soil available ammonium. Significance codes: 0.001 = ***, 0.01 = **, 0.05 = *, 0.1 = •.

Predictors	Estimates	Standard Error	p-value
(Intercept)	3.106	0.20	<0.001***
Soil ammonium	-0.0004094	0.0004902	0.12
Type [Disturbance]	-0.0197044	0.0402328	0.019 *
Date [week 2]	-0.0198662	0.0402328	0.21
Date [week 3]	-0.0002597	0.0402328	0.45
Ammonium*Type	-0.0040187	0.0006932	0.03*

Residual SE: 0.32 on 18 df. *Adjusted R²:* 0.38. *F-statistic:* 3.76. *p-value:* **0.017***

Conclusions & Recommendations

The goal of my dissertation was to use refined ecological theory and cross-scale experiments to assess patterns and mechanisms of carbon cycling response to disturbance across gradients of severity. Synthesizing across all chapters, I highlight three overarching conclusions. First, leveraging components of a multi-dimensional stability framework into assessments of C flux disturbance response revealed the utility of applying such a framework—more commonly used by community ecologists—to the interpretation and comparison of ecosystem function. Second, soil respiration can exhibit variable responses to the same partial disturbance source, which could partly be determined by dynamic fine-scale rhizosphere responses from both surviving and disturbed trees on a landscape. Third, temperate forests can sustain their net C balance across a gradient of disturbance severities in the initial resistance phase as a result of stable heterotrophic respiration and net primary production. This result adds to a growing understanding that temperate forests can be highly functionally resistant to the increasing threat of forest disturbances from insect pests and pathogens.

My work also revealed several remaining areas of investigation that will help resolve uncertainties about functional stability following changing forest disturbance regimes. First, to allow for broader adoption of the multi-dimensional stability framework I describe in chapter one, I suggest the inclusion of additional stability dimensions that quantify and capture the temporal variability of carbon fluxes through the resistance phase. Second, the consistently negative NEP values across a disturbance severity gradient that I found in chapter three warrants future investigations comparing across methodologies of estimating carbon balance. This is important for resolving whether these temperate forests are transitioning to carbon sources from

climate warming or if there were systematic biases in our biometric approaches. Because temperate forests are predicted remain a strong carbon sink, improving accuracy of biometric approaches for measuring NEP is essential for climate change mitigation efforts that rely on forest carbon capture and storage. Finally, through the exploratory analysis of fine-scale rhizosphere processes that might drive soil respiration disturbance response, I suggest that future experiments could use tightly controlled manipulations to examine the role of surviving trees for determining ecosystem functional stability following partial disturbance.

Vita

Kayla Cerise Mathes was born on July 4th, 1995 in Albuquerque, New Mexico and graduated from Bosque Preparatory High School in 2013. She received a Bachelor of Music in cello performance and a Bachelor of Science in Environmental Studies from the University of Michigan-Ann Arbor in 2018. During and immediately following her undergraduate education she worked as a laboratory assistant for a soil ecology research lab, teachers' assistant for a forest ecology course and a peer advisor for the Science Learning Center at the University of Michigan. She also serves as a cellist in the Richmond Symphony Orchestra.